

JSCSEN 73(2)131–258(2008)

UDC 54:66

ISSN 0352–5139

Journal of
the Serbian
Chemical Society

Electronic
version

VOLUME 73

NO 2

BELGRADE 2008

Available on line at



www.shd.org.yu/JSCS/

The full search of JSCS
is available through

DOAJ DIRECTORY OF
OPEN ACCESS
JOURNALS

www.doaj.org



www.shd.org.yu

ISSN 0352-5139

J. Serb. Chem. Soc. Vol. 73, No. 2 (2008)

JSCS@tmf.bg.ac.yu • www.shd.org.yu/JSCS

ISSN 0352-5139



CONTENTS

Organic Chemistry and Biochemistry

- R. R. Kamble, B. S. Sudha and D. G. Bhadregowda: Expeditious synthesis of 1,3,4-oxadiazole derivatives via sydnone..... 131
- M. Simonović, S. Zlatanović-Milošević, M. M. Vrvić and B. Simonović: Recombinant expression of monovalent and bivalent anti-TNT-antibodies – evaluation of different expression systems..... 139
- N. Ognjanović, D. Bezbradica and Z. Knežević: Optimization of the production of biodiesel by a commercial immobilized lipase in a solvent-free system using a response surface methodology 147
- M. V. Nikolić and Lj. Mojović: Characterization and degradation of pectin derived from Budimka apple 157

Inorganic Chemistry

- N. Geetha and S. Thirumaran: Characterization studies and cyclic voltammetry on nickel(II) amino acid dithiocarbamates with triphenylphosphine in the coordination sphere..... 169
- M. Hussain, M. Zaman, M. Hanif, S. Ali and M. Danish: Synthesis and structural characterization of organotin(IV) complexes formed with [O,O] donor atoms of carboxylic acids 179

Theoretical Chemistry

- A. Moghani: Q-Conjugacy character and Markaracter tables of tetraammineplatinum(II) . 189

Physical Chemistry

- D. Bajuk-Bogdanović, I. Holclajtner-Antunović, M. Todorović, U. B. Mioč and J. Zakrzewska: A study of 12-tungstosilicic and 12-molybdophosphoric acids in solution 197
- N. Štrbac, D. Živković, I. Mihajlović, B. Boyanov and Ž. Živković: Mechanism and kinetics of the oxidation of synthetic α -NiS 211

Electrochemistry

- F. Crisan and E. Salló: Periodic current oscillations of zinc in nitric acid solutions 221
- P. M. Živković, B. N. Grgur and K. I. Popov: The validity of the general polarization curve equation approximation for the process of metal deposition (Note)..... 227

Analytical Chemistry

- M. A. Karimi, M. M. Ardakani, R. Behjatmanesh-Ardakani, M. R. H. Nezhad and H. Amiryan: Individual and simultaneous determinations of phenothiazine drugs using PCR, PLS and (OSC)-PLS multivariate calibration methods 233
- R. Gong, D. Zhang, K. Zhong, M. Feng and X. Liu: Determination of trace copper in water samples by flame atomic absorption spectrometry after preconcentration on a phosphoric acid functionalized cotton chelator..... 249



www.shd.org.yu

J. Serb. Chem. Soc. 73 (2) 131–138 (2008)

JSCS–3695

JSCS@tmf.bg.ac.yu • www.shd.org.yu/JSCS

UDC 547.78+542.913:547.334:547.77

Original scientific paper

Expeditious synthesis of 1,3,4-oxadiazole derivatives *via* sydnones

RAVINDRA R. KAMBLE*, B. S. SUDHA and D. G. BHADREGOWDA

*Department of Chemistry and Food Science, Yuvaraja's College,
University of Mysore, Mysore – 570 005, India*

(Received 21 June, revised 1 August 2007)

Abstract: The clean cyclization of chalcones (**1a–c/2a–c**) with hydrazine hydrate under microwave irradiation afforded pyrazolines derivatised with sydnone (**3d–i/4d–i**), which underwent 1,3-dipolar cyclo-addition with acetic anhydride to form pyrazolines appended with 1,3,4-oxadiazoles (**5g–l/6g–l**). The newly synthesized compounds were confirmed by spectral and elemental analyses. In comparison to classical heating, the results indicate that microwave irradiation affords higher yields, shorter reaction times (4–12 min) and cleaner reactions.

Keywords: microwave irradiation; sydnones; chalcones; pyrazolines; 1,3,4-oxadiazoles.

INTRODUCTION

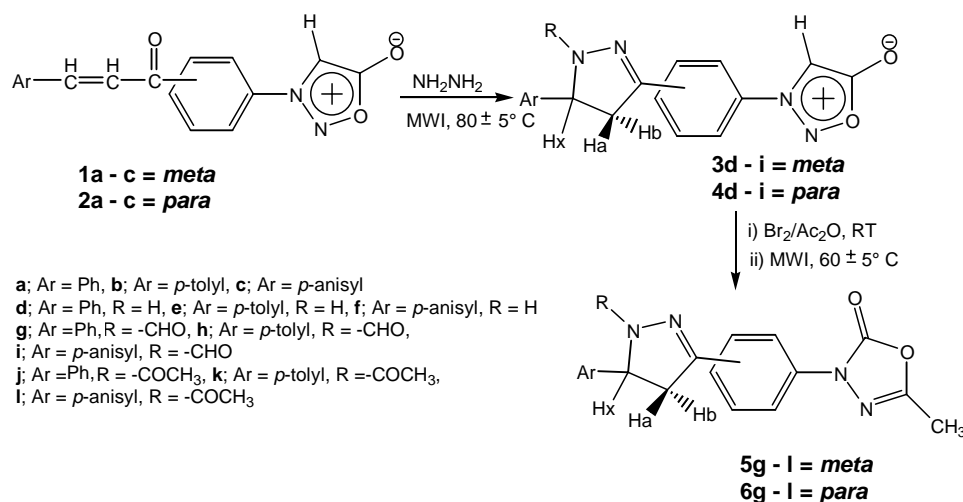
In recent years, a significant portion of the research in heterocyclic chemistry has been devoted to sydnones containing different moieties, as evident from the literature.^{1–4} Sydnones have played a crucial role in the development of theory in heterocyclic chemistry and have been used extensively as synthons in organic synthesis. It was reported that 1,3,4-oxadiazole derivatives, suitably substituted at the 2 and 5 positions, exhibited considerable antibacterial and antifungal activity.^{5–8} These heterocycles are of great interest to medicinal chemists for molecular manipulation and to biologists for further pharmacological evaluation. Pyrazolines and their derivatives are important biological agents and a significant amount of research activity has been directed towards this class of compounds. In particular, they are used as antitumor, antibacterial, antifungal, antiviral, antiparasitic, antitubercular and insecticidal agents.^{9–18} Some of these compounds also have anti-inflammatory, antidiabetic, anaesthetic and analgesic properties.^{19–22} As a result of studies related to the development of synthetic protocols using microwave irradiation, a novel and easy access to pyrazolines appended to 1,3,4-oxadiazoles is reported herein.

* Corresponding author. E-mail: ravichem1234@rediffmail.com

doi: 10.2298/JSC0802131K

RESULTS AND DISCUSSION

Chalcones (*meta* and *para* isomers), which were prepared according to a previously reported method,²³ undergo a rapid cyclization with hydrazine hydrate under microwave irradiations at $80 \pm 5^\circ\text{C}$ (240 W) to give pyrazolines **3d-i/4d-i** quantitatively in 4–12 min (Scheme 1). Poly(ethylene glycol) (PEG 200) and formic acid were used as the solvent for the preparation of **3d-f/4d-f** and **3g-i/4g-i**, respectively. Compounds **3d-i/4d-i** on bromination at $0-5^\circ\text{C}$ and heating under microwave at $60 \pm 5^\circ\text{C}$ (210 W) in acetic anhydride afforded **5g-l/6g-l**. The sydnone ring which is mesoionic undergoes 1,3-dipolar cyclo-addition reaction²⁴ with acetic anhydride to 1,3,4-oxadiazole. In addition, compounds **3d-i/4d-i** undergo *N*-acetylation of the pyrazoline ring to form **5j-l/6j-l**. These heterocyclic products were characterized based on their IR, ¹H-NMR, mass spectral and elemental analyses.



Scheme 1. The starting chalcones **1a-c/2a-c** and the intermediates 3-[3/4-(1-substituted-5-aryl-4,5-dihydro-1*H*-pyrazol-3-yl)phenyl]sydnone (**3d-i/4d-i**) and the final products after 1,3-dipolar cycloaddition, 5-methyl-3-[3/4-(1-substituted-5-aryl-4,5-dihydro-1*H*-pyrazol-3-yl)phenyl]-1,3,4-oxadiazol-2(3*H*)-ones (**5g-l/6g-l**).

On comparison of the synthesis by the microwave assisted method with that by the conventional method (randomly selected compounds),²⁵ it was observed that the reaction progressed very fast with excellent yields using the former method (Table I). Microwave irradiation facilitates polarisation of the molecule under irradiation, causing rapid reaction to occur.

EXPERIMENTAL

Materials

The microwave irradiations were performed using a commercial microwave oven M-2735A. The temperature approximation was realised using sealed capillaries containing compounds of

known melting points according to a reported method.²⁶ The approximate temperature along with the power in watts is given in the experimental procedures. TLC was run on silica gel G plates using acetone–benzene (1:3) as the irrigant. The melting points were determined in open capillaries and are uncorrected. The IR (KBr) spectra were recorded on a Nicolet Impact-410 FT-IR spectrometer and the NMR spectra in CDCl₃ (δ , ppm downfield from TMS) were recorded on a Bruker Varian-300 MHz FT-NMR spectrometer. *J* values are given in Hz. Elemental analyses were performed on a CEST 1106 elemental analyser. The mass spectra were recorded on EI-70 eV and FR ver. 1on UIC 002002 spectrometers.

TABLE I. Comparison of the reaction time required and yield

Compound	Thermal		Microwave	
	Time, h	Yield, %	Time, min	Yield, %
3d	4.0	60	5.0	82
3i	6.0	67	8.0	90
4d	4.5	65	7.0	92
4i	6.0	70	10.0	87
5g	1.0	66	7.0	90
5l	1.5	60	5.0	95
6g	1.0	52	8.0	90
6l	1.5	57	5.0	92

Methods

General procedure for 3d–i/4d–i: The hydrazine hydrate (0.012 mol) was added to a stirred solution of chalcone **1a–c/2a–c** (0.010 mol) in 5 ml of poly(ethylene glycol) (PEG 200) or formic acid (5 ml). The mixture was subjected to microwave heating at 80±5 °C (240 W) for several minutes, which after workup afforded the pyrazoline derivatives **3d–i/4d–i**. The crude products after crystallization using absolute ethanol gave the pure compounds in 80–95 % yield.

3-[3-(4,5-Dihydro-5-phenyl-1H-pyrazol-3-yl)phenyl]sydnone (3d): pale yellow crystals, m.p. 170–171 °C. Anal. Calcd. for C₁₇H₁₄N₄O₂: C, 66.66; H, 4.58; N, 18.30. Found: C, 66.60 H, 4.52, N, 18.28. IR (KBr, cm⁻¹): 3400, 3103, 1715, 1599. ¹H-NMR (300 MHz, CDCl₃, δ , ppm): 3.40 (1H, *dd*, C₄–H_b), 3.75 (1H, *dd*, C₄–H_a), 4.85 (1H, *dd*, C₅–H_x), 5.20 (1H, *s*, NH), 6.75 (1H, *s*, C₄–H), 6.9–7.8 (8H, *bm*, Ar–H), 7.98 (1H, *s*, C₂–Ar–H). MS (*m/z* (relative abundance, %)): 306 (M⁺, 55), 276 (32), 248 (45), 221 (100), 144 (90), 77 (55).

3-[3-(4,5-Dihydro-5-p-tolyl-1H-pyrazol-3-yl)phenyl]sydnone (3e): pale yellow crystals, m.p. 154–155 °C. Anal. Calcd. for C₁₈H₁₆N₄O₂: C, 67.50; H, 5.00; N, 17.50. Found: C, 67.45 H, 4.96, N, 17.46. IR (KBr, cm⁻¹): 3410, 3100, 1724, 1595. ¹H-NMR (300 MHz, CDCl₃, δ , ppm): 2.10 (3H, *s*, CH₃), 3.15 (1H, *dd*, C₄–H_b), 3.60 (1H, *dd*, C₄–H_a), 4.90 (1H, *dd*, C₅–H_x), 5.05 (1H, *s*, NH), 6.60 (1H, *s*, C₄–H), 7.0–7.75 (7H, *bm*, Ar–H), 8.05 (1H, *s*, C₂–Ar–H). MS (*m/z* (relative abundance, %)): 320 (M⁺, 64), 290 (40), 262 (50), 235 (100), 144 (82), 91 (50).

3-[3-(5-p-Anisyl-4,5-dihydro-1H-pyrazol-3-yl)phenyl]sydnone (3f): yellow crystals, m.p. 184–190 °C. Anal. Calcd. for C₁₈H₁₆N₄O₃: C, 64.29; H, 4.76; N, 16.66. Found: C, 64.23, H, 4.71, N, 16.62. IR (KBr, cm⁻¹): 3400, 3110, 1730, 1600. ¹H-NMR (300 MHz, CDCl₃, δ , ppm): 3.05 (1H, *dd*, C₄–H_b), 3.30 (1H, *dd*, C₄–H_a), 3.75 (3H, *s*, –OCH₃), 4.74 (1H, *dd*, C₅–H_x), 5.50 (1H, *s*, NH), 6.85 (1H, *s*, C₄–H), 7.15–7.90 (7H, *bm*, Ar–H), 7.95 (1H, *s*, C₂–Ar–H). MS (*m/z* (relative abundance, %)): 336 (M⁺, 70), 309 (45), 281 (49), 254 (100), 144 (85), 107 (47).

3-[3-(1-Formyl-4,5-dihydro-5-phenyl-1H-pyrazol-3-yl)phenyl]sydnone (3g): yellow crystals, m.p. 108–109 °C. Anal. Calcd. for C₁₈H₁₄N₄O₃: C, 64.67; H, 4.19; N, 14.67. Found: C, 64.65, H, 4.14, N, 16.72. IR (KBr, cm⁻¹): 3138, 1745, 1600, 1580. ¹H-NMR (300 MHz, CDCl₃,

δ , ppm): 3.18 (1H, *dd*, C₄-H_b), 3.39 (1H, *dd*, C₄-H_a), 4.45 (1H, *dd*, C₅-H_x), 6.70 (1H, *s*, C₄-H), 6.78–7.40 (8H, *bm*, Ar-H), 7.75 (1H, *s*, C₂-Ar-H), 8.9 (1H, *s*, -CHO); MS (*m/z* (relative abundance, %)): 334 (M⁺, 75), 306 (64), 276 (49), 248 (100), 221 (14), 144 (58), 77 (50).

3-[3-(1-Formyl-4,5-dihydro-5-p-tolyl-1H-pyrazol-3-yl)phenyl]sydnone (3h): yellow crystals, m.p. 184–185 °C. Anal. Calcd. for C₁₉H₁₆N₄O₃: C, 65.52; H, 4.60; N, 16.09. Found: C, 65.47, H, 4.54, N, 16.06. IR (KBr, cm⁻¹): 3145, 1737, 1605, 1610. ¹H-NMR (300 MHz, CDCl₃, δ , ppm): 2.4 (3H, *s*, CH₃), 3.05 (1H, *dd*, C₄-H_b), 3.45 (1H, *dd*, C₄-H_a), 4.75 (1H, *dd*, C₅-H_x), 6.70 (1H, *s*, C₄-H), 6.85–7.35 (7H, *bm*, Ar-H), 8.0 (1H, *s*, C₂-Ar-H), 9.0 (1H, *s*, -CHO); MS (*m/z* (relative abundance, %)): 350 (M⁺, 42), 322 (63), 292 (34), 264 (100), 144 (90), 107 (40).

3-[3-(5-p-Anisyl-1-formyl-4,5-dihydro-1H-pyrazol-3-yl)phenyl]sydnone (3i): yellow crystals, m.p. 201–202 °C. Anal. Calcd. for C₁₉H₁₆N₄O₃: C, 62.64; H, 4.40; N, 15.38. Found: C, 62.61, H, 4.38, N, 15.36. IR (KBr, cm⁻¹): 3132, 1740, 1585, 1595. ¹H-NMR (300 MHz, CDCl₃, δ , ppm): 3.20 (1H, *dd*, C₄-H_b), 3.49 (1H, *dd*, C₄-H_a), 3.74 (3H, *s*, -OCH₃), 4.60 (1H, *dd*, C₅-H_x), 6.78 (1H, *s*, C₄-H), 6.90–7.45 (7H, *bm*, Ar-H), 7.90 (1H, *s*, C₂-Ar-H), 10.0 (1H, *s*, -CHO). MS (*m/z* (relative abundance, %)): 366 (M⁺, 39), 338 (60), 308 (54), 280 (100), 144 (87), 107 (44).

3-[4-(4,5-Dihydro-5-phenyl-1H-pyrazol-3-yl)phenyl]sydnone (4d): yellow crystals, m.p. 160–161 °C. Anal. Calcd. for C₁₇H₁₄N₄O₂: C, 66.66; H, 4.58; N, 18.30. Found: C, 66.65 H, 4.54, N, 18.30. IR (KBr, cm⁻¹): 3395, 3114, 1730, 1600. ¹H-NMR (300 MHz, CDCl₃, δ , ppm): 3.24 (1H, *dd*, C₄-H_b), 3.45 (1H, *dd*, C₄-H_a), 4.62 (1H, *dd*, C₅-H_x), 5.15 (1H, *s*, NH), 6.50 (1H, *s*, C₄-H), 6.75–7.27 (9H, *bm*, Ar-H). MS (*m/z* (relative abundance, %)): 306 (M⁺, 62), 145 (24), 131 (26), 117 (100), 103 (15), 90 (50), 67 (75).

3-[4-(4,5-Dihydro-5-p-tolyl-1H-pyrazol-3-yl)phenyl]sydnone (4e): yellow crystals, m.p. 178–179 °C. Anal. Calcd. for C₁₈H₁₆N₄O₂: C, 67.50; H, 5.00; N, 17.50. Found: C, 67.48 H, 5.05, N, 17.55. IR (KBr, cm⁻¹): 3096, 1725, 1605. ¹H-NMR (300 MHz, CDCl₃, δ , ppm): 2.23 (3H, *s*, CH₃), 3.20 (1H, *dd*, C₄-H_b), 3.39 (1H, *dd*, C₄-H_a), 4.60 (1H, *dd*, C₅-H_x), 5.0 (1H, *s*, NH), 6.54 (1H, *s*, C₄-H), 6.70–7.25 (8H, *bm*, Ar-H); MS (*m/z* (relative abundance, %)): 320 (M⁺, 64), 159 (28), 132 (100), 105 (19), 103 (50), 67 (75), 40 (13).

3-[4-(5-p-Anisyl-4,5-dihydro-1H-pyrazol-3-yl)phenyl]sydnone (4f): yellow crystals, m.p. 127–128 °C. Anal. Calcd. for C₁₈H₁₆N₄O₃: C, 64.29; H, 4.76; N, 16.66. Found: C, 64.30, H, 4.75, N, 16.67. IR (KBr, cm⁻¹): 3100, 1730, 1600. ¹H-NMR (300 MHz, CDCl₃, δ , ppm): 3.18 (1H, *dd*, C₄-H_b), 3.25 (1H, *dd*, C₄-H_a), 3.80 (3H, *s*, -OCH₃), 4.75 (1H, *dd*, C₅-H_x), 4.95 (1H, *s*, NH), 6.60 (1H, *s*, C₄-H), 6.65–7.64 (8H, *bm*, Ar-H); MS (*m/z* (relative abundance, %)): 336 (M⁺, 65), 175 (35), 148 (100), 131 (32), 121 (22), 103 (54).

3-[4-(1-Formyl-4,5-dihydro-5-phenyl-1H-pyrazol-3-yl)phenyl]sydnone (4g): yellow crystals, m.p. 140–141 °C. Anal. Calcd. for C₁₈H₁₄N₄O₃: C, 64.67; H, 4.19; N, 16.76. Found: C, 64.60, H, 4.17, N, 16.78. IR (KBr, cm⁻¹): 3100, 1725, 1605, 1595. ¹H-NMR (300 MHz, CDCl₃, δ , ppm): 3.16 (1H, *dd*, C₄-H_b), 3.35 (1H, *dd*, C₄-H_a), 4.57 (1H, *dd*, C₅-H_x), 6.70 (1H, *s*, C₄-H), 6.9–7.40 (8H, *bm*, Ar-H), 10.50 (1H, *s*, -CHO); MS (*m/z* (relative abundance, %)): 334 (M⁺, 21), 306 (47), 145 (25), 131 (30), 117 (100), 103 (46), 95 (15), 90 (43), 67 (14), 29 (44), 40 (5).

3-[4-(1-Formyl-4,5-dihydro-5-p-tolyl-1H-pyrazol-3-yl)phenyl]sydnone (4h): yellow crystals, m.p. 161–162 °C. Anal. Calcd. for C₁₉H₁₆N₄O₃: C, 65.52; H, 4.60; N, 16.09. Found: C, 65.54, H, 4.61, N, 16.13. IR (KBr, cm⁻¹): 3110, 1725, 1610, 1625. ¹H-NMR (300 MHz, CDCl₃, δ , ppm): 2.34 (3H, *s*, CH₃), 3.12 (1H, *dd*, C₄-H_b), 3.47 (1H, *dd*, C₄-H_a), 4.80 (1H, *dd*, C₅-H_x), 6.54 (1H, *s*, C₄-H), 6.67–7.40 (8H, *bm*, Ar-H) 9.5 (1H, *s*, -CHO); MS (*m/z* (relative abundance, %)): 350 (M⁺, 52), 322 (28), 159 (16), 131 (100), 104 (6), 67 (20), 40 (7), 29 (10).

3-[4-(5-p-Anisyl-1-formyl-4,5-dihydro-1H-pyrazol-3-yl)phenyl]sydnone (**4i**): yellow crystals, m.p. 154–155 °C. Anal. Calcd. for C₁₉H₁₆N₄O₃: C, 62.64; H, 4.40; N, 15.38. Found: C, 62.61, H, 4.38, N, 15.36. IR (KBr, cm⁻¹): 3127, 1732, 1597, 1620. ¹H-NMR (300 MHz, CDCl₃, δ, ppm): 3.18 (1H, *dd*, C₄-H_b), 3.35 (1H, *dd*, C₄-H_a), 3.90 (3H, *s*, -OCH₃), 4.45 (1H, *dd*, C₅-H_x), 6.85 (1H, *s*, C₄-H), 7.0–7.57 (8H, *bm*, Ar-H), 10.5 (1H, *s*, -CHO); MS (*m/z* (relative abundance, %)): 366 (M⁺, 34), 338 (24), 177 (15), 131 (87), 150 (100), 123 (7), 67 (18), 40 (8), 29 (11).

General procedure for the synthesis of 5g-I/6g-I: A solution of bromine (0.011 mol) in 5 ml of acetic anhydride was added to the compound **3d-i/4d-i** (0.010 mol) in 5 ml of acetic anhydride at 0–5 °C over 30 min. The mixture was subjected to microwave heating at 60±5 °C (210 W) until the evolution of carbon dioxide fumes had ceased and then allowed to attain room temperature. The reaction mixture was poured into ice water and filtered. The crude product was filtered and crystallized using hot methanol to obtain pale yellow crystals of **5g-I/6g-I** in 90–95 % yield.

3-[3-(1-Formyl-4,5-dihydro-5-phenyl-1H-pyrazol-3-yl)phenyl]-5-methyl-1,3,4-oxadiazol-2(3H)-one (**5g**): pale yellow crystals, m.p. 111–112 °C. Anal. Calcd. for C₁₉H₁₆N₄O₃: C, 65.52; H, 4.60; N, 16.09. Found: C, 65.48; H, 4.58, N, 16.05. IR (KBr, cm⁻¹): 1775, 1652, 1599. ¹H-NMR (300 MHz, CDCl₃, δ, ppm): 1.94 (3H, *s*, C₅-CH₃), 3.10 (1H, *dd*, C₄-H_b), 4.1 (1H, *dd*, C₄-H_a), 5.5 (1H, *dd*, C₅-H_x), 7.2–8.1 (9H, *bm*, Ar-H), 8.2 (1H, *s*, C₂-Ar-H), 9.0 (1H, *s*, -CHO); MS (*m/z* (relative abundance, %)): 348 (M⁺, 67), 277 (63), 117 (100), 105 (22), 90 (67), 43 (23).

3-[3-(1-Formyl-4,5-dihydro-5-p-tolyl-1H-pyrazol-3-yl)phenyl]-5-methyl-1,3,4-oxadiazol-2(3H)-one (**5h**): pale yellow crystals, m.p. 165–166 °C. Anal. Calcd. for C₂₀H₁₈N₄O₃: C, 66.30; H, 4.97; N, 15.46. Found: C, 66.27; H, 4.92, N, 15.42. IR (KBr, cm⁻¹): 1773, 1640, 1585. ¹H-NMR (300 MHz, CDCl₃, δ, ppm): 2.0 (3H, *s*, C₅-CH₃), 2.4 (3H, *s*, Ph-CH₃), 3.05 (1H, *dd*, C₄-H_b), 4.0 (1H, *dd*, C₄-H_a), 5.4 (1H, *dd*, C₅-H_x), 7.0–7.9 (8H, *bm*, Ar-H), 8.0 (1H, *s*, C₂-Ar-H), 8.9 (1H, *s*, -CHO). MS (*m/z* (relative abundance, %)): 362 (M⁺, 74), 291 (65), 131 (100), 105 (20), 104 (87), 90 (67), 77 (12), 43 (23).

3-[3-(5-p-Anisyl-1-formyl-4,5-dihydro-1H-pyrazol-3-yl)phenyl]-5-methyl-1,3,4-oxadiazol-2(3H)-one (**5i**): yellow crystals, m.p. 215–216 °C. Anal. Calcd. for C₂₀H₁₈N₄O₄: C, 63.49; H, 4.76; N, 14.81. Found: C, 63.45; H, 4.74, N, 14.79. IR (KBr, cm⁻¹): 1765, 1645, 1599. ¹H-NMR (300 MHz, CDCl₃, δ, ppm): 2.20 (3H, *s*, CH₃), 3.0 (1H, *dd*, C₄-H_b), 3.80 (1H, *dd*, C₄-H_a), 5.0 (1H, *dd*, C₅-H_x), 6.90–7.60 (8H, *bm*, Ar-H), 7.89 (1H, *s*, C₂-Ar-H), 9.0 (1H, *s*, -CHO); MS (*m/z* (relative abundance, %)): 378 (M⁺, 42), 307 (65), 147 (100), 120 (78), 105 (20), 104 (87), 90 (68), 43 (20).

3-[3-(1-Acetyl-4,5-dihydro-5-phenyl-1H-pyrazol-3-yl)phenyl]-5-methyl-1,3,4-oxadiazol-2(3H)-one (**5j**): pale yellow crystals, m.p. 301–302 °C. Anal. Calcd. for C₂₀H₁₈N₄O₃: C, 66.29; H, 4.97; N, 15.46. Found: C, 66.25; H, 4.95, N, 15.42; IR (KBr, cm⁻¹): 1765, 1648, 1600. ¹H-NMR (300 MHz, CDCl₃, δ, ppm): 2.15 (3H, *s*, C₅-CH₃), 2.62 (3H, *s*, COCH₃), 3.4 (1H, *dd*, C₄-H_b), 3.9 (1H, *dd*, C₄-H_a), 5.0 (1H, *dd*, C₅-H_x), 6.95–7.8 (9H, *bm*, Ar-H), 7.85 (1H, *s*, C₂-Ar-H), 10.0 (1H, *s*, -CHO); MS (*m/z* (relative abundance, %)): 362 (M⁺, 66), 291 (47), 263 (23), 117 (100), 105 (24), 90 (50), 43 (45).

3-[3-(1-Acetyl-4,5-dihydro-5-p-tolyl-1H-pyrazol-3-yl)phenyl]-5-methyl-1,3,4-oxadiazol-2(3H)-one (**5k**): pale yellow crystals, m.p. 181–182 °C. Anal. Calcd. for C₂₁H₂₀N₄O₃: C, 67.02; H, 5.32; N, 14.89. Found: C, 67.00; H, 5.29, N, 14.85. IR (KBr, cm⁻¹): 1770, 1655, 1605. ¹H-NMR (300 MHz, CDCl₃, δ, ppm): 2.12 (3H, *s*, C₅-CH₃), 2.4 (3H, *s*, Ph-CH₃), 2.50 (3H, *s*, COCH₃), 3.12 (1H, *dd*, C₄-H_b), 3.8 (1H, *dd*, C₄-H_a), 4.57 (1H, *dd*, C₅-H_x), 7.05–7.75 (8H, *bm*, Ar-H), 7.9 (1H, *s*, C₂-Ar-H), 9.7 (1H, *s*, -CHO). MS (*m/z* (relative abundance, %)): 376 (M⁺, 58), 348 (25), 305 (28), 131 (100), 105 (39), 43 (28).

3-[3-(1-acetyl-5-p-anisyl-4,5-dihydro-1H-pyrazol-3-yl)phenyl]-5-methyl-1,3,4-oxadiazol-2(3H)-one (**5l**): yellow crystals, m.p. 224–225 °C. Anal. Calcd. for C₂₁H₂₀N₄O₄: C, 64.28; H, 5.10; N, 14.28. Found: C, 64.25; H, 5.07, N, 14.25. IR (KBr, cm⁻¹): 1762, 1648, 1592. ¹H-NMR (300 MHz, CDCl₃, δ, ppm): 2.15 (3H, s, C₅-CH₃), 2.36 (3H, s, COCH₃), 3.30 (1H, dd, C₄-H_b), 3.67 (3H, s, OCH₃), 3.85 (1H, dd, C₄-H_a), 4.85 (1H, dd, C₅-H_x), 6.82–7.70 (8H, bm, Ar-H), 7.90 (1H, s, C₂-Ar-H), 10.05 (1H, s, -CHO); MS (*m/z* (relative abundance, %)): 392 (M⁺, 20), 364 (45), 321 (30), 147 (100), 120 (58), 105 (42).

3-[4-(1-Formyl-4,5-dihydro-5-phenyl-1H-pyrazol-3-yl)phenyl]-5-methyl-1,3,4-oxadiazol-2(3H)-one (**6g**): pale yellow crystals, m.p. 185–186 °C. Anal. Calcd. for C₁₉H₁₆N₄O₃: C, 65.52; H, 4.60; N, 16.09. Found: C, 65.51; H, 4.56, N, 16.10. IR (KBr, cm⁻¹): 1772, 1648, 1603. ¹H-NMR (300 MHz, CDCl₃, δ, ppm): 1.9 (3H, s, C₅-CH₃), 3.25 (1H, dd, C₄-H_b), 3.96 (1H, dd, C₄-H_a), 4.98 (1H, dd, C₅-H_x), 7.0–8.4 (9H, bm, Ar-H), 10.0 (1H, s, -CHO); MS (*m/z* (relative abundance, %)): 348 (M⁺, 46), 305 (37), 130 (58), 103 (100), 90 (67), 29 (15).

3-[4-(1-Formyl-4,5-dihydro-5-p-tolyl-1H-pyrazol-3-yl)phenyl]-5-methyl-1,3,4-oxadiazol-2(3H)-one (**6h**): pale yellow crystals, m.p. 220–221 °C. Anal. Calcd. for C₂₀H₁₈N₄O₃: C, 66.30; H, 4.97; N, 15.46. Found: C, 66.35; H, 5.00, N, 15.44. IR (KBr, cm⁻¹): 1765, 1635, 1602. ¹H-NMR (300 MHz, CDCl₃, δ, ppm): 1.99 (3H, s, C₅-CH₃), 2.47 (3H, s, Ph-CH₃), 3.24 (1H, dd, C₄-H_b), 3.65 (1H, dd, C₄-H_a), 5.0 (1H, dd, C₅-H_x), 6.95–7.45 (8H, bm, Ar-H), 9.0 (1H, s, -CHO); MS (*m/z* (relative abundance, %)): 362 (M⁺, 63), 319 (33), 144 (100), 117 (60), 104 (21), 29 (17).

3-[4-(5-p-Anisyl-1-formyl-4,5-dihydro-1H-pyrazol-3-yl)phenyl]-5-methyl-1,3,4-oxadiazol-2(3H)-one (**6i**): yellow crystals, m.p. 148–149 °C. Anal. Calcd. for C₂₀H₁₈N₄O₄: C, 63.49; H, 4.76; N, 14.81. Found: C, 63.48; H, 4.77, N, 14.80. IR (KBr, cm⁻¹): 1780, 1655, 1588. ¹H-NMR (300 MHz, CDCl₃, δ, ppm): 2.06 (3H, s, C₅-CH₃), 3.52 (1H, dd, C₄-H_b), 3.74 (3H, s, -OCH₃), 3.95 (1H, dd, C₄-H_a), 5.0 (1H, dd, C₅-H_x), 6.95–7.52 (8H, bm, Ar-H), 9.3 (1H, s, -CHO); MS (*m/z* (relative abundance, %)): 378 (M⁺, 52), 335 (77), 160 (94), 133 (100), 120 (21), 29 (14).

3-[4-(1-Acetyl-4,5-dihydro-5-phenyl-1H-pyrazol-3-yl)phenyl]-5-methyl-1,3,4-oxadiazol-2(3H)-one (**6j**): pale yellow crystals, m.p. 170–171 °C. Anal. Calcd. for C₂₀H₁₈N₄O₃: C, 66.29; H, 4.97; N, 15.46. Found: C, 66.30; H, 4.90, N, 15.50. IR (KBr, cm⁻¹): 1774, 1657, 1606. ¹H-NMR (300 MHz, CDCl₃, δ, ppm): 1.98 (3H, s, CH₃), 2.43 (3H, s, COCH₃), 3.26 (1H, dd, C₄-H_b), 3.87 (1H, dd, C₄-H_a), 4.98 (1H, dd, C₅-H_x), 6.97–7.72 (9H, bm, Ar-H), 10.4 (1H, s, -CHO). MS (*m/z* (relative abundance, %)): 362 (M⁺, 67), 320 (54), 187 (100), 144 (90), 90 (45), 43 (56).

3-[4-(1-Acetyl-4,5-dihydro-5-p-tolyl-1H-pyrazol-3-yl)phenyl]-5-methyl-1,3,4-oxadiazol-2(3H)-one (**6k**): pale yellow crystals, m.p. 218–219 °C. Anal. Calcd. for C₂₁H₂₀N₄O₃: C, 67.02; H, 5.32; N, 14.89. Found: C, 67.00; H, 5.29, N, 14.85. IR (KBr, cm⁻¹): 1785, 1637, 1584. ¹H-NMR (300 MHz, CDCl₃, δ, ppm): 2.0 (3H, s, C₅-CH₃), 2.30 (3H, s, Ph-CH₃), 2.47 (3H, s, COCH₃), 3.12 (1H, dd, C₄-H_b), 3.8 (1H, dd, C₄-H_a), 4.57 (1H, dd, C₅-H_x), 7.05–7.75 (8H, bm, Ar-H), 7.9 (1H, s, C₂-Ar-H), 9.7 (1H, s, -CHO); MS (*m/z* (relative abundance, %)): 376 (M⁺, 40), 334 (50), 201 (100), 174 (88), 104 (14), 43 (11).

3-[4-(1-Acetyl-5-p-anisyl-4,5-dihydro-1H-pyrazol-3-yl)phenyl]-5-methyl-1,3,4-oxadiazol-2(3H)-one (**6l**): yellow crystals, m.p. 162–163 °C. Anal. Calcd. for C₂₁H₂₀N₄O₄: C, 64.28; H, 5.10; N, 14.28. Found: C, 64.27; H, 5.12, N, 14.32. IR (KBr, cm⁻¹): 1762, 1648, 1592. ¹H-NMR (300 MHz, CDCl₃, δ, ppm): 2.15 (3H, s, C₅-CH₃), 2.55 (3H, s, COCH₃), 3.30 (1H, dd, C₄-H_b), 3.64 (3H, s, -OCH₃), 3.94 (1H, dd, C₄-H_a), 5.12 (1H, dd, C₅-H_x), 6.80–7.54 (8H, bm, Ar-H), 9.45. (1H, s, -CHO); MS (*m/z* (relative abundance, %)): 392 (M⁺, 66), 350 (48), 217 (100), 147 (75), 120 (64), 43 (10).

CONCLUSION

This work demonstrated a rapid, efficient and environmentally friendly method of synthesis of bisheterocycles containing sydnone and 1,3,4-oxadiazole derivatized with pyrazoline under microwave heating. The method is convenient, inexpensive with good yields and is useful for the synthesis the bioactive molecules. The pharmacological assay of the newly synthesized molecules is in progress.

Acknowledgements. One of the authors (RRK) wishes to acknowledge the financial support of the University of Mysore and to the Principal, Yuvaraja's College, Mysore for the laboratory facilities. In addition, the authors would like to thank USIC, University of Mysore, for performing the spectral analyses.

ИЗВОД

ЕФИКАСНА СИНТЕЗА 1,3,4-ОКСАДИАЗОЛСКИХ ДЕРИВАТА ПРЕКО СИДНОНА

RAVINDRA R. KAMBLE, B. S. SUDHA и D. G. BHADREGOWDA

Department of Chemistry and Food Science, Yuvaraja's College, University of Mysore, Mysore – 570 005, India

Чистом циклизацијом халкона **1a-c/2a-c** са хидразин-хидратом под дејством микро-таласног зрачења добијени су пиразолини **3d-i/4d-i** дериватизовани сидноном. 1,3-Диполарном циклоадицијом са анхидридом сирћетне киселине граде се пиразолини **5g-l/6g-l** који садрже 1,3,4-оксадиазолски фрагмент. Структура ових једињења потврђена је на основу спектралних података и елементалне анализе. У поређењу са стандардним загревањем, добијени резултати указују на то да се микро-таланим зрачењем, у реакцијама које су чистије, постиже већи принос, уз краће реакционо време (4–12 min).

(Примљено 21. јуна, ревидирано 1. августа 2007)

REFERENCES

1. C. V. Yelamagad, U. S. Hiremath, B. V. Badami, *Indian J. Chem.* **33B** (1994) 674
2. B. M. Patil, B. V. Badami, G. S. Puranik, *Indian Drugs* **32** (1995) 439
3. J. R. Kavali, B. V. Badami, *Farmaco* **55** (2000) 406
4. J. R. Kavali, B. V. Badami, *J. Chem. Res.* (2000) 546
5. K. Mogliah, D. S. Chowdary R. B. Rao, *Indian J. Chem.* **40B** (2001) 43
6. V. R. Shah, M. Vadodaria, A. R. Parikh, *Indian J. Chem.* **36B** (1997) 100
7. K. Ladva, P. Patel, P. Upadhyay, H. Parekh, *Indian J. Chem.* **35B** (1996) 1062
8. X. W. Su, X. P. Hui, C. H. Chu, Z. Y. Zhang, *Indian J. Chem.* **40B** (2001) 15
9. E. C. Taylor, H. Patel, H. Kumar, *Tetrahedron* **48** (1992) 8089
10. S. G. Roelfvan, C. Arnold, K. Wellnga, *J. Agric. Food Chem.* **84** (1979) 406
11. G. H. Keats, GB 1,209,631 (1970)
12. R. M. Kedar, N. N. Vidhale, M. M. Chincholkar, *Orient. J. Chem.* **13** (1997) 143
13. A. Singh, S. Rathod, B. N. Berad, S. D. Patil, A. G. Dosh, *Orient. J. Chem.* **16** (2000) 315
14. H. Z. Katri, S. A. Vunii, *J. Indian Chem. Soc.* **58** (1981) 168
15. N. B. Das, A. S. Mitra, *Indian J. Chem.* **16B** (1978) 638
16. D. Azarifar, M. Shaebanzadeh, *Molecules* **7** (2002) 885
17. B. Shivarama Holla, P. M. Akberali, M. K. Shivananda, *Farmaco* **55** (2000) 256
18. E. Palaska, M. Aytemir, I. Tayfun, K. Erol, E. Dilek, *Eur. J. Med. Chem. Chim. Ther.* **36** (2001) 539

19. H. G. Garge, Chandraprakash, *J. Pharm. Sci.* **14** (1971) 649
20. H. A. Regaila, A. K. El-Bayonk, M. Hammad, *Egypt. J. Chem.* **20** (1979) 197
21. R. Krishna, B. R. Pande, S. P. Bharthwal, S. S. Parmar, *Eur. J. Med. Chem.* **15** (1980) 567
22. M. I. Husain, S. Shukla, *Indian J. Chem.* **25B** (1986) 983
23. R. R. Kamble, B. S. Sudha, *Indian J. Pharm. Sci.* **68** (2006) 249
24. R. R. Kamble, S. B. Sudha, *J. Serb. Chem. Soc.* **71** (2006) 331
25. Conventional method was done according to the report; R. R. Kamble, *Ph.D. Thesis*, Karnatak University, Dharwad, India, 2001, p. 122
26. R. J. Giguere, T. L. Bray, S. M. Duncan, *Tetrahedron Lett.* **27** (1986) 4949.



www.shd.org.yu

J. Serb. Chem. Soc. 73 (2) 139–145 (2008)

JSCS–3696

JSCS@tmf.bg.ac.yu • www.shd.org.yu/JSCS

UDC 662.237.3:66–95:579.23:579.67

Original scientific paper

Recombinant expression of monovalent and bivalent anti-TNT-antibodies – evaluation of different expression systems

MLADEN SIMONOVIĆ^{1*}, SVETLANA ZLATANOVIĆ-MILOŠEVIĆ²,
MIROSLAV M. VRVIĆ^{3#} and BRANISLAV SIMONOVIĆ¹

¹Institute for General and Physical Chemistry, Studentski trg 12–16, 11000 Belgrade, ²Faculty of Mathematics and Natural Sciences, University of Kragujevac, Radoja Domanovića 12, 34000 Kragujevac and ³Faculty of Chemistry, University of Belgrade, Studentski trg 12–16, 11000 Belgrade, Serbia

(Received 7 February, revised 2 July 2007)

Abstract: Monoclonal 11B3 anti-TNT (trinitrotoluene) antibody was expressed as a monovalent and bivalent form using different prokaryotic and eukaryotic expression systems. Recombinant expression in *Escherichia coli*, mammalian cells and the methylotrophic yeast *Pichia pastoris* was performed to obtain disulfide-linked and glycosylated antibody forms. The generation of antibody and subsequent evaluation of the expression rates were performed using intracellular, excretory and periplasmic expression techniques. All methods involved striving for native expressed antibody with maintenance of its functionality only.

Keywords: TNT; antibody; recombinant expression; 11B3; scFv.

INTRODUCTION

For protein production in the laboratory, the most suitable prokaryotic system is the gram-negative bacterium *Escherichia coli* because of its rapid growth in high cell densities, easy generic and availability of a large number of vector systems. The first demonstrated expression of functional fragments of antibodies was for *E. coli* in prokaryotic periplasma. The secretion in periplasma was forced by genetic fusion of antibody fragments with a signal sequence of some periplasmic protein.^{1,2} The building of disulfide bridges is ensured through the oxidative nature of the periplasmic compartment.³

Protein expression without a signal sequence results in it remaining in the cytoplasm. Native isolation with ultrasound is possible if the protein is soluble in the cytoplasm. It has to be considered that cytoplasm is not an oxidative compartment, and hence the actual protein must go through redox active systems to achieve its functionality.

* Corresponding author. E-mail: mladen@iofh.bg.ac.yu

Serbian Chemical Society member.

doi: 10.2298/JSC0802139S

In addition to *E. coli*, other organisms can be used in which antibody fragments were successfully expressed and partially secreted into the medium, which is an enormous advantage for preparative and commercial expression. For easier laboratory expressions, each organism should be matched with *E. coli* regarding its ease of handling and diversity of possibilities.

In yeasts, the eukaryotic folding and post-translational modifications are merged through simple cultivation. The methylotrophic species *Pichia pastoris* can metabolize methanol as the only carbon source and also secrete and process recombinant proteins.^{4,5} The high yields and functionality of the secreted recombinant immunoglobulins underline the importance of yeasts for this application. For scFv (single chain fragment variable) molecules, yields of over 100 mg l⁻¹ were obtained, which exceed the expression in *E. coli* by more than hundred times.⁶

Without doubt, the usage of mammalian cells (COS, CHO, HEK, *etc.*) is the most suitable approach for expression of recombinant proteins. The problems with post-translational modifications are thereby almost excluded. The conversion of antibody fragments into complete immunoglobulins of different isotypes and their expression in mammalian cells have been demonstrated many times with no loss of binding activity.⁷⁻¹⁰

The use of recombinant antibody has significant advantages compared with conventional antibody and its use has become more popular nowadays due to the fact that no animals are required in the manufacturing procedure of the recombinant antibodies. In addition, the manufacturing time is relatively short compared with the conventional method. Moreover, the quality of the final products is higher than those manufactured by the non-recombinant method.

In this work, recombinant antibodies specific for TNT were expressed in mono- and bi-valent format in different expression systems. The aim of the work was, on the one hand, to examine the expression efficiency in prokaryotic and eukaryotic systems and, on the other, to use these antibodies for the detection of TNT and its derivatives. The best expressing system should then be used for the commercial production of the most sensitive antibody format for TNT detection.

EXPERIMENTAL

Vectors

The vectors pcDNA3.1+ and pPICZ α -ABC for eukaryotic expression in mammalian cells and yeast *Pichia pastoris* were commercially purchased from Invitrogen Life Technologies (Karlsruhe, Germany). The *E. coli* expression vector pET26b(+) was purchased from Novagen (Schwalbach, Germany) and the phagemid-vector pHEN2 from G. Winter, Center of Protein Engineering, MRC Cambridge, UK.

Antibody fragments

The gene for the scFv-fragment 11B3 of mouse origin, as well as the genes for the C_H2 and C_H3 regions of human IgG was available.

Oligonucleotides

The employed oligonucleotides were synthesized by Metabion (Martinsried) (Table I).

TABLE I. Utilized oligonucleotides

Name	Sequence 5'-3'	Target region	Restriction sites
11B3 Bsi for	Gatccgtacgtgtgggatggcccaggtgaag	11B3-scFv	<i>Bsi</i> WI
11B3 Asc back	Gatcggcgcgccacctaggacggtcagcttg	11B3-scFv	<i>Asc</i> I
11B3 Sfi for (pPICZ α B)	Gatcggcccagccggccttatggcccaggtgaag	11B3-scFv	<i>Sfi</i> I
11B3 Nde for	Ggaattccatatggcccaggtgaagctg	11B3-scFv	<i>Nde</i> I
11B3 Not back (pET)	Attcttatgcgccgcccgtttatttcagctt	11B3-scFv	<i>Not</i> I

Standard molecular biology techniques

PCR, ligation, restriction, DNA dephosphorylation, agarose gel electrophoresis, DNA extraction from agarose gels, classic plasmid preparation, alcohol precipitation, DNA quantification, *etc.* were performed according to standard protocols.¹¹

Production of competent E. coli cells, transformation and expression

Electrocompetent *E. coli* cells, transformation, periplasmatic and intracellular expression were performed according to standard protocols.¹¹⁻¹³

Standard techniques in protein biochemistry

Immobilized metal ion affinity chromatography for protein purification using a Ni-NTA (nickel nitrilotriacetate) matrix, PAGE (polyacrylamide gel electrophoresis), protein determination, Western blot, dialysis, antibody purification *via* the Fc region using protein A/G-PLUS-agarose, *etc.* were generally performed according to standard protocols.¹¹

Eukaryotic expression in yeast and mammalia

Antibody expression in yeast *P. pastoris* and mammalia was performed according to standard protocols.^{11,14} For the expression in *P. pastoris*, the standard vector pPICZIgGscFv-Fc, which already contained an α -factor as a signal sequence and an expression cassette (C_{H2} and C_{H3} genes), was available. Using restriction sites *Sfi*I and *Asc*I, any scFv can be cloned into the cassette and a dimer IgG Δ C1, with constant C_{H2} and C_{H3} regions, is generated as the result of the expression.

For expression of the IgG Δ C1-dimer in mammalian cells, HEK (humane embryo kidney) cells were mostly used. The available vector was pcDNA3.1/Zeo, which contained a CMV promoter, a rat signal sequence, a gene for zeocine resistance and an expression cassette with the genes for the IgG domains C_{H2} and C_{H3} .

RESULTS

Starting from the TNT-specific scFv-fragment of mouse origin, named 11B3, monovalent and bivalent antibodies were generated. The fragment was produced in different formats, *i.e.*, it was expressed in a monovalent form as scFv and the scFv were further used for the generation of bivalent antibodies. In order to use the scFv in the bivalent form, the IgG Δ C1 constructs were made. To analyze the binding properties of antibodies, the free TNP-Tris (trinitrophenol-tris-(hydroxymethyl)aminomethane), as well as the TNP-protein conjugates were used.

Monovalent antibody 11B3-scFv

For the cloning and expression of the monovalent antibody, a vector pet26b(+) with a stronger T7-promoter was chosen, in which the amplified 11B3-scFv gene was inserted between the restriction sites *Nde*I and *Not*I. During the insertion, the signal sequence was removed, which meant a predisposition for intracellular expression in *E. coli* strain BL21 DE3. The expression was performed for 3 hours at 25 °C using the lactose analog IPTG (isopropyl- β -D-thiogalactopyranoside) as inducer. The protein was purified from the cytosol supernatant with a NiNTA-matrix and subsequently analyzed by SDS-PAGE and immunoblot. The band of 28 kDa on the membrane for the Western-blot confirmed the successful expression of the antibody (Fig. 1).

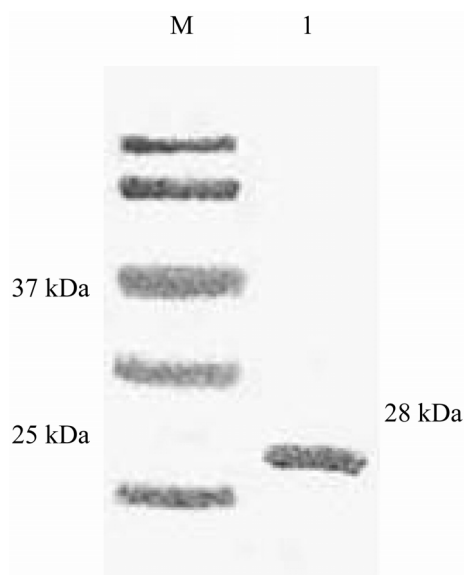


Fig. 1. Analysis of purified 11B3-scFv using immunoblot. 15 μ l of protein probe (1) was separated under reducing conditions on a 12 % SDS-gel together with 10 μ l of protein marker (M). The presence of protein was confirmed after transfer onto a PVDF-membrane and detection with murine anti-His-IgG-antibody (1: 2500) and anti-mouse-IgG-AP conjugate (1: 2500).

The determination of the protein concentration gave a value of 65 μ g/ml. The antibody was further biotinylated for usage in the TNP-assay.

Bivalent construct 11B3-IgG Δ C1

The bivalent construct 11B3-IgG Δ C1 is a synthetic molecule obtained after cloning the murine 11B3-gene in the expression cassette with constant C_H2 and C_H3 regions of the human gamma heavy chain. Expression of 11B3-IgG Δ C1 was performed parallel in two expression systems, *i.e.*, yeast *Pichia pastoris* and the human cell line HEK293.

Expression in human HEK293 cells

As the expression cassette, the vector pcDNA3.1 was available, which had a strong viral promoter and genes for the constant regions of the human gamma

heavy chain. The restriction sites *Bsi*I and *Asc*I were chosen for the cloning of the 11B3-gene. After ligation and transformation, characterization of the clones was performed with PCR. The obtained amplicates confirmed the cloning of the 11B3-scFv insert in the vector.

The recombinant DNA was further employed for the production of stable secreting cell lines. From *ca.* 300 ml expression supernatant, the antibody was purified using protein A-agarose and analyzed by Western blot (Fig. 2). The eluted amount of 4.5 ml gave a total protein quantity of about 410 μ g (90 μ g/ml); hence the expression rate for the 300 ml culture was about 1.37 μ g/ml. The purified protein was directly used in the assay for confirming its functionality. This immunocomponent proved to be very sensitive in the assay for detection of TNT-derivatives. Using 60 μ l of antibody solution at a concentration of 225 ng/ml, 25 fmol TNP-Tris was identified.



Fig. 2. Immunoblot of purified 11B3-IgG Δ C1. 10 μ l of protein marker (M) and 10 μ l of protein sample (1) were separated on a 7.5 % SDS-gel under non-reducing conditions. The presence of protein was verified after transfer onto a PVDF-membrane and detection with anti-human-IgG-AP conjugate (1:2500).

Expression in yeast

After ligation of scFv and transformation, the clones were controlled using PCR. One of the selected clones was chosen for inoculation of the overnight culture with zeocine and subsequently for DNA isolation. The isolated DNA was then linearized and inserted into yeast cells using electroporation.

After yeast electroporation with yeast DNA, a three-day-expression was performed with one of selected clones. A very small quantity of the protein was detected on a PVDF (poly(vinylidene difluoride)) membrane with anti-human-IgG (1:2500) conjugated with AP (alkaline phosphatase) or HRP (horseradish peroxidase). No protein was visualized on an SDS-gel. Accordingly, expression in HEK-cells was preferred.

DISCUSSION

Cloning and expression of recombinant immunoreagents

The bivalent 11B3-IgG Δ C1-construct was successfully expressed in the stable human embryo cell line HEK293. Deletion of the C_H1 region offered the advantage of a lower molecular weight, which contributed to the enhanced secretion. The high expression yield facilitated the purification of the 11B3-antibody on a protein A-matrix. The only problem with this antibody was the determination of its molecular weight, which was necessary for the precise determination of the protein concentration. According to the primary sequence, computer calculations gave a value of 104 kDa. An apparent appearance of these antibodies on an SDS-gel and Western blot was at about 130 kDa due to glycosylation. The functionality of this antibody and its binding properties were successfully verified in ELISA for detection of TNT-derivatives. According to these results, it can be concluded that this construct expressed in mammalian showed complete and correct folding and oxidation. Alternatively, 11B3-IgG Δ C1 was expressed in yeast cells but, due to low yields, this expression was not the subject of further investigations.

Monoclonal 11B3-scFv was expressed in two different systems. First, it was supposed to have been expressed under a Lac-promoter with a signal sequence, but this failed as the antibody was expressed mostly within inclusion bodies in the cytosol. It was further attempted to perform intracellular expression without a signal sequence under the stronger T7-promoter. This expression gave better antibody yields, which were about 0.5 μ g per ml of culture. For detection of monovalent antibodies in ELISA, biotinylation was performed in order to detect these antibodies with the streptavidine–HRP conjugate.

The reason for the bad expression efficiency can be a frequent presence of codons for some amino acids in the gene sequence.¹⁵ The origin of the scFv-gene can be the reason for the difference in expression efficiency. Another reason could be potential problems in the post-translational modifications or folding at 11B3-scFv.³ It could also be possible that more hydrophobic domains were formed in 11B3-scFv, whereby insolubility of the protein occurred. Some experiments concerning higher yields of expressed protein were performed under a lower temperature and IPTG concentration,¹⁶ but no improved expression was registered. Solubility enhancement of 11B3-scFv can be achieved by co-expression of bacterial chaperons¹⁶ or eukaryotic disulfide isomerases,¹⁷ which should be a future line of research. It has already been confirmed that the fusion of 11B3-scFv with the enzyme β -lactamase gave a higher expression rate than for the single antibody.

Acknowledgements. The experimental part of this study was performed at the University of Hamburg, Germany, under financial support of the German Academic Exchange Service. Special thanks to Prof. Dr. Reinhard Bredehorst and Dr. Edzard Spillner for constructive discussions and ideas during this project.

ИЗВОД

РЕКОМБИНАНТНА ЕКСПРЕСИЈА МОНОВАЛЕНТНИХ И БИВАЛЕНТНИХ АНТИ-
-ТНТ-АНТИТЕЛА – ЕВАЛУАЦИЈА РАЗЛИЧИТИХ ЕКСПРЕСИОНИХ СИСТЕМА

МЛАДЕН СИМОНОВИЋ¹, СВЕТЛАНА ЗЛАТАНОВИЋ-МИЛОШЕВИЋ²,
МИРОСЛАВ М. ВРВИЋ³ и БРАНИСЛАВ СИМОНОВИЋ¹

¹Институт за општу и физичку хемију, Студентски брџ 12–16, 11000 Београд, ²Природно-математички факултет, Универзитет у Крагујевцу, Радоја Домановића 12, 34000 Крагујевац и ³Хемијски факултет, Универзитет у Београду, Студентски брџ 12–16, 11000 Београд

Моноклонско 11В3 антители специфично за TNT (тринитротолуен) експримирано је у моновалентном и бивалентном облику користећи различите прокариотске и еукариотске експресионе системе. Рекombинантна експресија у *Escherichia coli*, ћелијама сисара и метило-трофном квасцу *Pichia pastoris* изведена је да би се добиле гликозиловане и дисулфидним мостовима везане форме антитела. Стварање антитела и евалуација приноса експресије изведени су применом техника интрацелуларне, екскреторне и периплазматске експресије. Све методе укључивале су тежњу за експресијом антитела искључиво у нативном облику што је очувало његову функционалност.

(Примљено 7. фебруара, ревидирано 2. јула 2007)

REFERENCES

1. A. Skerra, A. Pluckthun, *Science* **240** (1988) 1038
2. M. Better, C. P. Chang, R. R. Robinson, A. H. Horwitz, *Science* **240** (1988) 1041
3. R. Glockshuber, T. Schmidt, A. Pluckthun, *Biochemistry* **31** (1992) 1270
4. J. M. Cregg, T. S. Vedvick, W. C. Raschke, *Biotechnology (N.Y.)* **11** (1993) 905
5. C. A. Scorer, R. G. Buckholz, J. J. Clare, M. A. Romanos, *Gene* **136** (1993) 111
6. R. Ridder, R. Schmitz, F. Legay, H. Gram, *Biotechnology (N.Y.)* **13** (1995) 255
7. G. A. Huls, I. A. Heijnen, M. E. Cuomo, J. C. Koningsberger, L. Wiegman, E. Boel, A. R. van der Vuurst de Vries, S. A. Loyson, W. Helfrich, G. P. van Berge Henegouwen, M. van Meijer, J. de Kruif, T. Logtenberg, *Nat. Biotechnol.* **17** (1999) 276
8. L. Persic, A. Roberts, J. Wilton, A. Cattaneo, A. Bradbury, H. R. Hoogenboom, *Gene* **187** (1997) 9
9. L. Norderhaug, T. Olafsen, T. E. Michaelsen, I. Sandlie, *J. Immunol. Methods* **204** (1997) 77
10. E. Boel, S. Verlaan, M. J. Poppelier, N. A. Westerdaal, J. A. Van Strijp, T. Logtenberg, *J. Immunol. Methods* **239** (2000) 153
11. F. M. Ausubel, *Current protocols in molecular biology*, Wiley, New York, 1996
12. R. C. Sharma, R. T. Schimke, *Biotechniques* **20** (1996) 42
13. S. Fiedler, R. Wirth, *Anal. Biochem.* **170** (1988) 38
14. C. R. Wood, M. A. Boss, J. H. Kenten, J. E. Calvert, N. A. Roberts, J. S. Emtage, *Nature* **314** (1985) 446
15. J. Schaber, C. Rispe, J. Wernegreen, A. Bunes, F. Delmotte, F. J. Silva, A. Moya, *Gene* **352** (2005) 109
16. M. A. Heo, S. H. Kim, S. Y. Kim, Y. J. Kim, J. Chung, M. K. Oh, S. G. Lee, *Protein Expr. Purif.* **47** (2006) 203
17. M. Schlapschy, S. Grimm, A. Skerra, *Protein Eng. Des. Sel.* **19** (2006) 385.



www.shd.org.yu

J. Serb. Chem. Soc. 73 (2) 147–156 (2008)

JSCS–3697

Journal of
the Serbian
Chemical Society



JSCS@tmf.bg.ac.yu • www.shd.org.yu/JSCS

UDC 66.011+665.75.000.57.002.2:577.15

Original scientific paper

Optimization of the production of biodiesel by a commercial immobilized lipase in a solvent-free system using a response surface methodology

NEVENA OGNJANOVIĆ, DEJAN BEZBRADICA[#] and ZORICA KNEŽEVIĆ^{**}

Faculty of Technology and Metallurgy, Karnegijeva 4, 11000 Belgrade, Serbia

(Received 14 March, revised 2 July 2007)

Abstract: Response surface methodology was used for the evaluation of the effects of various factors on the synthesis of biodiesel catalyzed with immobilized lipase from *Rhizomucor miehei* in a solvent-free system. The production of biodiesel was optimized and model response equations were obtained, enabling the prediction of biodiesel production from the values of the four main factors. It would seem that the reaction temperature and the amount of water predominantly determined the conversion process while the methanol/oil molar ratio had no significant influence on the reaction rate. The temperature and amount of water showed negative interactive effects on the observed reaction rate per amount of enzyme. However, there were no significant interactions among the other variables according to the test of statistical significance. The highest yield of 10.15 mol kg⁻¹ enzyme was observed at 45 °C with a 6:1 methanol to oil molar ratio and with no added water in the system.

Keywords: lipases from *Rhizomucor miehei*; biodiesel; response surface methodology.

INTRODUCTION

Biodiesel (fatty acid methyl esters), used as alternative diesel engine fuel, has become increasingly important due to the diminishing petroleum reserves and the environmental consequences of exhaust gases from petroleum-fueled engines. Biodiesel has several advantages: it comes from renewable sources and, as such, it does not contribute to new carbon dioxide emission, it is biodegradable, its combustion products have reduced levels of particulates, carbon monoxide, sulfur oxides, hydrocarbons and soot.¹

Industrially, biodiesel is produced by the methanolysis of waste oil using alkaline catalysts.² There are several drawbacks to this conventional chemical production, such as the cost of the refined feedstock, the recovery of glycerol, the

[#] Serbian Chemical Society member.

^{**}Corresponding author. E-mail: zknez@tmf.bg.ac.yu

doi: 10.2298/JSC0802147O

necessity to exclude the catalyst, undesirable side reactions, removal of inorganic salts and high reaction temperature. To overcome such drawbacks, there have been some attempts to develop and optimize methods for the production of biodiesel from a variety of lipids *via* different chemical or enzymatic catalysis.^{3,4} Although the concept of biodiesel production without the use of any catalyst in supercritical methanol seems to be a very promising approach, the consumption of methanol was relatively high and the method required a high temperature of 350 °C and a pressure of 45 MPa, which would increase the production costs.⁵ Due to the high-energy costs of chemical processes, the application of lipase in the oleochemical industry has become more attractive. The employment of lipases as biocatalysts allows mild reaction conditions and easy recovery of glycerol without purification or chemical waste production.^{6,7}

Considerable research has been performed on the transesterification of vegetable oils and animal fats with different acyl acceptors using various free or immobilized lipases as catalysts in organic solvents or solvent-free systems.^{8–10} However, the majority of enzymatic syntheses of biodiesel were performed in organic solvents, which are not suitable from the application viewpoint because of the toxicity and flammability of the solvent, damaging effects on the environment and consequential requirement for solvent removal. Thus, to enable enzymatic processes to be competitive, enzymatic solvent-free systems have been developed.^{7,9–13}

It was shown that immobilized *Rhizomucor miehei* lipase (Lipozyme RM-IM) is a suitable catalyst for the alcoholysis of several oils and fats with primary alcohols in *n*-hexane.¹⁴ Alcoholysis with relatively long-chain linear alcohols proceeds efficiently even in an organic solvent-free system but organic solvent-free methanolysis typically does not give high conversions.¹⁵ The main obstacle for using methanol as a substrate is its detrimental effect on the lipase activity, as several studies reported that a high methanol concentration could lead to serious inactivation of lipase.^{11,15} In order to circumvent this limitation, a three-step batch methanolysis process was developed and conversions of around 80 % were achieved even without solvent.⁸ Additionally, the possibility of increasing the yield of methyl esters by a surplus of methanol was studied.^{8,9} However, like most studies dealing with enzymatic methanolysis of vegetable oils, the experiments were based on the conventional one-at-a-time variation of the parameters, which often does not demonstrate the interactive effects of the parameters. Considering the high demand and benefits, improved knowledge of the relationships between the important transesterification variables and biodiesel yield is necessary to develop an efficient lipase catalytic process.

In this study, the effects of various factors on the methanolysis of sunflower oil by a commercial lipozyme lipase from *Rhizomucor miehei* was studied in a solvent-free system. Response surface methodology (RSM) and 5-level-4-factor

central composite rotatable design (CCRD) was performed to evaluate the effect of each of the analyzed factors, as well as the interactive effects of these factors on the synthesis of the methyl ester. This kind of experimental design reduces the number of experiments to be performed, thus reducing the costs, and gives knowledge of the interaction among the variables within the studied range. Although an increasing number of results published in the field of biodiesel synthesis in an organic solvent are based on experimental design,^{16,17} a systematic study related to the transesterification of vegetable oil with the immobilized *R. miehei* lipase in a solvent-free system has not hitherto been performed.

EXPERIMENTAL

Materials

Commercial lipase from *R. miehei* immobilized on a macroporous anion exchange resin (Lipozyme RM-IM) was kindly gifted by Novo Nordisk (Bagsvaerd, Denmark). Refined sunflower oil "Sunce" (Sunce a.d., Sombor) and methanol (purity > 99.8 %, Sigma, USA) were used as the reactants for the enzymatic reaction. Methyl myristate (Fluka, Switzerland) was used as the internal standard. All other chemicals were of reagent-grade.

Alcoholysis reaction

The synthesis was performed in 100 ml stoppered flasks, as a three-step methanolysis process. The first portion of methanol and the total amount of oil were added at the start of the reaction; the second portion of methanol was added after 10 h, while the third portion was added after 25 h, according to previously obtained results.¹⁸ The total reaction time was 50 h. Appropriate amounts of enzyme, methanol and water were added in the reaction media according to the experimental design (Table I). The amount of enzyme varied from 1–5 %, water 0–10 % and substrate molar ratio 3–9. The mixture was agitated on a shaker at 150 rpm at different temperatures (25–65 °C).

Analysis of the samples

The contents of methyl ester in the reaction mixture were quantified using a GS Varian 3400 instrument with a fused silica capillary column (5 m×0.53 mm×0.5 µm). The column temperature was held at 60 °C for 1 min, then heated to 110 °C at 50 °C min⁻¹, heated again to 170 °C at 4 °C min⁻¹ and then raised to 340 °C at 20 °C min⁻¹ and maintained at this temperature for 45 min. The temperatures of the injector and detector were set at 300 °C and 340 °C, respectively. Methyl myristate served as the internal standard.

Experimental design and statistical analysis

The experiments were conducted employing a central composite design, which aids the investigation of linear, quadric and cross product effects of four factors, each varied at five levels.¹⁹ The factors studied were enzyme concentration, water concentration, methanol to oil molar ratio and temperature during the transesterification reaction. The assay conditions for the reaction parameters were taken at zero level (center point), level one (+1 and -1) and level two (+2 and -2) (Table I). The design of the experiments employed is also presented in Table I. For data evaluation, response surface methodology (RSM) was used, and a second order polynomial equation was tested (for both response variables). The coefficients of the response function and their statistical significance were evaluated by the method of least squares using MATLAB software (version 6.5, Release 13, The MathWorks, Juc, Matick, MA, USA). Only the significant terms ($p \leq 0.05$) were considered for the final reduced model. Response sur-

faces and contour plots were obtained using the fitted model, by keeping two independent variables at a constant value while changing the other two variables. The Fisher test was used to determine the adequacy of the model and the Student distribution to evaluate the significance of the coefficients.

TABLE I. The obtained results of various runs of the central composite design with coded and actual values of variables (numbers in parenthesis represent coded independent variable levels)

Run	Temperature °C	Enzyme amount %	Content of water %	Substrate molar ratio $n_{\text{methanol}}/n_{\text{oil}}$	Rate of biodiesel production mmol h^{-1}	Rate of biodiesel production per enzyme amount $\text{mmol h}^{-1} \text{g}^{-1}$
1	35 (-1) ^a	2 (-1)	2.5(-1)	4.5 (-1)	0.0882	0.147
2	55 (1)	2 (-1)	2.5(-1)	4.5 (-1)	0.0517	0.0862
3	35 (-1)	4 (1)	2.5(-1)	4.5 (-1)	0.156	0.130
4	55 (1)	4 (1)	2.5(-1)	4.5 (-1)	0.139	0.115
5	35 (-1)	2 (-1)	7.5(1)	4.5 (-1)	0.110	0.183
6	55 (1)	2 (-1)	7.5(1)	4.5 (-1)	0.0369	0.0615
7	35 (-1)	4 (1)	7.5(1)	4.5 (-1)	0.131	0.109
8	55 (1)	4 (1)	7.5(1)	4.5 (-1)	0.0636	0.0530
9	35 (-1)	2 (-1)	2.5(-1)	7.5 (1)	0.0535	0.0891
10	55 (1)	2 (-1)	2.5(-1)	7.5 (1)	0.139	0.231
11	35 (-1)	4 (1)	2.5(-1)	7.5 (1)	0.109	0.0906
12	55 (1)	4 (1)	2.5(-1)	7.5 (1)	0.0617	0.0514
13	35 (-1)	2 (-1)	7.5(1)	7.5 (1)	0.0603	0.101
14	55 (1)	2 (-1)	7.5(1)	7.5 (1)	0.0316	0.0527
15	35 (-1)	4 (1)	7.5(1)	7.5 (1)	0.132	0.110
16	55 (1)	4 (1)	7.5(1)	7.5 (1)	0.0496	0.0413
17	25 (-2)	3 (0)	5(0)	6 (0)	0.152	0.169
18	65 (2)	3 (0)	5(0)	6 (0)	0.0746	0.0828
19	45 (0)	1 (-2)	5(0)	6 (0)	0.0318	0.106
20	45 (0)	5 (2)	5(0)	6 (0)	0.169	0.113
21	45 (0)	3 (0)	0(-2)	6 (0)	0.183	0.203
22	45 (0)	3 (0)	10(2)	6 (0)	0.0617	0.0685
23	45 (0)	3 (0)	5(0)	3 (-2)	0.0474	0.0527
24	45 (0)	3 (0)	5(0)	9 (2)	0.0966	0.107
25	45 (0)	3 (0)	5(0)	6(0)	0.0474	0.0527
26	45 (0)	3 (0)	5(0)	6 (0)	0.0515	0.0573
27	45 (0)	3 (0)	5(0)	6 (0)	0.0318	0.0353
28	45 (0)	3 (0)	5(0)	6 (0)	0.0978	0.109
29	45 (0)	3 (0)	5(0)	6 (0)	0.0431	0.0480
30	45 (0)	3 (0)	5(0)	6 (0)	0.0882	0.0980

^aThe numbers in parenthesis represent coded independent variable levels

RESULTS AND DISCUSSION

In this study, response surface methodology was used to optimize and understand the relationships between the important reaction parameters in the lipase-catalyzed transesterification of sunflower oil with methanol in a solvent-free sys-

tem. The objective was to obtain basic information concerning the relationships between these variables and the response (the reaction rate), aiming at a better control of the enzymatic process.

Based on the experimental results, two models were obtained. The first one presents the influence of individual and interactive effects on the reaction rate and the second one presents the same effects on the reaction rate per unit amount of enzyme. The second model allows the economic efficiency of the process to be optimized, since the cost of the enzyme represents a significant constituent of the overall costs of the process.

Statistical analysis was performed on the experimental results and the main and interaction effects of the variables were estimated. The amount of the enzyme had the largest influence on the reaction rate. Temperature and the amount of water had the next largest linear effects. The methanol to oil molar ratio did not significantly influence the production of biodiesel. An insignificant factor, but with a very high value, was the interactive effect between temperature and water content.

After eliminating the insignificant terms based on the composite rotatable design, a second order model (Eq. 1) was obtained with three significant parameters, without interactions:

$$Y_1 = 0.0596 - 0.0180x_1 + 0.0233x_2 - 0.0181x_3 + 0.0131 x_1^2 + 0.0154 x_3^2 \quad (1)$$

where Y_1 (mmol h^{-1}) is the rate of biodiesel production.

The response surface and contour plots of the predicted reaction rate as a function of process variables obtained from RSM analysis are presented in Fig. 1. Over the entire investigated range of enzyme concentration, the yield of the transesterification increased with increasing amount of enzyme in the reaction mixture (Figs. 1a and 1b). On the other hand, the effects of reaction temperature and amount of added water were described with quadratic equation with minimum values. The minimum rate of biodiesel production was achieved at 52 °C and 6.7 % of added water, while high rates were observed at high water content and a low temperature or at a low water content and a high temperature (Fig. 1c).

The transesterification reactions were performed over a wide range of temperatures, *i.e.*, from 25 to 65 °C. The response surface plot (Fig. 1a) clearly shows that increasing the temperature first led to a steep decrease of the rate of production of biodiesel until 45 °C. Further increasing of the temperature resulted in a slight increase of the rate of synthesis. The highest activity in examined temperature range was observed at the lowest applied temperature of 25 °C. The highest activity of the immobilized *R. miehei* lipase at the lowest employed temperature suggests that the lipase, like some other lipases, such as that from *Pseudomonas cepacia*,¹⁷ *Candida rugosa*²⁰ or porcine pancreatic lipase,²¹ was inactivated when it was subjected to a higher temperature for a long period.

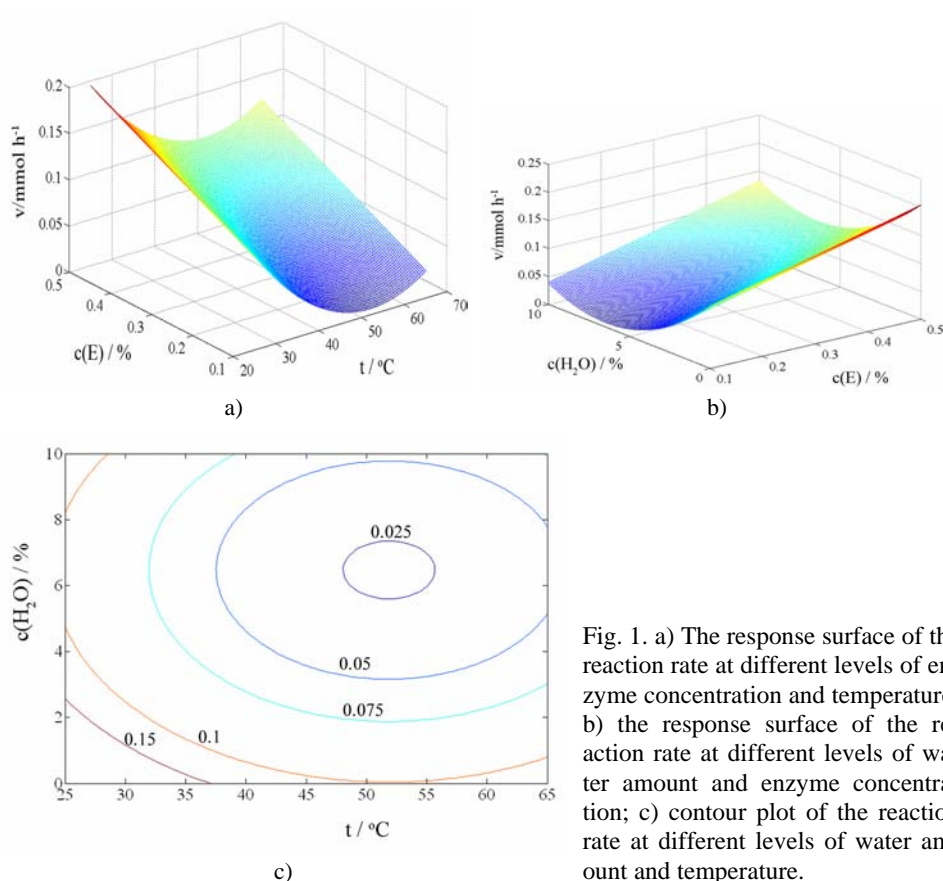


Fig. 1. a) The response surface of the reaction rate at different levels of enzyme concentration and temperature; b) the response surface of the reaction rate at different levels of water amount and enzyme concentration; c) contour plot of the reaction rate at different levels of water amount and temperature.

It is clear that significant parameters in the second model are temperature, water content and the interactive effect between temperature and water. From the experimental data and after eliminating the insignificant parameters, for the analysis of the factors on the reaction rate per unit amount of enzyme, the second order model (Eq. 2) with two significant parameters together with their interaction was obtained:

$$Y_2 = 0.0714 - 0.0198x_1 - 0.0227x_3 + 0.0163x_1^2 + 0.0191x_3^2 - 0.0219x_1x_3 \quad (2)$$

where Y_2 (mmol h⁻¹ g⁻¹) is the rate of biodiesel production per unit amount of enzyme.

The effect of both significant parameters on the specific rate of biodiesel production is illustrated in the response surface plot given in Fig. 2, from which it can be observed that high yields were obtained at low temperature and high water content or *vice versa*.

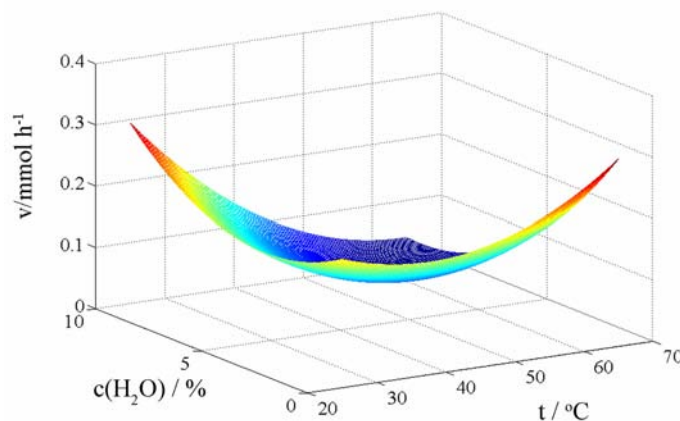


Fig. 2. The response surface of the reaction rate per unit amount of enzyme at different levels of water amount and temperature.

Comparing the two obtained models, it is clear that in the first model the amount of enzyme is the most significant factor with positive effect on the production rate of biodiesel, whereas in the second model it did not influence the production rate of biodiesel per unit amount of enzyme. These findings indicate that, although with increasing amount of enzyme in the system the rate of biodiesel production was increased, it is not economically justified. However, reports can be found that increasing the enzyme concentration up to 30 % led to an increase in the yield of biodiesel.⁷ This implies that the rate of transesterification per unit amount of enzyme should be the response variable of choice in the development of the best method for evaluation of the effectiveness of a production process of biodiesel.

In both models, the methanol/oil molar ratio (3:1–9:1) was not a significant factor for the synthesis of biodiesel. In a majority of related studies, the methanol/oil molar ratio significantly influenced the yield of methyl esters. For example, Soumanou *et al.* also investigated the influence of methanol on the yield of biodiesel, with the same lipase, and obtained best results with 3:1 methanol/oil molar ratio.⁸ In this case, the enzyme concentration was significantly higher (10 %), and even a slight increase of excess methanol resulted in the almost complete inactivation of the lipase. In a different study, the best results were obtained at 4:1 alcohol/oil molar ratio with an even higher amount of enzyme (27 %). However, the activity of the immobilized enzyme from *Candida antarctica* decreased at higher methanol concentrations (5:1 and 6:1).¹⁰

The addition of water exhibited a negative effect on the reaction rate. The highest activity was achieved without addition of water to the reaction mixture (Figs. 1b and 1c). Increasing the amount of added water up to 6.5 % led to a steep decrease of activity but further increase of the amount of water led to a slight

increase of the transesterification activity. Such a behavior is a consequence of the complex reaction mechanism of enzymatic transesterification.²² The amount of water in the system should be a compromise between minimizing hydrolysis and maximizing enzyme activity for the transesterification reaction.¹¹ Immobilized enzymes, however, show the highest activity in low-water systems. The highest initial rate of the transesterification reaction using immobilized *Pseudomonas fluorescens* was achieved at 0.3 % of added water.²³ The capability of lipase from *R. miehei* to catalyze reactions at exceptionally low activity of water, a_w , was documented in a previous study.²⁴ It was reported that the enzyme remained highly active at a water activity below 0.0001.

In this study, according to the test of statistical significance, only one interactive effect was observed, *i.e.*, a negative interactive effect between the temperature and water content on the reaction rate per unit amount of enzyme. It can be seen from the response surface (Fig. 2) that a higher reaction rate could be obtained at a high temperature and low water content, or *vice versa*. The transesterification activity of lipase *R. miehei* rapidly decreased with the combined increase of both the amount of water and temperature, probably due to lipase denaturation. Additionally, with excess water, the hydrolysis of methyl esters is favorable, especially at high temperatures.

CONCLUSIONS

The response surface methodology proved to be a valuable tool for evaluating the effects of various factors on the lipase-catalyzed synthesis of biodiesel fuel from sunflower oil. The reaction temperature and the amount of added water significantly influenced the rate of biodiesel production and these effects were adequately described by a quadratic model. Most importantly, RSM enabled the determination of a negative interactive effect between temperature and the amount of water, which would have been unseen in a classical investigation of the effects by variation of one factor while keeping the other parameters at fixed values. Thus, the highest yield of biodiesel was achieved at 45 °C and without water addition. Additionally, the results of this research imply that the choice of output parameter is of crucial importance, since different models were obtained with two particular response variables. The enzyme concentration had the most pronounced effect on the rate of biodiesel production but had no effect on the rate of biodiesel production per unit amount of enzyme. This fact implies that enzymatic synthesis of biodiesel with high amounts of lipase is not economically acceptable in a batch process, in spite of a certain increase of the product yield.

ИЗВОД

ОПТИМИЗОВАЊЕ ПОСТУПКА ПРОИЗВОДЊЕ БИОДИЗЕЛА КОМЕРЦИЈАЛНОМ ЛИПАЗОМ У СИСТЕМУ БЕЗ ОРГАНСКОГ РАСТВОРАЧА ПРИМЕНОМ МЕТОДОЛОГИЈЕ ОДЗИВНИХ ПОВРШИНА

НЕВЕНА ОГЊАНОВИЋ, ДЕЈАН БЕЗБРАДИЦА и ЗОРИЦА КНЕЖЕВИЋ

Технолошко-металурички факултет, Карнегијева 4, 11000 Београд

Циљ овог рада била је оптимизација процеса синтезе биодизела коришћењем имобилисане липазе из *Rhizomucor miehei*. У овом раду испитан је утицај основних процесних параметара на принос биодизела: температуре, моларног односа метанол/уље, концентрације ензима и концентрације воде у систему без органског растварача. Оптимизација процеса ензимске синтезе је извршена коришћењем ротатабилног композиционог плана. За обраду података коришћена је методологија одзивних површина. Установљено је да се утицај фактора на брзину ензимске реакције може описати моделом другог реда са три фактора, без међусобне интеракције. Статистичка анализа показује да је најзначајнији параметар количина ензима у реакционој смеси. Повишена температура је имала негативан утицај на брзину ензимске реакције, као и повећана концентрација воде. За анализу утицаја различитих фактора на брзину ензимске реакције по количини ензима, добијен је модел другог реда, са два значајна параметра са међусобном интеракцијом. Из модела се види да је модел изузетно стабилан при малом садржају воде, а да реакцији погодује велика количина воде само при ниским температурама. Највећи принос, од 10,15 mol kg⁻¹ ензима, остварен је при следећим параметрима реакције: 45 °С, моларни однос метанол/уље 6:1 и без додате воде у систем.

(Примљено 14. марта, ревидирано 2. јула 2007)

REFERENCES

1. J. M. Encinar, J. F. Gonzales, J. J. Rodriguez, A. Tejedor, *Energy Fuels* **16** (2002) 443
2. A. W. Schwab, M. O. Bagby, B. Freedman, *Fuel* **66** (1987) 1372
3. S. Saka, D. Kusdiana, *Fuel* **80** (2001) 225
4. Y. Shimada, Y. Watanabe, A. Sugihara, Y. Tominaga, *J. Mol. Catal. B: Enzym.* **17** (2002) 133
5. D. Kusdiana, S. Saka, *Fuel* **80** (2001) 693
6. D. Wei, X. Yuanyan, L. Dehua, J. Zeng, *J. Mol. Catal. B: Enzym.* **30** (2004) 125
7. O. Kose, M. Tuter, H. A. Aksoy, *Bioresour. Technol.* **83** (2002) 125
8. M. M. Soumanou, U. T. Bornscheuer, *Enzyme Microb. Technol.* **33** (2003) 97
9. M. Kaieda, T. Samukawa, A. Kondo, H. Fukuda, *J. Biosci. Bioeng.* **91** (2001) 12
10. M. Kaieda, T. Samukawa, T. Matsumoto, K. Ban, A. Kondo, Y. Shimada, H. Noda, K. Ohtsuka, E. Izumoto, H. Fukuda, *J. Biosci. Bioeng.* **88** (1999) 627
11. H. Noureddini, X. Gao, R. S. Philkana, *Bioresour. Technol.* **96** (2005) 769
12. C. G. Laudani, M. Habulin, M. Primozic, Z. Knez, G. Della Porta, E. Reverchon, *Bioprocess Biosyst. Eng.* **29** (2006) 119
13. F. J. Hernandez, A. P. de los Rios, D. Gomez, M. Rubio, G. Villora, *Appl. Catal. B* **67** (2006) 121
14. L. A. Nelson, T. A. Foglia, W. N. Marmer, *J. Am. Oil Chem. Soc.* **73** (1996) 1191
15. A. Salis, M. Pinna, M. Monduzzi, V. Solinas, *J. Biotechnol.* **119** (2005) 291
16. G. Vicente, A. Coteron, M. Martimez, J. Aracil, *Ind. Crops Prod.* **8** (1998) 29
17. C. J. Shieh, H. F. Liao, C. C. Lee, *Bioresour. Technol.* **88** (2003) 103

18. Z. Knežević, N. Ognjanović, D. Bezbradica, in *Proceedings of the 1st International Symposium on Environmental Biocatalysis*, Cordoba, Spain, 2006, p. 56
19. G. E. P. Box, W. G. Hunter, J. S. Hunter, *Statistics for experimenters: An introduction to design, data analysis and model building*, Wiley, New York, 1978
20. Z. Knežević, N. Milosavić, D. Bezbradica, Ž. Jakovljević, R. Prodanović, *Biochem. Eng. J.* **30** (2006) 269
21. B. Manohar, S. Divakar, *Process Biochem.* **39** (2004) 847
22. H. Fukuda, A. Kondo, H. Noda, *J. Biosci. Bioeng.* **92** (2001) 405
23. M. Iso, B. Chen, M. Eguchi, T. Kudo, S. Shrestha, *J. Mol. Catal. B: Enzym.* **16** (2001) 53
24. R. H. Valivety, P. J. Halling, A. R. Macrae, *FEBS Lett.* **301** (1992) 258.



www.shd.org.yu

J. Serb. Chem. Soc. 73 (2) 157–167 (2008)

JSCS–3698

JSCS@tmf.bg.ac.yu • www.shd.org.yu/JSCS

UDC 542.92:664.29+582.734.3

Original scientific paper

Characterization and degradation of pectin derived from Budimka apple

MILOŠ V. NIKOLIĆ¹ and LJILJANA MOJOVIĆ^{2*}

¹"Srbijanka" Food-Processing Industry, 14 000 Valjevo and ²Faculty of Technology and Metallurgy, Department of Biochemical Engineering and Biotechnology University of Belgrade, Karnegijeva 4, 11000 Belgrade, Serbia

(Received 26 February, revised 1 August 2007)

Abstract: The characterization of apple pectin and its oligogalacturonic fractions derived from the autochthones apple variety Budimka, characteristic for central Serbia, is described in this paper. After extraction, the apple pectin was subjected to controlled enzymatic hydrolysis by polygalacturonase (PG) and pectin lyase (PL) from *Aspergillus niger* and then fractionated by ion-exchange column chromatography on Dowex 1X-8 (200–400 mesh). Saturated oligogalacturonic acids, obtained by controlled hydrolysis with PG, were efficiently separated by elution with a gradient of Na acetate buffer (pH 6.0), while unsaturated oligogalacturonic acids, obtained by controlled hydrolysis with PL, were separated on the same resin, using a gradient of Na formate buffer (pH 4.7) as the eluent. The yields of the fractions with the particular degree of polymerization (*DP*) were also determined. The total content of neutral saccharides in the original Budimka apple pectin was detected by HPLC analysis of the 4-nitrobenzoyl derivatives of the sugar, and amounted to 5.31 %. Among the neutral saccharides, contents of galactose, glucose, rhamnose, arabinose, xylose and mannose were detected.

Keywords: degradation; fractionation; oligogalacturonic acids; Budimka apple pectin; polygalacturonase; pectin lyase; neutral saccharides.

INTRODUCTION

Budimka apple is an autochthon apple variety specific for the region of central Serbia. This apple type is very resistant to climate and ecological conditions and has low agricultural demands, making it a good candidate for organic food products. In addition, it is well known for its sharp flavor and deep yellow to red color, which sometimes extends into the fruit, as well as for its good balance of acids and sugars. It is highly sought after by industry to bring a real apple flavor to juices and ciders. For these reasons, the Budimka is treasured in Serbia both

* Corresponding author. E-mail: lmojovic@tmf.bg.ac.yu

doi: 10.2298/JSC0802157N

fresh and for baked dishes. Moreover, the beneficial and even anticancerogenic health effects of the apple pectin and phenols are well documented.^{1,2}

Despite a large range of industrial utilization and export of these apples or apple-based products, including commercial pectin, no systematic study on the degradation and characterization of this pectin has been performed. Significant changes related to the characteristics and technological properties of fruit products during maturation, storing and canning are related to the physico-chemical transformations of pectins caused by the action of pectic enzymes. Both naturally present (endogenous) and introduced enzymes (exogenous) catalyze the decomposition of pectins.

Previously,³ the extraction of apple pectin from Budimka apples was studied and some general properties of the isolated pectin were determined, such as its high degree of polymerization (*DP*) and high degree of esterification (*DE*). These characteristics, together with the particular content of phenolics and neutral saccharides largely determine the technological properties and specific quality of products derived from Budimka apple.

The aim of the present study was to characterize chemically Budimka apple pectin and the fractions obtained by enzymatic degradation. For these purposes, homologous series of saturated and unsaturated oligogalacturonic acids were obtained by enzymatic hydrolysis of pectin compounds from the Budimka apple using polygalacturonase (PG) and pectin lyase (PL) from *Aspergillus niger*.

EXPERIMENTAL

Pectin extraction and purification

Budimka apples from the Arilje locality (central Serbia) were collected for investigation during the year 2004. The extraction and purification of polygalacturonic acids from Budimka apple was described previously.³ The resulting pectin preparations had a degree of esterification (*DE*) of 75 %, an average degree of polymerization of 134 % and consisted of 93 % galacturonic acids.

Enzymes and chemicals

Enzymes. The pectic acid was degraded by polygalacturonase (PG; EC.3.2.1.15) from *Aspergillus niger* (Sigma, declared activity of 5–20 U/mg) to obtain a mixture of saturated oligogalacturonides and hydrolyzed by pectin lyase (PL; EC.4.2.2.10) also from *A. niger* (Sigma, declared activity of 50–100 U/mg).

Chemicals. D(+)-galacturonic acid monohydrate (Sigma, USA) was used as the standard for chromatographic analysis. Sugars and sugar alcohols were purchased from Merck (Darmstadt, Germany). 4-Nitrobenzoyl chloride (4-NBCl; analytical grade, Fluka), used to obtain 4-nitrobenzoyl sugar derivatives, was recrystallized once from petroleum ether (Sigma) b.p. 60–70 °C. The melting point of 4-NBCl after recrystallization was between 71–73 °C. Analytical grade pyridine (Fluka), used for derivatization, was refluxed for 3 h with NaOH (Merck), distilled (b.p. 115–116 °C) and stored over NaOH. 4-Dimethylaminopyridine *purum* was also purchased from Fluka. The reagent solution for derivatization of the neutral saccharides was prepared by dissolving 100 mg of 4-NBCl in 1 ml of pyridine with gentle warming. All other reagents and solvents were of analytical or HPLC grade.

Enzymatic hydrolysis

Preparation of saturated oligogalacturonides. Mixtures of saturated oligogalacturonic acids were obtained by incubating apple pectin in Erlenmeyer flasks in a thermostated water bath with shaking (150 rpm) with an appropriate amount of *A. niger* fungal polygalacturonase (FPG) at 35 °C for different reaction times. The reaction mixture usually contained 1 % PGA (w/v), 0.15 M NaCl in acetate buffer (0.05 M) and 0.15 mg ml⁻¹ of FPG (w/v). In order to obtain different types of oligogalacturonides, the following conditions were applied: for pentamer to octamer 30 to 60 min at pH 6.0; for dimer to pentamer 12 h at pH 6.0; for dimer to tetramer 20 h at pH 6.0; for dimer to trimer 30 h at pH 6.0. The dimer was obtained by incubation at pH 3.5 for 48 h. The enzymatic reactions were terminated by addition of 10 g of celite and activated charcoal *per* 1000 ml and by heating for 5 min at 100 °C. This warm suspension was then filtered and the filtrate loaded onto a Dowex-50W (H⁺) column and eluted with two volumes of bidistilled water (flow rate 48.9 cm h⁻¹). In this way, the uronides were transformed into free acids. The eluate was concentrated under vacuum to about 10 % (w/v) of galacturonic acids. The mixture of the obtained saturated oligogalacturonides was stored in a refrigerator until further separation of the particular oligogalacturonic fractions was performed.

Preparation of unsaturated oligogalacturonides. The samples were prepared in the same way as for the saturated oligogalacturonides except that they were incubated with 0.1 mg ml⁻¹ PL from *A. niger*. Also, the same incubation times were applied to collect the unsaturated oligogalacturonides of particular chain length. Upon termination of the enzymatic reaction, the suspension was filtered and the filtrate loaded onto a Dowex-50W (H⁺), as described above, in order to transform the uronides into free acids. When a hydrolysate contained too much monomer (D-galacturonic acid), this compound was removed from the pectin hydrolysate by precipitation as the sodium strontium salt. The removal of the monomer enabled a better separation of the higher oligogalacturonic acids. The eluate was concentrated under vacuum to about 10 % (w/v) of galacturonic acids. The mixture was refrigerated until further separation of the particular oligogalacturonic fractions was performed.

Analytical methods

The anhydrogalacturonic acid (AGA) content in the pectin preparations was determined by a photometric method with carbazole in 80 % sulfuric acid and borate ions were added. The absorbance of the solutions was compared to that obtained from standard solutions of galacturonic acid subjected to the same procedure.⁴

The unsaturated oligogalacturonides content was monitored by measuring the absorbance increase in the reaction mixture at 232 nm, due to double C₄–C₅ bond formation in the pectin molecule during the enzymatic reaction. The absorbance was measured using a Zeiss PMQ II spectrophotometer. The degree of degradation of the pectin was calculated from the ratio of the measured increase of the absorbance and the theoretical increase that should have occurred if the enzyme were to break all the glycoside bonds. The theoretical absorbance increase was calculated from the concentration of pectin acids, the degree of polymerization and the molar extinction coefficient (ϵ) for unsaturated bonds according to Macmillan and Vaughn.⁵

The degree of polymerization (*DP*) of the substrate was estimated by determining the ratio of AGA to the content of reducing groups (AGA/CHO), according to Liu and Luh.⁶ The reducing group content was determined using the method of Somogyi.⁷

The degree of esterification (*DE*) was evaluated by the cuprizonic method of Keijbets and Pilnik.⁸

The methanol content was determined using chromotropic acid.⁹

The phenolics were determined after saponification of pectin substrate with 1 M NaOH. The phenolics were measured using the Folin–Ciocalteu reagent (FCR) and vanillin–sulfuric

acid reagent (VSR). FCR reacted with monomers and higher phenolic polymers according to the method of Ribereau-Gayon.¹⁰ VSR reacted approximately stoichiometrically with phenolic compounds of medium and lower degrees of polymerization, as described by Goldstein and Swain.¹¹ Changes in the degree of polymerization of the phenolics in the samples were monitored from the ratio of the values obtained by the two methods.

The molecular mass, M_r , was estimated by determining the end-groups according to Voragen *et al.*¹²

Ion-exchange chromatography of the oligogalacturonic acids

The saturated oligogalacturonic acids were fractionated using a modified procedure of Nagel and Wilson.¹³ The material obtained after digestion of 10 g of pectin was separated by column chromatography employing a Dowex 1X-8 column (200–400 mesh). A typical column measured 30×700 mm² and had a volume of about 500 ml. The column was loaded with 150 ml of the 10 % oligogalacturonic acid solution. Saturated oligogalacturonic acids were eluted using sodium acetate buffer (pH 6.0) at a linear concentration gradient from 0.2 to 0.8 M. Before elution, the column was washed with 1 l of distilled water. Unsaturated oligogalacturonic acids were separated using the same column but with a different eluent. They were eluted using sodium formate buffer (pH 4.7) at a concentration gradient of 0.1–0.6 M. In this way, the fractions which presented homologous series of saturated and unsaturated oligogalacturonic acids from dimer to octamer, were eluted. The fractions collected were tested for the content of uronide using the carbazole method⁴ and for the content of unsaturated uronide by measuring the absorbance increase at 232 nm.⁵

Purification of the oligogalacturonic acids

After analysis for their uronide content, the fractions of the oligogalacturonic acids from the individual peaks were pooled and precipitated with SrCl₂. The SrCl₂ was added in 100 % excess and the salts of the uronic acids were precipitated in 4 volumes of 92 % ethanol. Then the dimers and trimers were precipitated in 70 % ethanol and finally in 60 % ethanol, while the oligogalacturonic acids with longer chains were precipitated in 50 % ethanol. After filtration, the precipitates were dried under vacuum over CaCl₂. To ensure the purity of the individual uronides, the salts from several column runs were combined, converted to the free acids by treatment with Dowex-50 W (H⁺) and rechromatographed. Only those fractions shown by TLC to contain the desired oligogalacturonides were pooled.

TLC of the oligogalacturonic acids

After column separation, the obtained fractions were identified and determined by thin layer chromatography, TLC. The TLC analyses were performed on cellulose TLC plates (Eastman E-13255). Each spot contained 35–85 µg (depending on the experiment) of the sample. The plates were developed in an ascending direction at 23 °C with ethyl acetate: acetic acid: water (4:2:3, v/v/v). The spots were visualized by spraying the plates with 10 % ammonia solution followed with bromophenol blue according to Liu and Luh.⁶ For quantitative assay, an aliquot of 85 µg of hydrolysate was applied for each spot. Quantitative analysis of the oligogalacturonic acid was performed by scraping the acidic spots from the thin-layer plates and analyzing for the content of anhydrogalacturonic acid by the carbazole method described above.

Determination of neutral saccharides

The neutral saccharides were determined by liquid chromatography (HPLC) analysis on a Spectra-Physics Sp 8000 instrument, with a Rheodyne fixed injector (20 µl) using a Bio Rad HPX-87P column (30 cm×7.8 mm, packed with 9 µm spherical sulfonated polystyrene-divinylbenzene beads with 8 % of cross-linked bonds). The neutral saccharides present in the

samples of the oligogalacturonic acid fractions were derivatized prior to the HPLC analysis. Detection of the derivates was performed at 260 nm, which is the extinction maximum for 4-nitrobenzoyl sugar derivatives at ambient temperature. An acetonitrile–water mixture (400:100) was used as the eluent. The flow rate was 1.0 ml min^{-1} . The derivatization of saccharides was performed with 4-NBCl in pyridine according to a modified procedure described by Nachtmann *et al.*^{14,15} The reaction was performed in stoppered 10-ml centrifuge tubes. Fifty μl of the samples with 10 % (w/v) of galacturonic acids were mixed with 150 μl of the reagent solution (prepared by dissolving 100 mg of 4-NBCl in 1 ml of pyridine with gentle warming), well shaken, and reacted for 10 min at room temperature. After the reaction, the derivatives were extracted. The pyridine was first removed in a desiccator under a water suction vacuum. The centrifuge tubes were then flushed with an air or nitrogen stream and 2 ml of a 5 % NaHCO_3 solution containing 5 mg of 4-dimethylaminopyridine was added. The excess reagent was hydrolyzed after 5 min of treatment in an ultrasonic bath. A blank treated simultaneously should yield a clear solution. The derivatives were then extracted with 2 ml of chloroform and treated with 2 ml of a 5 % NaHCO_3 solution and twice with 3 ml of a 0.05 M HCl solution containing 5 % NaCl. This led to the quantitative isolation of the derivatives and complete exclusion of excess reagent and pyridine.

RESULTS AND DISCUSSION

Separation of oligogalacturonides

The yields of saturated and unsaturated oligogalacturonic acids obtained by enzymatic decomposition of pectin preparations from Budimka apple are given in Table I. The saturated and unsaturated di- to octagalacturonides were separated using the same Dowex-1X8 ion-exchange column chromatography but with different eluents. As shown in Table I, the overall yield of saturated oligogalacturonic acids was 60.13 % (w/w), which was higher than the overall yield of unsaturated oligogalacturonic acids, amounting to 53.45 %. In both cases, trimers were obtained in the largest amount (16.76 % for saturated oligogalacturonic acids and 12.25 % for unsaturated oligogalacturonic acids), followed by dimers (12.45 % for saturated oligogalacturonic acids and 9.61 % for unsaturated oligogalacturonic acids) and tetramers (9.21 and 9.02 %, respectively), and the amounts decreased towards oligogalacturonic acids with higher degrees of polymerization, up to octamer. The method employed for the determination of the degree of polymerization (*DP*) of the fractions of the oligogalacturonic acids, *i.e.*, according to the ratio of AGA to the content of reducing groups (AGA/CHO), was found to be an effective and precise method for both the saturated and unsaturated oligogalacturonic acids (Table I).

The fractions of oligogalacturonic acids present in the incubation mixtures obtained by enzyme action were identified by TLC on the basis of the R_{ga} values, which are presented in Table I (the R_{ga} values represent the relationship between the migration distance of the sample spot and that of the standard). It is obvious that the oligogalacturonic acid fractions identified by the R_{ga} values corresponded very well to the *DP* calculated on the basis of the AGA and CHO contents. The purity of the identified TLC spots, which was determined by scraping of the

acidic spots from the thin-layer plates and analyzing for the content of anhydrogalacturonic acid by the carbazole method (data not presented), was more than 98 %, thus indicating that a very good separation was achieved.

TABLE I. Yield of saturated and unsaturated oligogalacturonic acids (*DP* 2–8) obtained from 10.0 g of pectin preparation (extracted from Budimka apple) containing 93 % polygalacturonic acid (*DE* 75, *DP* 134)

Oligogalactouronic acid	<i>DP</i>	R_{ga}	Saturated			Unsaturated		
			Obtained amount, g	Yield w/w %	AGA/CHO	Obtained amount, g	Yield w/w %	AGA/CHO
Dimer	2	0.67	1.16	12.45	2.01	0.92	9.61	2.02
Trimer	3	0.51	1.56	16.76	3.09	1.19	12.25	3.07
Tetramer	4	0.39	0.86	9.21	3.97	0.87	9.02	4.06
Pentamer	5	0.28	0.69	7.43	4.99	0.68	6.98	4.98
Hexamer	6	0.21	0.54	5.84	6.01	0.63	6.45	5.97
Heptamer	7	0.15	0.46	4.95	7.02	0.52	5.39	7.03
Octamer	8	0.11	0.32	3.49	7.98	0.38	3.95	8.05
Total	–	–	5.59	60.13	–	5.19	53.65	–

The presented results demonstrate that it was possible to employ the same column but with different eluents to separate the unsaturated and saturated uronides. It was noticed that the elution power of the acetate buffer used for the separation of the saturated oligogalacturonides was stronger than the elution power of the formate buffer used for the separation of the unsaturated oligogalacturonides. Thus, a higher concentration of the eluent was applied for the elution of the unsaturated uronides than that used for the elution of the saturated uronides of the same chain length.

The elution profiles for the saturated and unsaturated oligogalacturonic acids are shown in Figs. 1 and 2, respectively. It can be seen that the unsaturated uronides were eluted as broader peaks (Fig. 2). The first small peak at the beginning of the elution profile of the saturated oligogalacturonic acids (Fig. 1) was not part of the homologous series of oligogalacturonides. Moreover, the first two small peaks of the profile of the unsaturated oligogalacturonic acids (Fig. 2) were also not part of the homologous series of oligogalacturonides. This was confirmed by TLC analysis.

Determination of saccharides

The content of neutral saccharides (rhamnose, galactose, arabinose, xylose, mannose and glucose) in the original apple sample is presented in Fig. 3. The content of the total neutral saccharides was also determined in the saturated and unsaturated fractions of oligogalacturonic acids and expressed relative to the content of dry mass (Tables II and III), as well as the content of individual saccharides (data not presented).

The total content of neutral saccharides in the original Budimka apple pectin amounted to 5.31 % (Fig. 3). Galactose was present in the greatest amount (1.16 %)

in the original sample, while the content of mannose was the lowest (0.63 %). The contents of rhamnose, arabinose, xylose and glucose were similar and below 1 % in the Budimka apple pectin. The presented results of the neutral saccharides indicated a heteropolysaccharide content of Budimka apple pectin compounds, since a larger content of different saccharides in the isolated fractions of oligogalacturonic acids was detected. These sugars are integral constituent of pectic polysaccharides, which was indicated by the failure of fractionations by ion-exchange chromatography. Generally, the neutral sugar side chains are linked to rhamnogalacturonan segments within the pectin molecule.¹⁶ The presence of xylose and glucose could be explained, in part, by the presence of xyloglucans, which have been shown to be associated with pectic material,¹⁷ or by xylogalacturonan.¹⁸

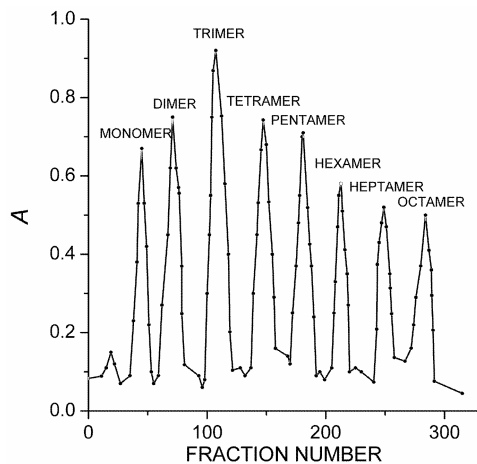


Fig. 1. The elution profile for saturated oligogalacturonic acids (*DP* 2–8) isolated by ion-exchange chromatography on a Dowex 1X-8 column (200–400 mesh), acetate form, in a step-wise gradient using 0.2–0.8 M Na-acetate buffer at pH 6.0.

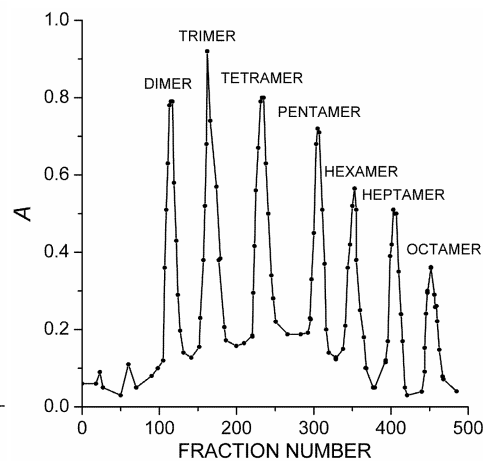


Fig. 2. The elution profile of unsaturated oligogalacturonic acids (*DP* 2–8) separated by ion-exchange chromatography on a Dowex 1X-8 column (200–400 mesh), formate form, in a step-wise gradient using 0.2–0.8 M sodium formate buffer (pH 4.7).

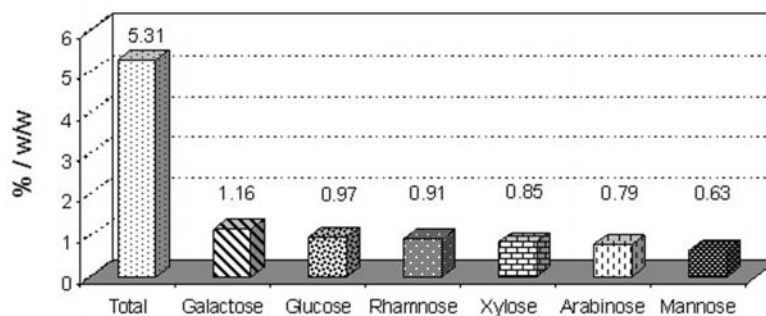


Fig.3. Total and individual content of individual neutral saccharides (galactose, glucose, rhamnose, xylose, arabinose and mannose) determined in Budimka apple pectin.

TABLE II. Composition of the original Budimka apple pectin sample and of saturated oligogalacturonic acids fractions (*DP* 2–8) of the pectin separated on a Dowex 1X-8 (acetate) column

Quantities in %	Original sample	Oligogalacturonic acid							
		Di-	Tri-	Tetra-	Penta-	Hexa-	Hepta-	Octa-	
Degree of esterification	75	68.2	63.5	59.4	58.6	56.9	56.8	53.0	
Degree of polymerization	134	2.07	2.95	3.01	4.97	6.03	7.02	8.09	
M_r (end groups) / g mol ⁻¹	17400	9500	17300	29300	27890	31090	37800	40780	
Galacturonic acid content	93	94.7	95.2	93.9	89.4	88.7	86.0	83.7	
Neutral sacch. content	5.31	3.41	3.24	4.63	5.47	5.33	6.28	7.91	
Methanol content	0.070	0.070	0.050	0.050	0.050	0.050	0.040	0.040	
Content of phenolics	VSR	0.15	0.02	0.02	0.02	0.03	0.06	0.07	0.6
	FCR	3.25	1.53	1.32	0.62	0.64	0.69	2.77	2.43
	VSR/FCR	4.6	6.5	4.6	4.4	3.9	3.3	2.5	2.4
Humidity	5.7	8.6	8.2	6.5	7.3	8.9	9.50	9.65	
Ash	0.37	0.68	0.79	0.78	0.92	0.64	0.50	0.65	

TABLE III. Composition of the unsaturated oligogalacturonic acids fractions (*DP* 2–8) of Budimka apple pectine separated on a Dowex-1X8 (formate) column

Quantities in %		Oligogalacturonic acid						
		Di-	Tri-	Tetra-	Penta-	Hexa-	Hepta-	Octa-
Degree of esterification		72.5	70.8	64.7	61.9	58.7	57.3	54.8
Degree of polymerization		2.07	3.05	4.09	5.00	6.09	7.05	8.00
M_r (end groups) / g mol ⁻¹		19500	27480	32720	39650	46900	53000	58390
Galacturonic acid content		91.7	88.4	85.3	81.9	78.9	75.3	72.8
Neutral sacch. content		3.43	3.65	4.40	4.75	5.05	5.55	5.65
Methanol content		0.03	0.09	0.08	0.05	0.07	0.05	0.06
Content of phenolics	VSR	1.97	1.36	0.64	0.86	0.46	0.58	0.58
	FCR	6.35	5.92	4.79	4.53	4.28	4.19	2.43
	VSR/FCR	4.13	4.72	5.78	7.05	8.03	10.68	10.84
Humidity		7.5	7.0	6.8	6.4	6.9	6.3	7.2
Ash		0.63	0.69	0.75	0.81	0.75	0.68	0.55

The amounts of neutral sugars found in the pectin preparations corresponded to those presented in a study on a model of cell wall structure by Talmadge *et al.*¹⁹ Smaller amounts of rhamnose and galactose were observed in fractions containing compounds of lower M_r , confirming that these two sugars might be incorporated into the main chain of the pectin molecule. The successive increase of the content of rhamnose and galactose in the oligogalacturonides with longer chains suggested (data not presented) the assumption that these sugars are included in the main chain of the pectin molecules. Direct evidence for L-rhamnose as an integral constituent in several pectic acids, for example, that from alfa (lucerne) has been obtained by the isolation of aldobiouronic acid 2-*O*-(α -D-galactopyranosyluronic acid)-L-rhamnose, as a product of partial acid hydrolysis.²⁰ Other neutral residues in pectins are probably attached as side chains as depicted on the partial structure shown in Fig. 4.

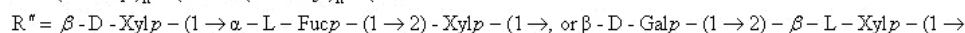
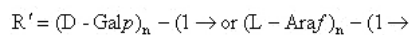
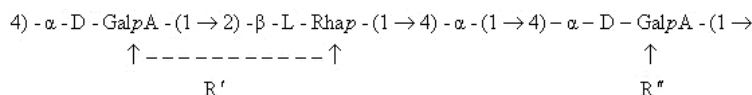


Fig. 4. Model of the partial structure of the neutral residues of pectin compounds.

Chemical composition of the fractions of oligogalacturonic acids

The overall chemical composition of the fractions of saturated and unsaturated oligogalacturonic acids fractions (*DP* 2–8) of Budimka apple pectin are presented in Tables II and III, respectively. It can be seen from these Tables that the degrees of esterification of both the saturated and unsaturated oligogalacturonic acids decreased with increasing chain length of the oligogalacturonic acid. The elution of poorly methylated pectin compounds was possible only at higher buffer concentrations. This leads to the conclusion that pectin binding to ion-exchange resins depends on both the number of free carboxyl groups and the strength of the negative charges in the macromolecule. The extent of esterification in the isolated saturated oligogalacturonic fractions ranged from 68.2 to 53.0 (Table II), while in the unsaturated oligogalacturonic acids, it ranged from 72.5 to 54.8 (Table III). The decrease of the degree of esterification in the isolated oligomers from di- to octamer was accompanied by an increase in the total content of phenolics. It is supposed that the presence of phenolics in pectin compounds amplifies the negative charge of the molecule, which influences the strength of the bonds formed with ion-exchange resins. Most of the phenolics contained in the chain of pectin compounds are not directly bound to pectin since, under the employed experimental conditions for the separation of oligogalacturonides by ion-exchange chromatography, the eluates contained some 96 % of the starting uronides and about 10 % of the starting amount of phenolics in the analyzed pectin preparations.

Oligomers of increasing M_r were eluted with increasing buffer concentration, for both the saturated and unsaturated oligogalacturonic acid fractions (Tables II and III). The gel-filtration effect on the ion-exchange material used for the isolation of oligogalacturonides cannot be the reason for this trend because the sequence of M_r values in the eluted fractions would be reversed in such a case. It is assumed that other bonds are formed, besides the ionic ones (*e.g.*, van der Waals bonds), which are independent of the degree of esterification. Their number and strength would increase with increasing pectin chain length. Moreover, the presence of phenolic hydroxyl groups may lead to an amplification of this effect.

CONCLUSIONS

The isolation of pure homologous fractions, according to the degree of polymerization, of saturated and unsaturated oligogalacturonic acids obtained by

controlled enzymatic hydrolysis of the Budimka variety of apple could be simply and efficiently performed by ion exchange chromatography on a Dowex 1X-8 column.

The saturated oligogalacturonic acids, obtained by controlled hydrolysis with FPG, were eluted with a gradient of Na acetate buffer, pH 6.0, while the unsaturated oligogalacturonic acids (4,5-dehydrogalacturonosyl unit on the non-reducing end), obtained by controlled hydrolysis with PL, were separated on the same resin but using a gradient of Na formate buffer, pH 4.7, as the eluent. The total yields of oligogalacturonic acids recovered from the hydrolysate of polygalacturonic acid were 60.13 % for the saturated (*DP* 2–8) and 53.65 % for the unsaturated (*DP* 2–8) forms. It was confirmed that the separated oligogalacturonides were very pure (\approx 99 % of AGA).

The presence of neutral saccharides, *i.e.*, rhamnose, galactose, arabinose, xylose, mannose and glucose, in the original Budimka apple pectin and in the obtained fractions was confirmed by HPLC analysis of 4-nitrobenzoyl sugar derivatives. The total content of neutral saccharides in the original Budimka apple pectin amounted to 5.31 %. The contents of rhamnose, arabinose, xylose and glucose were similar and below 1 % in the Budimka apple pectin.

The degree of esterification of the isolated oligogalacturonic acids decreased with increasing chain length.

ИЗВОД

ДЕГРАДАЦИЈА И КАРАКТЕРИЗАЦИЈА ПЕКТИНА ЈАБУКЕ СОРТЕ БУДИМКА

МИЛОШ В. НИКОЛИЋ¹ и ЉИЉАНА МОЈОВИЋ²

¹"Србијанка", 14 000 Ваљево и ²Универзитет у Београду, Технолошко-металуришки факултет, Карнегијева 4, 11000 Београд

У овом раду је испитиван хемијски састав и карактеристике пектина јабуке аутохтоне сорте будимка, која је карактеристична за регион централне Србије. Након екстракције пектина из јабуке, извршена је контролисана ензимска хидролиза помоћу ензима полигалактуроназе (PG) и пектин-лијазе (PL) из *Aspergillus niger* и добијени хидролизати су фракционисани помоћу јоноизмењивачке колоне Dowex 1X-8. Сепарација засићених олигогалактуронских киселина, добијених контролисаним хидролизом помоћу полигалактуроназе је ефикасно извршена градијентном елуцијом са Na-ацетатним пуфером, pH 6,0, док је сепарација незасићених олигогалактуронских киселина добијених контролисаним хидролизом са пектин-лијазом извршена на истој јоноизмењивачкој колони, али коришћењем Na-формијатног пуфера pH 4,7. Такође је утврђен принос индивидуалних фракција различитог степена полимеризације. Укупан садржај неутралних сахара, који је утврђен помоћу HPLC је износио 5,31 %. Неутралне шећере пектина јабуке будимка чине рамноза, арабиноза, ксилоза, маноза и глукоза.

(Примљено 26. фебруара, ревидирано 1. августа 2007)

REFERENCES

1. J. Boyer, R. H. Liu, *Nutrition J.* **3** (2004) 5
2. S.W. Barth, C. Fähndrich, A. Bub, H. Dietrich, B. Watzl, F. Will, K. Briviba, G. Rechkemmer, *Carcinogenesis* **26** (2005) 1414
3. M. Nikolić, L. Mojović, *Food Chem.* **101** (2007) 1

4. K. A. Taylor, J. G. Buchanan-Smith, *Anal. Biochem.* **201** (1992) 190
5. J. D. Macmillan, R. H. Vaughn, *Biochemistry* **3** (1964) 564
6. Y. K. Liu, B. S. Luh, *J. Food Sci.* **43** (1978) 721
7. M. Somogyi, *J. Biol. Chem.* **195** (1952) 19
8. M. J. H. Keijbets, W. Pilnik, *Potato Res.* **17** (1974) 169
9. International Standards ISO, 1388/1
10. P. Ribereau-Gayon, in *Plant Phenolics*, P. H. Heywood, Ed., Oliver & Boyd, Edinburgh, 1972, p. 169
11. J. L. Goldstein, T. Swain, *Phytochemistry* **2** (1963) 371
12. A. G. J. Voragen, F. M. Rambouts, M. J. Hoajdank, W. Pilnik, *Lebensm. – Wiss. Technol.* **4** (1971) 7
13. C. W. Nagel, T. M. Wilson, *J. Chromatogr.* **41** (1964) 410
14. F. Nachtmann, H. Spitzzy, R. W. Frei, *Anal. Chem.* **48** (1976) 1576
15. F. Nachtmann, K. W. Budna, *J. Chromatogr.* **136** (1977) 279
16. *Pectins and Their Manipulation*, G. B. Seymour, J. P. Knox, Eds., CRC Press, Boca Raton, 2002, pp. 1–29
17. R. R. Selvendran, M. A. O'Neill, in *Methods of Biochemical Analysis*, Vol. 32, D. Glick, Ed., Wiley, 1987, pp. 25–123
18. A. Kikuchi, Y. Edashige, T. Ishii, S. Satoh, *Planta* **200** (1996) 369
19. K. W. Talmadge, K. Keegstra, W. D. Bauer, P. Albersheim, *Plant Physiol.* **51** (1973) 158
20. W. Pigman, D. Horton, A. Herp, *The Carbohydrates*, Academic Press, New York, 1970, pp. 516–521.



www.shd.org.yu

J. Serb. Chem. Soc. 73 (2) 169–177 (2008)

JSCS–3699

Journal of
the Serbian
Chemical Society

JSCS@tmf.bg.ac.yu • www.shd.org.yu/JSCS

UDC 546.742+547.466+547.496.2:543.4:543.57

Original scientific paper

Characterization studies and cyclic voltammetry on nickel(II) amino acid dithiocarbamates with triphenylphosphine in the coordination sphere

NATESAN GEETHA and SUBBIAH THIRUMARAN*

Department of Chemistry, Annamalai University, Annamalainagar – 608 002, India

(Received 18 January, revised 10 July 2007)

Abstract: Nickel(II) amino acid dithiocarbamate complexes of the composition $[\text{Ni}(\text{AA}(\text{dtc})(\text{PPh}_3)(\text{NCS})]$, $[\text{Ni}(\text{AA}(\text{dtc})(\text{PPh}_3)(\text{CN})]$ and $[\text{Ni}(\text{AA}(\text{dtc})(\text{PPh}_3)_2]\text{ClO}_4$ [$\text{AA}(\text{dtc})$ = dithiocarbamate derivatives of amino acids, *i.e.*, glycine (glydtc), L-*iso*-leucine (*i*-leudtc) and L-proline (prodtc)] were synthesized. The compounds were characterized by IR and electronic spectroscopy, thermal analysis, cyclic voltammetry and conductivity measurements. In the case of the mixed ligand complexes, the thioureide $\nu(\text{C}-\text{N})$ values were shifted to higher wave numbers compared to $[\text{Ni}(\text{AA}(\text{dtc})_2]$. This observation shows the increased strength of the thioureide bond due to the presence of the π -accepting phosphine. Electronic spectral studies suggest square planar geometry for the complexes. Thermal analyses of the complexes are in keeping with the proposed formulae. Almost all the complexes showed signs of decay above 170 °C. At around 390 °C, the final mass corresponded to NiS. Cyclic voltammetry showed a decrease of the electron density on the nickel in the mixed ligand complexes compared to $[\text{Ni}(\text{AA}(\text{dtc})_2]$.

Keywords: amino acid dithiocarbamate; triphenylphosphine; nickel(II); IR; electronic spectra; cyclic voltammetry.

INTRODUCTION

Group VIII dithiolates containing planar MS_4 chromophores show interesting variations in their reactions with Lewis bases.^{1,2} Unlike its congeners, nickel(II) is a borderline acceptor and its planar dithiocarbamate ligand prefers to react with Lewis bases, such as phosphines, rather than hard nitrogenous bases. Nickel(II) dithiocarbamates in their reaction with PR_3 form NiS_2P_2 chromophores.^{3,4}

Nickel(II) complexes with phosphine ligands have been studied for their anti-cancer activity.⁵ Many proteins contain cysteine and methionine residues and hence dithiocarbamate derivatives of α -amino acids may be valid models for the study of the coordination of proteins to metal ions. The complexes formed between metal

* Corresponding author. E-mail: sthirumaran@yahoo.com

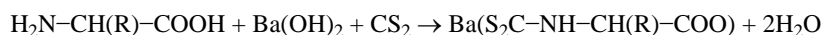
doi: 10.2298/JSC0802169G

ions and dithiocarbamate derivatives of amino acids have been reported.⁶⁻⁸ In order to understand the influence of SCN^- and CN^- donors on the coordination environment around a nickel atom and on the thioureide bond, in this work, the synthesis and characterization of mixed-ligand complexes *i.e.*, $[\text{Ni}(\text{AAdtc})(\text{PPh}_3)(\text{NCS})]$, $[\text{Ni}(\text{AAdtc})(\text{PPh}_3)(\text{CN})]$ and $[\text{Ni}(\text{AAdtc})(\text{PPh}_3)_2]\text{ClO}_4$, were studied.

EXPERIMENTAL

Synthesis of the ligands

The dithiocarbamate-derivatives of the α -amino acids glycine, L-*iso*-leucine and L-proline were synthesized following a method similar to that described by Musil and Irgolic.⁹ The amino acid (0.050 mol) was reacted with an aqueous solution of $\text{Ba}(\text{OH})_2 \cdot 8\text{H}_2\text{O}$ (0.055 mol) and the suspension was magnetically stirred until total dissolution was achieved. In order to prevent precipitation of barium carbonate, the presence of air was avoided. Acetone was then added, until its content was *ca.* 40 % of the total volume and CS_2 (0.060 mol) was added dropwise. Formation of the barium salt occurs according to the reaction:



The solution was kept at 0 °C for 12 h. Addition of ethanol resulted in a white precipitate, which was filtered and washed with diethyl ether. Purification was performed by dissolution in water and precipitation with ethanol.

Preparation of nickel(II)-dithiocarbamate complexes

A solution of $\text{NiCl}_2 \cdot 6\text{H}_2\text{O}$ (0.001 mol) was added dropwise to an aqueous solution of the barium salt (0.001 mol) of the corresponding dithiocarbamate ligand. The light green nickel(II) solution immediately became dark and a precipitate formed, which was characterized as $\text{Ba}[\text{Ni}(\text{S}_2\text{C}-\text{NH}-\text{CH}(\text{R})-\text{COO})_2] \cdot 3\text{H}_2\text{O}$. In order to remove the barium cation from the complex, the aqueous solution was transferred to a separating funnel and diethyl ether was added. Then the stoichiometric amount of 0.10 M HCl was added to generate BaCl_2 , which remained in the aqueous layer. It should be noted that the acid solution was added after the diethyl ether, hence, the neutral complex was removed to the organic phase before it was destroyed by the acidic medium:



Upon evaporation of the diethyl ether, the olive green $\text{Ni}(\text{AAdtc})_2$ complex separated.

Preparation of $[\text{Ni}(\text{AAdtc})(\text{PPh}_3)(\text{NCS})]$ [AAdtc = glydtc (1), i-leudtc (2), prodtc (3)]

A mixture of $\text{Ni}(\text{AAdtc})_2$ (0.001 mol), $\text{NiCl}_2 \cdot 6\text{H}_2\text{O}$ (0.001 mol), PPh_3 (0.002 mol) and NH_4SCN (0.002 mol) was refluxed for 3 h in acetonitrile (30 cm³) and methanol (10 cm³). The purple red solution was filtered and left to evaporate. After two days, a purple red solid had separated out, which was re-crystallized from CHCl_3 .

Preparation of $[\text{Ni}(\text{AAdtc})(\text{PPh}_3)(\text{CN})]$ [AAdtc = glydtc (4), i-leudtc (5), prodtc (6)]

A mixture of $\text{Ni}(\text{AAdtc})_2$ (0.001 mol), $\text{NiCl}_2 \cdot 6\text{H}_2\text{O}$ (0.001 mol), PPh_3 (0.002 mol) and KCN (0.002 mol) was refluxed for 3 h in acetonitrile (30 cm³) and methanol (10 cm³). The orange solution was filtered and left to evaporate. After two days, an orange solid separated out, which was recrystallized from Me_2CO .

Preparation of $[\text{Ni}(\text{AAdtc})(\text{PPh}_3)_2]\text{ClO}_4$ [AAdtc = glydtc (7), i-leudtc (8), prodtc (9)]

A mixture of $\text{Ni}(\text{AAdtc})_2$ (0.001 mol), $\text{NiCl}_2 \cdot 6\text{H}_2\text{O}$ (0.001 mol), PPh_3 (0.002 mol) and NaClO_4 (0.001 mol) in CHCl_3 (50 cm³) and EtOH (4 cm³) was refluxed for 3 h. The resulting

purple red solution was filtered and left to evaporate. After 2 days, a purple red solid separated, which was recrystallized from CHCl_3 .¹⁰

Analytical and physical measurements

Reagent grade, high purity materials (BDH/Merck) were used as supplied. The nitrogen content in the complex was determined by the Kjeldahl method and the nickel content was determined by the standard EDTA method. The conductivity studies were performed using a Pico Model 201 conductivity bridge. Acetone and acetonitrile were used as solvents. The conductance measurements were recorded at room temperature (27 °C). The concentration of the compounds was $1 \times 10^{-3} \text{ mol dm}^{-3}$ in all measurements. IR Spectra were recorded as KBr pellets with a Nicolet Avatar 360 FT-IR spectrophotometer (range 400–4000 cm^{-1}). UV-Vis spectra were recorded on a Hitachi U-2001 double beam UV-spectrophotometer. A Perkin-Elmer TGA7 instrument was used for the thermal analysis. The heating rate of the furnace was fixed at 20 °C min^{-1} . An ECDA 001 electrochemical system was used for recording the cyclic voltammograms of the complexes. The working electrode was made of glassy carbon. The counter electrode was a Pt wire and reference electrode was Ag/AgCl. Pure dichloromethane was used as the solvent and tetrabutylammonium perchlorate (0.10 M) as the supporting electrolyte. The scan rate employed was 100 mV s^{-1} . All measurements were recorded at room temperature (27 °C) in an oxygen free atmosphere, provided by bubbling purified nitrogen through the solution. The concentration of the compounds was $1 \times 10^{-3} \text{ mol dm}^{-3}$.

RESULTS AND DISCUSSION

The conductivity measurements indicated the non-electrolytic nature of the complexes **1–3** and **4–6** and the 1:1 electrolytic nature of the complexes **7–9**,¹¹ Table I.

Infrared spectra

The important IR bands are listed in Table I. The energy of the $\nu(\text{C–N})$ band was intermediate between the stretching frequencies associated with typical single and double bonded carbon and nitrogen atoms.¹² The $\text{Ni}(\text{AA}(\text{dtc})_2)$ complexes showed the thioureide stretching bands at *ca.* 1500 cm^{-1} . In the case of the mixed ligand complexes, the $\nu(\text{C–N})$ values were found to be larger than those of the parent dithiocarbamates. This observation shows the increased strength of the thioureide bond due to the presence of the π -accepting phosphine. In general, the glydtc and *i*-leudtc complexes showed higher thioureide $\nu(\text{C–N})$ values than the prodtc complexes because the heterocyclic ring system has a smaller tendency to release electrons to the N–C bond.¹³

The $\nu(\text{C–N})$ bands (single bonded) appeared at *ca.* 1100 cm^{-1} , while in the mixed ligand complexes containing the perchlorate anion, a band due to ClO_4^- ions also appeared in this region. The IR spectral bands at 2090 cm^{-1} $\nu(\text{C}\equiv\text{N})$ and 830 cm^{-1} $\nu(\text{C–S})$ for the complexes **1–3** may imply the assumption that the NCS group is coordinated to the nickel *via* the nitrogen atom.¹⁴ In the case of complexes **4–6**, the $\nu(\text{C}\equiv\text{N})$ frequency at *ca.* 2135 cm^{-1} indicates the CN^- group is bonded to the metal through the carbon atom.¹⁵

The $\nu(\text{C–S})$ asymmetric stretching bands are located prominently at *ca.* 1000 cm^{-1} in all the complexes and the $\nu(\text{C–S})$ symmetric bands appear as weak absorptions

at *ca.* 690 cm^{-1} . All the complexes show bands at $1700 \pm 30 \text{ cm}^{-1}$, indicating the presence of free carboxylic groups.¹⁶ This observation shows that the carboxylic group is not involved in the coordination.

TABLE I. Important IR bands, conductance and analytical data for the complexes

Compound	Important infrared spectral bands cm^{-1}				λ_m S $\text{cm}^2 \text{ mol}^{-1}$	Found (Calcd.) %	
	$\nu(\text{C-N})$ (Thioureide)	$\nu(\text{C-N})$ (Single bonded)	$\nu(\text{C-N})$ (NCS/CN)	$\nu(\text{C-S})$		Ni	N
	[Ni(glydtc)(PPh ₃)(NCS)] (1)	1542	1098	2094			
[Ni(i-leudtc)(PPh ₃)(NCS)] (2)	1520	1098	2091	1030	10.04 ^a	9.8 (10.1)	4.6 (4.8)
[Ni(prodctc)(PPh ₃)(NCS)] (3)	1510	1099	2088	1034	8.01 ^a	10.3 (10.4)	4.6 (4.9)
[Ni(glydtc)(PPh ₃)(CN)] (4)	1536	1098	2137	1028	14.56 ^b	11.5 (11.9)	5.4 (5.6)
[Ni(^l leudtc)(PPh ₃)(CN)] (5)	1540	1097	2137	1026	15.30 ^b	10.6 (10.7)	4.8 (5.1)
[Ni(prodctc)(PPh ₃)(CN)] (6)	1511	1097	2132	1028	9.88 ^b	10.8 (11.0)	4.9 (5.2)
[Ni(glydtc)(PPh ₃) ₂ ClO ₄] (7)	1539	1115	–	1028	121.76 ^a	6.8 (7.1)	1.3 (1.7)
[Ni(^l leudtc)(PPh ₃) ₂ ClO ₄] (8)	1529	1099	–	1028	118.46 ^a	6.6 (6.7)	1.4 (1.6)
[Ni(prodctc)(PPh ₃) ₂ ClO ₄] (9)	1512	1090	–	1028	138.80 ^a	6.5 (6.8)	1.2 (1.6)

^aMeasured in acetone solution, $[\text{Ni}^{+2}] = 10^{-3} \text{ mol dm}^{-3}$ at 27 °C; ^bmeasured in acetonitrile solution, $[\text{Ni}^{+2}] = 10^{-3} \text{ mol dm}^{-3}$ at 27 °C

Electronic spectra

In all the nickel(II) complexes, the bands which appear below 350 nm are due to intraligand $\pi-\pi^*$ transitions, mainly associated with N=C=S and S=C=S groups (Table II). Several authors ascribe the intense bands at 390 nm to either metal \rightarrow ligand or ligand \rightarrow metal charge transfer.¹⁷ In addition to these charge transfer bands, the electronic spectra show weak bands at 490 and 650 nm, due to the d-d transitions. In the dialkyldithiocarbamate complexes of nickel(II), similar bands were reported and ascribed to transitions from the lower filled d-orbitals to the unoccupied $d_{x^2-y^2}$ orbitals.¹⁸ The two bands at 650 and 490 nm correspond to $d_{xy} \rightarrow d_{x^2-y^2}$ and $d_{z^2} \rightarrow d_{x^2-y^2}$ transitions, respectively.

The strong bands at around 490, 435 and 440 nm for the complexes **1–9** can be attributed to d-d electron transitions, Table I. Comparison of the information already available on similar compounds of this type leads to the conclusion that the coordination around the metal ions should be square planar.^{3,4}

TABLE II. Electronic spectral bands, thermogravimetric data and cyclic voltammetric reduction potentials

Compound	λ_{\max} / nm	Decomp. temp. °C	Weight loss, %		Final residue	Reduction potential, V
			Exp.	Calcd.		
[Ni(glydte)(PPh ₃)(NCS)] (1)	332, 385, 485	182–382	83.4	82.8	NiS	-0.816
[Ni(<i>i</i> -leudte)(PPh ₃)(NCS)] (2)	258, 329, 490	180–368	82.7	84.5	NiS	-0.837
[Ni(prodte)(PPh ₃)(NCS)] (3)	252, 329, 491	192–377	84.0	84.1	NiS	-0.841
[Ni(glydte)(PPh ₃)(CN)] (4)	218, 254, 321, 432	167–394	80.7	81.7	NiS	-1.092
[Ni(<i>l</i> -leudte)(PPh ₃)(CN)] (5)	241, 309, 438	190–370	82.7	83.6	NiS	-1.001
[Ni(prodte)(PPh ₃)(CN)] (6)	225, 309, 433	177–376	82.0	83.3	NiS	-1.010
[Ni(glydte)(PPh ₃) ₂ ClO ₄] (7) ^a	239, 258, 324, 440	–	–	–	–	-0.645
[Ni(<i>l</i> -leudte)(PPh ₃) ₂ ClO ₄] (8) ^a	256, 325, 440	–	–	–	–	-0.652
[Ni(prodte)(PPh ₃) ₂ ClO ₄] (9) ^a	256, 327, 440	–	–	–	–	-0.617

^aThe decomposition of the complexes containing the perchlorate anion were not performed owing to their possible explosive character

Thermal analysis

TG Techniques were employed to follow the thermal behavior of complexes 1–6. Representative thermograms of [Ni(glydte)(PPh₃)(NCS)] and [Ni(*i*-leudte)(PPh₃)(NCS)] are given in Fig. 1. According to the results obtained, the

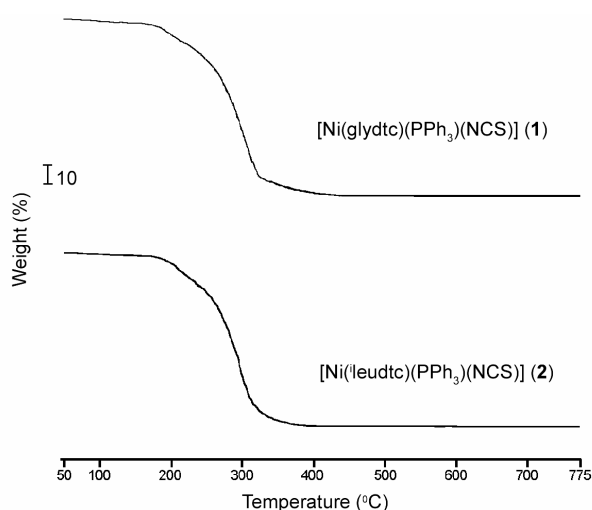


Fig. 1. Thermograms of [Ni(glydte)(PPh₃)(NCS)] (1) and [Ni(*i*-leudte)(PPh₃)(NCS)] (2).

complexes are not volatile and their decomposition occurs in different steps; the main features are summarized in Table I. Thermogravimetric studies on the complexes confirmed their proposed molecular formulae. The thermograms of all the complexes show an initial decomposition around 180 °C, which indicates the absence of solvent molecules. Complexes **1**, **3**, **6** and **9** show similar behavior with three main processes. The other complexes show two main processes, probably corresponding to pyrolysis of the organic matter existing in these compounds. The final product of the decomposition is nickel sulfide, as confirmed by the experimental and expected weight loss measurements.

Cyclic voltammetry

The cyclic voltammetry reduction potentials are given in Table II. Representative cyclic voltammograms of $[\text{Ni}(\text{prodtc})_2]$ and $[\text{Ni}(\text{prodtc})(\text{PPh}_3)(\text{NCS})]$ are given in Fig. 2. The reduction potential for the parent $\text{Ni}(\text{AAdtc})_2$ complexes is observed around -1.3 V. All the mixed-ligand complexes **1–9** show one electron

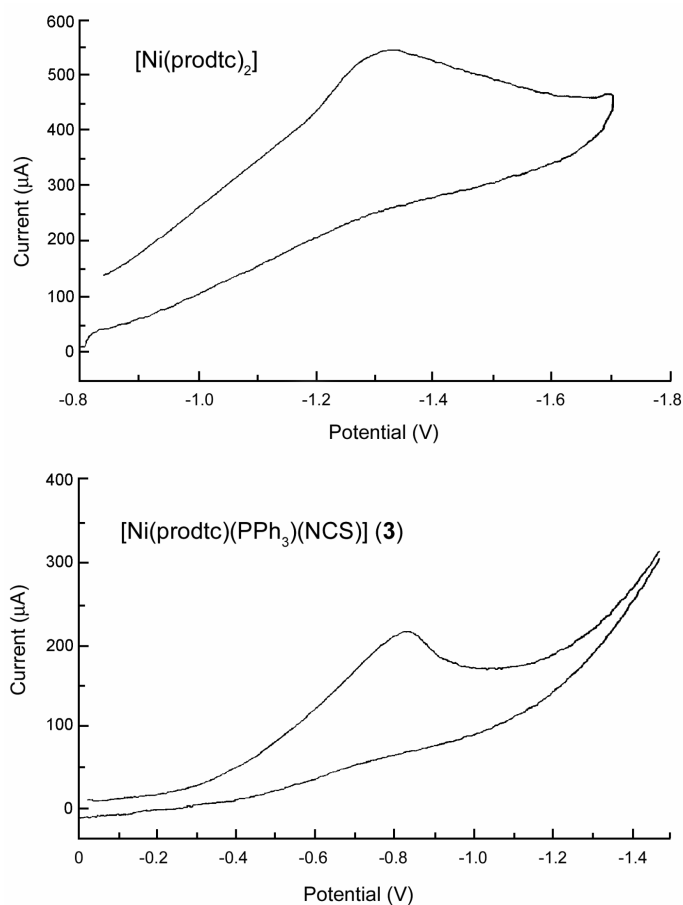
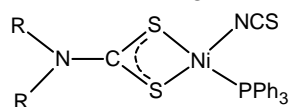
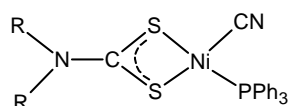
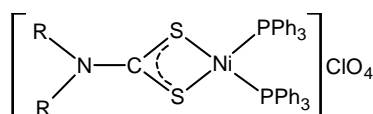


Fig. 2. Cyclic voltammograms of $[\text{Ni}(\text{prodtc})_2]$ and $[\text{Ni}(\text{prodtc})(\text{PPh}_3)(\text{NCS})]$ (**3**).

reduction at lower potentials. The reductions are irreversible. The lower reduction potentials observed for complexes **1–9** indicate the ease of electron addition in the mixed-ligand complexes. The mesomeric drift of the electron density from the dithiocarbamate moiety towards the metal centre contributes to lower reduction potential from the normal reduction potentials of Ni(dtc)₂ complexes around -1.3 V.¹⁹ Comparison of [Ni(AAdtc)(PPh₃)₂]ClO₄ with the other types of complexes show that the reduction potentials decrease in the following order: Ni(AAdtc)₂ > [Ni(AAdtc)(PPh₃)(CN)] (**4–6**) > [Ni(AAdtc)(PPh₃)(NCS)] (**1–3**) > [Ni(AAdtc)(PPh₃)₂]ClO₄ (**7–9**), indicating the influence of the PPh₃, NCS and CN ligands, respectively, on the mesomeric drift of the electron density towards nickel.

Infrared spectral studies on the complexes show the contribution of the thioureide form to the structures. In the case of mixed-ligand complexes, the $\nu(\text{C-N})$ (thioureide) values shift to higher wave numbers compared to the Ni(AAdtc)₂ complexes. This observation is an indication of the increased electron density on nickel in the mixed ligand complexes and, hence, these complexes are expected

[Ni(AAdtc)(PPh₃)(NCS)][Ni(AAdtc)(PPh₃)(CN)][Ni(AAdtc)(PPh₃)₂]ClO₄

R₂NCS₂ = AAdtc = glydtc (HOOC-CH₂-NH-CS₂),

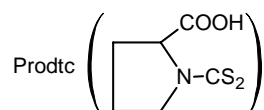
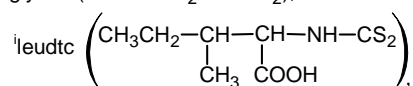


Fig. 3. Proposed structures of the complexes.

to be more difficult to reduce. However, in reality, the mixed-ligand complexes are the most easily reduced. The reason probably is extensive π -back bonding with the phosphorous atom, which drains the excess negative charge on the metal and hence the low reduction potential.

Based on the above observations, the structures proposed for these complexes are given in Fig. 3.

ИЗВОД

КАРАКТЕРИЗАЦИЈА И ЦИКЛИЧНА ВОЛТАМЕТРИЈА НИКАЛ(II)
АМИНОКИСЕЛИНСКИХ ДИТИОКАРБАМАТА СА
ТРИФЕНИЛФОСФИНОМ У КООРДИНАЦИОНОЈ СФЕРИ

NATESAN GEETHA и SUBBIAH THIRUMARAN

Department of Chemistry, Annamalai University, Annamalainagar – 608 002, India

Синтетисани су комплекси никла(II) са аминокиселинским дитиокарбаматима састава: $[\text{Ni}(\text{AAdtc})(\text{PPh}_3)(\text{NCS})]$, $[\text{Ni}(\text{AAdtc})(\text{PPh}_3)(\text{CN})]$ и $[\text{Ni}(\text{AAdtc})(\text{PPh}_3)_2]\text{ClO}_4$ [(AAdtc = дитиокарбаматни деривати аминокиселина, тј. глицина (glydtc), L-изолеуцина (*i*-leudtc) и L-пролина (prodtc)]. Једињења су окарактерисана IR и електронском спектроскопијом, термичком анализом, цикличном волтаметријом и мерењима проводљивости. У случају комплекса са мешовитим лигандима, тиоуреидне $\nu(\text{C}-\text{N})$ вредности померају се ка већим таласним бројевима у поређењу са $[\text{Ni}(\text{AAdtc})_2]$. Ово указује на јачу тиоуреидну везу због присуства π -акцепторског фосфина. Електронска спектрална проучавања указују на квадратно-планарну геометрију ових комплекса. Скоро сви комплекси показују знаке распада изнад 170 °C. На око 390 °C коначна маса одговарала је NiS. Циклична волтаметрија комплекса указује на смањење електронске густине на никлу у мешовито-лигандним комплексима у поређењу са $[\text{Ni}(\text{AAdtc})_2]$.

(Примљено 18. јануара, ревидирано 10. јула 2007)

REFERENCES

1. A. Chakravarthy, *Prog. Inorg. Chem.* **7** (1966) 83
2. J. P. Fackler Jr., W. C. Siegel, *Inorg. Chem.* **8** (1969) 163
3. C. K. Jorgenson, *Inorg. Chem.* **3** (1964) 120
4. R. Pastroek, J. Kamenicek, J. Marek, D. Dastyh, Z. Sindelar, *Polyhedron* **19** (2000) 1713
5. P. S. Jarret, O. M. N. Dhubhghaill, P. J. Sadler, *J. Chem. Soc. Dalton Trans.* (1993) 1863
6. B. Macias, P. Malet, R. Paradinas, V. Rives, M. V. Villa, *Inorg. Chim. Acta* **127** (1999) 288
7. S. Thirumaran, K. Ramalingam, *Trans. Metal Chem.* **25** (2000) 60
8. I. R. Baird, B. R. Camneron, R. T. Skerlj, *Inorg. Chim. Acta* **353** (2003) 107
9. A. Musil, K. Irgolic, *Z. Anal. Chem.* **208** (1965) 352
10. W. J. Geary, *Coord. Chem. Rev.* **7** (1971) 81
11. R. Baggio, A. Frigerio, E. B. Halac, D. Vega, M. Percec, *J. Chem. Soc. Dalton Trans.* (1992) 549
12. C. Moncotrigiano, G. C. Pellacani, C. Preti, *J. Inorg. Nucl. Chem.* **36** (1974) 3709
13. R. Pastorek, Z. Travenicek, E. Kvapilova, Z. Sindelar, F. Brezina, J. Marek, *Polyhedron* **18** (1999) 151
14. B. Arul Prakasam, K. Ramalingam, G. Bocelli, R. Olla, *Z. Anorg. Allg. Chem.* **630** (2004) 301
15. M. Castillo, M. J. Criado, B. Macias, V. Vaquero, *Inorg. Chim. Acta* **124** (1986) 127

16. W. Beck, M. Givnth, M. Castillo, H. Zippel, *Chem. Ber.* **11** (1978) 1246
17. C. K. Jorgenson, *J. Inorg. Nucl. Chem.* **24** (1962) 1571
18. K. Ramalingam, G. Aravamudan, M. Seshasayee, *Inorg. Chim. Acta* 128 (1987) 231.



www.shd.org.yu

J. Serb. Chem. Soc. 73 (2) 179–187 (2008)

JSCS–3700

JSCS@tmf.bg.ac.yu • www.shd.org.yu/JSCS

UDC *Organotin(IV)+547.595:542.913

Original scientific paper

Synthesis and structural characterization of organotin(IV) complexes formed with [O,O] donor atoms of carboxylic acids

MUKHTIAR HUSSAIN¹, MUHAMMAD ZAMAN¹, MUHAMMAD HANIF¹,
SAQIB ALI^{1*} and MUHAMMAD DANISH²

¹Department of Chemistry, Quaid-i-Azam University, Islamabad–45320 and

²Department of Chemistry, University of Sargodha, Sargodha, Pakistan

(Received 14 May, revised 22 October 2007)

Abstract: Organotin(IV) carboxylates of the general formula R_nSnL_{4-n} (where $R = \text{Me}$, $n\text{-Bu}$ or Ph , and $L = \alpha\text{-phenyl-2,3-(methylenedioxy)cinnamate}$ anion or $2\text{-}(2,3\text{-dimethylanylino)nicotinate}$ anion) have been prepared. The mono-, di- and tri-organotin(IV) carboxylates were synthesized by the reaction of organotin(IV) oxides or hydroxides with a stoichiometric amount of the ligand acids at an elevated temperature in dry toluene. The composition of the synthesized organotin(IV) complexes, the bonding behavior of the donor groups and structural assignments were studied by elemental analysis, FT-IR, ^1H -, ^{13}C -NMR and mass spectrometry. The spectral data suggest that the ligand acts in a bidentate manner, coordinating through the oxygen atoms. These spectroscopic techniques revealed a distorted tetrahedral geometry in the solution state for the tri-organotins, while a mean coordination number between five to six for the di-organotin(IV) dicarboxylates. In the solid phase, the tri-organotins were essentially trigonal bipyramidal polymeric while the di-organotins were octahedral. However, mono-organotin tricarboxylates were predicted to exist in the octahedral state both in solution as well as in the solid phase.

Keywords: organotin(IV) complexes; O-donor ligands; IR, NMR and mass spectrometry.

INTRODUCTION

In general, tri-organotin(IV) compounds display a larger array of biological activity than their di-organotin and mono-organotin analogues. This has been attributed to their ability to bind proteins.¹ Furthermore, many organotin(IV) carboxylates were found to possess anticancer activity in a variety of tumor cells and the structure of these organotin(IV) compounds were characterized in the solid phase and in solution.² Di-alkyltin(IV) compounds have a selective effect on lymphocytes^{3,4} and hence can be used in cancer chemotherapy.

* Corresponding author. E-mail: drsa54@yahoo.com

doi: 10.2298/JSC0802179H

In addition to their medicinal and pesticidal impact,^{5–12} tin compounds have a fascinating solution and solid phase chemistry, which led to countless publications, reviews and books based on structural elucidation in both phases.^{11–13} It is well known that organotin carboxylates have versatile molecular structures, such as monomers, dimers, tetramers, oligomeric ladders and hexameric drums, *etc.*, both in the solid phase and in solution. It has also been demonstrated that the different structural types are formed due to the presence of additional coordinating sites (S, N or O, *etc.*) along with a carboxylic moiety.^{13–15} Herein, organotin(IV) complexes of α -phenyl-2,3-(methylenedioxy)cinnamic acid (HL¹, Fig. 1) and 2-(2,3-dimethylanilino)nicotinic acid (HL², Fig. 1) and their special characterization to ascertain their geometry in the solid and solution phase are reported.

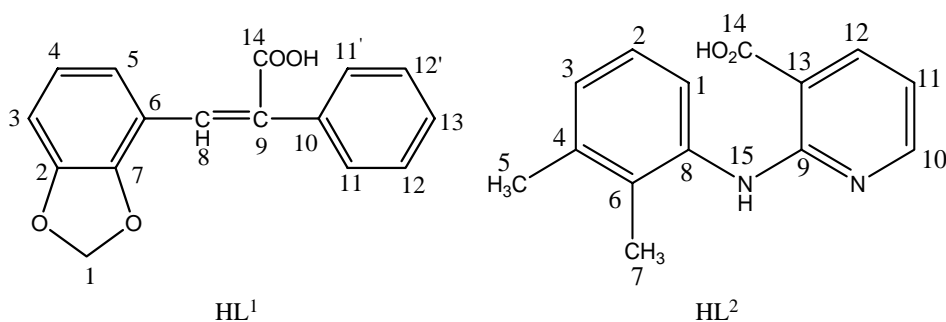


Fig. 1. α -Phenyl-2,3-(methylenedioxy)cinnamic acid (HL¹) and 2-(2,3-dimethylanilino)nicotinic acid (HL²), with the numbering scheme.

EXPERIMENTAL

Materials and Methods

Analytical grade organotin chlorides, oxides, hydroxide, 2,3-dihydroxybenzaldehyde, 2,3-dimethylaniline, NaOH (> 97%), 2-chloronicotinic acid and benzene were purchased from Aldrich, Fluka and Alfa-Aesar (Johnson Matthey Chemical Company). The organic solvents, such as toluene, chloroform and acetone, were purchased from Merck (Germany) and dried *in situ* using standard procedures.^{16,17}

Melting points were determined with melting point apparatus model MPD Mitamura Riken Kogyo (Japan) and are uncorrected. The infrared spectra were recorded on a Bio-Rad Excalibur FT-IR Model FTS 3000MX as KBr pellets. The ¹H- and ¹³C-NMR spectra in solution (CDCl₃) were recorded at ambient temperature on a Bruker 300 MHz FT NMR spectrometer using deuterated chloroform and benzene as internal references. The elemental analyses were performed using a CHNS-932 elemental analyzer, Leco Corporation (USA). The mass spectrometric analyses were performed on a MAT-312 mass spectrometer.

Synthesis

The acid ligands, α -phenyl-2,3-(methylenedioxy)cinnamic acid (HL¹) and 2-(2,3-dimethylanilino)nicotinic acid (HL²) were prepared according to a standard procedure.¹⁸ The new organotin(IV) compounds were prepared according to the following procedure.

The ligand acid, RCOOH (HL¹, 10 mmol, 2.68 g; HL², 10 mmol, 2.42 g) and the stoichiometric amount of the organotin(IV) compound (Me₂SnO, Bu₂SnO, Ph₃SnOH, BuSn(O)OH,

BuSn(OH)₂Cl were suspended in dry toluene (100 ml) in a two-necked round bottom flask (250 ml), equipped with a Dean–Stark apparatus, magnet bar and water condenser. The contents were refluxed for 6–8 h with continuous removal of the formed water then cooled to room temperature and toluene was removed under reduced pressure. The resulting solid was recrystallized from a chloroform/*n*-hexane mixture (1:4).

RESULTS AND DISCUSSION

The physical properties, yields and elemental analysis of the compounds are given in Table I.

TABLE I. Physical properties of the synthesized organotin(IV) complexes

Comp. No.	Compound	Molecular formula	M_r g mol ⁻¹	M.p. °C	Yield %	Content calcd.(found), %		
						C	H	N
1	Me ₂ SnL ¹ ₂	C ₃₄ H ₂₈ O ₈ Sn	682.69	230–231	68	59.76 (60.20)	4.10 (4.32)	–
2	Bu ₂ SnL ¹ ₂	C ₄₀ H ₄₀ O ₈ Sn	766.69	71–72	78	62.60 (61.96)	5.21 (5.01)	–
3	Ph ₃ SnL ¹	C ₃₄ H ₂₆ O ₄ Sn	616.69	115–116	77	66.15 (65.79)	4.21 (4.32)	–
4	BuSnL ¹ ₃	C ₅₂ H ₄₂ O ₁₂ Sn	976.69	147–148	71	63.88 (64.12)	4.30 (4.41)	–
5	BuSnClL ¹ ₂	C ₃₆ H ₃₁ O ₈ ClSn	745.19	150–151	80	57.97 (58.00)	4.16 (3.97)	–
6	Bu ₂ SnL ² ₂	C ₃₆ H ₄₄ N ₄ O ₄ Sn	714.19	100–101	68	60.48 (60.21)	6.16 (6.16)	7.84 (7.48)
7	Ph ₃ SnL ²	C ₃₂ H ₂₈ N ₂ O ₂ Sn	590.19	158–160	70	65.06 (64.97)	4.74 (4.69)	4.74 (4.71)
8	BuSnL ² ₃	C ₄₆ H ₄₈ N ₆ O ₆ Sn	898.19	155–157	72	61.45 (60.74)	5.34 (5.50)	9.35 (9.21)
9	BuSnClL ² ₂	C ₃₂ H ₃₅ N ₄ O ₄ ClSn	692.69	219–220	74	55.43 (55.43)	5.05 (4.96)	8.09 (7.29)

IR spectroscopy

The infrared spectra of the prepared compounds were recorded in the range 4000–400 cm⁻¹ as KBr discs. The absorption bands were assigned by comparison with earlier reports^{19,20} and important absorption frequencies, such as $\nu(\text{COO})$, $\nu(\text{Sn-O})$, $\nu(\text{Sn-C})$ and $\nu(\text{O-CH}_2)$ are listed in Table II. In the spectra, medium to weak bands in the region 490–434 cm⁻¹ are assigned to Sn–O, whereas those in the region 571–529 cm⁻¹ indicate the presence of Sn–C bonds.²¹ Complexation by deprotonation of the acid ligand was evidenced by the absence of a $\nu(\text{O-H})$ broad band in the range 3434–3424 cm⁻¹, which was supplemented by the pronounced change in $\Delta\nu$, ($\Delta\nu = \nu(\text{COO})_{\text{asy}} - \nu(\text{COO})_{\text{sym}}$), which is important to describe the tin–carboxylate–chelate interaction.²² Hence, the carboxylate group acts as a bidentate ligand in these complexes in the solid state.

TABLE II. Infrared spectral data (cm⁻¹) of organotin (IV) carboxylates

Compd. No.	Compound	$\nu(\text{COO})$		$\Delta\nu$	$\nu(\text{Sn-C})$	$\nu(\text{Sn-O})$	$\nu(\text{OCH}_2)$ (ring)	$\nu(\text{NH})$
		Asym.	Sym.					
HL ¹	Acid ¹	1695	1420	275	–	–	928	–
1	Me ₂ SnL ¹ ₂	1630	1451	179	539	490	926	–
2	Bu ₂ SnL ¹ ₂	1677	1497	180	537	485	930	–
3	Ph ₃ SnL ¹	1605	1449	156	–	446	927	–
4	BuSnL ¹ ₃	1625	1453	172	531	460	929	–
5	BuSnCIL ¹ ₂	1626	1452	174	535	488	931	–
HL ²	Acid ²	1678	1468	210	–	–	–	3316
6	Bu ₂ SnL ² ₂	1649	1465	184	529	434	–	3304
7	Ph ₃ SnL ²	1608	1427	181	–	473	–	3314
8	BuSnL ² ₃	1635	1446	189	579	461	–	3376
9	BuSnCIL ² ₂	1630	1455	175	571	470	–	3318

¹H-NMR spectroscopy

The characteristic resonance peaks in the ¹H-NMR spectra for the complexes are given in Tables III and IV. The expected resonances are assigned on the basis of their peak multiplicity, intensity pattern and/or tin satellites. The signals due to the –OH group in the acid ligands (HL¹, HL²), at 12.00 and 11.46 ppm, respectively, are absent in all the complexes, which suggests the replacement of the carboxylic proton by the organotin(IV) moiety. The methyl protons of the dimethyltin(IV) derivative appear as a sharp singlet around 1.22 ppm, both with well-defined tin satellites; the coupling constants are included in Tables III and IV.^{23–27} Theoretically, the phenyl ring protons must give doublet of doublets or a double doublet of doublets on the *meta* and *para* positions but the presence of more than one ring in these compounds results in a complex multiplet pattern. It was noticed that in most of these complexes, the ¹H- and ¹³C-NMR signals are broad, hence satellites due to ^{*n*}*J* [¹¹⁹Sn – ¹H] or ^{*n*}*J* [¹¹⁹Sn – ¹³C] couplings are not clearly visible. This shows that there is a competition in the coordination behavior of the carboxylate oxygens for the tin center.

TABLE III. ¹H-NMR data of the organotin(IV) derivatives of α -phenyl-2,3-(methylenedioxy)cinnamic acid^a

¹ H No.	HL ¹ Acid	Me ₂ SnL ¹ ₂	<i>n</i> -Bu ₂ SnL ¹ ₂	Ph ₃ SnL ¹	<i>n</i> -BuSnL ¹ ₃	<i>n</i> -BuCILSnL ¹ ₂
1	5.95 (s)	5.89 (s)	5.89 (s)	5.89 (s)	5.85 (s)	5.88 (s)
3	6.21 (<i>d</i> , 8.4)	6.27 (<i>d</i> , 8.1)	6.25 (<i>d</i> , 8.1)	6.25 (<i>d</i> , 8.1)	6.21 (<i>d</i> , 8.1)	6.23–6.15 (<i>m</i>)
4	6.49 (<i>t</i> , 7.8)	6.52 (<i>t</i> , 7.8)	6.52 (<i>t</i> , 7.8)	6.51 (<i>t</i> , 8.1)	6.52 (<i>t</i> , 7.8)	6.51 (<i>t</i> , 7.8)
5	6.70 (<i>d</i> , 7.5)	6.70 (<i>d</i> , 7.5)	6.51 (<i>d</i> , 7.5)	6.67 (<i>d</i> , 7.8)	6.65 (<i>d</i> , 7.2)	6.69 (<i>d</i> , 7.8)
8	8.05 (<i>m</i>)	8.09 (<i>m</i>)	8.06 (<i>m</i>)	8.06 (<i>m</i>)	8.06 (<i>m</i>)	8.06 (<i>m</i>)
11,11'	7.29–7.26(<i>m</i>)	7.42–7.31 (<i>m</i>)	7.40–7.35 (<i>m</i>)	7.40–7.34 (<i>m</i>)	7.37–7.38 (<i>m</i>)	7.36–7.28 (<i>m</i>)
12,12',13	7.39–7.37 (<i>m</i>)	7.30–7.18 (<i>m</i>)	7.30–7.27 (<i>m</i>)	7.29–7.28 (<i>m</i>)	7.21–7.11 (<i>m</i>)	7.36–7.28 (<i>m</i>)
14	12.00 (s)	–	–	–	–	–
α	–	1.22 ² <i>J</i> [78]	1.65–1.70 (<i>m</i>)	–	1.90–1.96 (<i>m</i>)	1.90–1.96 (<i>m</i>)
β	–	–	–	7.6 (<i>m</i>)	–	–

TABLE III. Continued

¹ H No.	HL ¹ Acid	Me ₂ SnL ¹ ₂	<i>n</i> -Bu ₂ SnL ¹ ₂	Ph ₃ SnL ¹	<i>n</i> -BuSnL ¹ ₃	<i>n</i> -BuClSnL ¹ ₂
γ	–	–	1.35–1.42 (<i>m</i>)	7.45 (<i>m</i>)	1.46–1.39 (<i>m</i>)	1.17–1.15 (<i>m</i>)
δ	–	–	0.89 (<i>t</i> , 7.0)	7.80 (<i>m</i>)	0.86 (<i>t</i> , 7.2)	0.88 (<i>t</i> , 7.0)

^aMultiplicity is given as *s* = singlet, *d* = doublet, *t* = triplet, *m* = multiplet. ³*J* [¹H, ¹H] in Hz are given, along with the multiplicity in parenthesis. Protons α–δ belong to the R groups. ²*J* [¹¹⁹Sn – ¹H] are not visible, except for dimethyl derivative, due to the broadness of the peaks

TABLE IV. ¹H-NMR data of the organotin(IV) derivatives of 2-(2,3-dimethylanilino)nicotinic acid^a

¹ H No.	(HL ²) Acid	<i>n</i> -Bu ₂ SnL ² ₂	Ph ₃ SnL ²	<i>n</i> -BuSnL ² ₃	<i>n</i> -BuClSnL ² ₂
1	7.03 (<i>d</i> , 7.5)	7.02 (<i>d</i> , 6.6)	7.00 (<i>d</i> , 7.5)	6.60 (<i>d</i> , 6.9)	6.67 (<i>d</i> , 7.1)
2	6.72 (<i>d</i> , 5.4)	6.95 (<i>d</i> , 5.5)	6.68 (<i>d</i> , 4.8)	6.62 (<i>d</i> , 6.6)	7.56 (<i>d</i> , 4.7)
3	7.50 (<i>d</i> , 7.8)	7.38 (<i>d</i> , 7.3)	7.16 (<i>d</i> , 7.2)	6.78 (<i>d</i> , 7.9)	7.04 (<i>d</i> , 7.1)
5	2.21 (<i>s</i>)	2.21 (<i>s</i>)	2.36 (<i>s</i>)	2.35 (<i>s</i>)	2.35 (<i>s</i>)
7	2.36 (<i>s</i>)	2.31 (<i>s</i>)	2.18 (<i>s</i>)	2.35 (<i>s</i>)	2.33 (<i>s</i>)
10	8.8 (<i>d</i> , 2.1)	8.40 (<i>d</i> , 3.3)	8.31 (<i>d</i> , 3.0)	8.12 (<i>d</i> , 2.1)	8.78 (<i>d</i>)
11	7.12–7.20 (<i>m</i>)	7.00–7.07 (<i>m</i>)	7.74–7.93 (<i>m</i>)	7.10–7.38 (<i>m</i>)	7.04–7.27 (<i>m</i>)
12	7.57–7.60 (<i>m</i>)	7.72–7.75 (<i>m</i>)	7.58–7.60 (<i>m</i>)	7.73–7.77 (<i>m</i>)	7.04–7.27 (<i>m</i>)
14	11.46 (<i>s</i>)	–	–	–	–
15	5.4 (<i>s</i>)	5.4 (<i>s</i>)	5.4 (<i>s</i>)	5.4 (<i>s</i>)	5.4 (<i>s</i>)
α	–	1.70–1.74 (<i>m</i>)	–	1.90–1.96 (<i>m</i>)	1.90–1.94 (<i>m</i>)
β	–	–	7.50 (<i>m</i>)	–	–
γ	–	1.38–1.45 (<i>m</i>)	7.44 (<i>m</i>)	1.17 (<i>m</i>)	1.15 (<i>m</i>)
δ	–	0.90 (<i>t</i> , 7.0)	7.78 (<i>m</i>)	0.88 (<i>t</i> , 7.0)	0.90 (<i>t</i> , 7.0)

^aMultiplicity is given as *s* = singlet, *d* = doublet, *t* = triplet, *m* = multiplet. ³*J* [¹H, ¹H] in Hz are given, along with the multiplicity in parenthesis. Protons α–δ belong to the R groups.

¹³C-NMR spectroscopy

The characteristic resonance peaks in the ¹³C-NMR spectra of the complexes as well as those of the ligand acids (HL¹, HL²) are given in Tables V and VI. The ¹³C-NMR spectral data for the R– groups attached to the tin atom, where R = Me, *n*-Bu, and Ph, were assigned by the incremental method and comparison with analogous compounds, on the basis of ^{*n*}*J* [¹¹⁹Sn – ¹³C] coupling constants.^{28–31} The carboxylate carbon shifts to a lower field region in all the complexes, indicating participation of the carboxyl group in the coordination to tin(IV).³⁰ For tri-organotin compounds, the magnitudes of the ¹*J* [¹¹⁹Sn – ¹³C] coupling suggest the typical tetrahedral geometry around the tin atom in solution, di-organotin- and mono-organotin derivatives are expected to be octahedral in solution as well as in the solid state.^{1,29,30}

Mass Spectrometry

The fragment ions with their *m/z* (%) values for the compounds are given in Tables VII and VIII. Molecular ion peaks were observed only for complexes **3**, **6** and **7**, while for the other complexes, these were either absent or of very low intensity. In tri-organotin derivatives, the primary decomposition is due to the

loss of the R group, while di-organotin derivatives prefer the elimination of one ligand. Secondary decomposition is a consequence of the loss of either the R group or CO₂ molecules. However, the latter is the more frequent and probable pathway. In case of di-organotin derivatives, primary decomposition is mostly due to the loss of one ligand. However, if primary decomposition is due to the loss of the R group then there is successive elimination of two CO₂ molecules.^{30,31} Complexes with the general formula RSnClL₂ and RSnL₃ behave in a similar manner to di-organotin carboxylates after the release of the chloride ion and L group, respectively. Peaks for [R₃Sn]⁺ and [RSn]⁺ have either very low intensities or are absent, thus indicating that fragmentation through these species is not favorable.

TABLE V. ¹³C-NMR data of the organotin(IV) derivatives of α -phenyl-2,3-(methylenedioxy)cinnamic acid^a

¹³ C No.	(HL ¹) Acid	Me ₂ SnL ¹ ₂	<i>n</i> -Bu ₂ SnL ¹ ₂	Ph ₃ SnL ¹	<i>n</i> -BuSnL ¹ ₃	<i>n</i> -BuClSnL ¹ ₂
1	101.22	101.11	101.08	101.01	101.01	101.18
2	147.43	147.35	147.35	147.28	147.22	147.37
3	109.28	108.98	108.87	108.62	108.79	113.51
4	121.74	121.88	121.89	121.94	121.78	121.75
5	121.08	121.05	121.00	120.73	120.85	121.05
6	116.90	117.25	117.38	117.68	117.41	116.93
7	147.38	147.06	147.02	146.79	147.32	137.47
8	135.23	136.86	136.11	135.72	136.12	136.27
9	132.24	137.18	137.19	137.50	137.87	137.77
10	134.59	132.89	133.84	133.86	129.06	134.99
11,11'	128.14	127.96	126.79	126.53	126.52	126.52
12,12'	131.19	129.70	128.70	128.88	128.69	128.49
13	129.74	128.46	128.07	128.45	128.19	128.12
14	172.92	177.15	176.98	176.47	177.81	177.21
α	–	4.92	22.68 [654]	129.30 [611]	22.73	24.17
β	–	–	22.72	137.0	31.96	24.17
γ	–	–	13.65	128.88	26.00	25.79
δ	–	–	13.65	128.19	13.70	13.63

^a¹J [¹¹⁹Sn – ¹³C] is only visible for the di-*n*-butyl and triphenyl derivative and are given in square brackets, while it could not be measured for the others due to broadness of the peaks. Carbons α – δ belong to the R groups

TABLE VI. ¹³C-NMR data of the organotin(IV) derivatives of 2-(2,3-dimethylanilino)nicotinic acid^a

¹³ C No.	(HL ²) Acid	Bu ₂ SnL ² ₂	Ph ₃ SnL ²	<i>n</i> -BuSnL ² ₃	<i>n</i> -BuClSnL ² ₂
1	112.59	114.04	112.11	112.38	112.61
2	126.71	125.59	126.03	126.77	126.50
3	122.12	122.13	121.98	121.87	122.08
4	137.70	136.74	137.91	137.58	137.08
5	20.70	19.61	20.86	20.78	20.78
6	125.87	125.45	125.59	125.32	125.95
7	13.90	13.06	13.85	13.41	13.64

TABLE VI. Continued

¹³ C No.	(HL ²) Acid	Bu ₂ SnL ² ₂	Ph ₃ SnL ²	<i>n</i> -BuSnL ² ₃	<i>n</i> -BuClSnL ² ₂
8	142.16	142.27	141.94	141.82	141.50
9	161.32	167.64	161.90	161.60	161.03
10	156.80	152.83	153.45	157.44	155.97
11	120.80	119.63	119.45	120.36	120.89
12	137.86	137.28	137.33	137.58	137.19
13	108.87	108.99	107.45	109.38	108.61
14	171.27	173.45	173.59	173.65	173.85
α	–	19.93 [650]	129.02 [615]	20.70	13.92
β	–	20.21	137.33	27.75	22.72
γ	–	26.01	128.60	26.67	26.35
δ	–	13.36	129.02	13.92	14.16

^{a1J} [¹¹⁹Sn – ¹³C] is only visible for the di-*n*-butyl and triphenyl derivative and are given in square brackets, while it could not be measured for the others due to broadness of the peaks. Carbons α – δ belong to the R groups

TABLE VII. Mass spectral data (*m/z* (%)) of the organotin(IV) complexes of α -phenyl-2,3-(methylenedioxy)cinnamic acid at 70 eV

Fragment ion	Me ₂ SnL ¹ ₂	<i>n</i> -Bu ₂ SnL ¹ ₂	Ph ₃ SnL ¹	<i>n</i> -BuSnL ¹ ₃	<i>n</i> -BuSnClL ¹ ₂
[R ₂ SnOO] ⁺	182(6)	209(8)	306(7)	–	–
[R ₃ Sn] ⁺	–	–	351(10)	–	–
[RSn] ⁺	135(15)	177(10)	197(12)	177(7)	177(9)
[C ₆ H ₄] ⁺	76(11)	76(9)	76(16)	76(11)	76(16)
[Sn] ⁺	120(6)	120(5)	120(8)	120(5)	120(4)
[OCOL ¹] ⁺	268(24)	268(67)	268(19)	268(94)	268(84)
[C ₁₅ H ₁₁ O ₂] ⁺	223(12)	223(26)	223(5)	223(32)	223(44)
[SnO ₂ CH ₂] ⁺	165(100)	165(100)	–	165(100)	165(100)
[C ₄ H ₉] ⁺	–	–	57(100)	–	–

Table VIII. Mass spectral data (*m/z* (%)) of organotin(IV) complexes of 2-(2,3-dimethylamino) nicotinic acid at 70 eV

Fragment ion	<i>n</i> -Bu ₂ SnL ² ₂	Ph ₃ SnL ²	<i>n</i> -BuSnL ² ₃	<i>n</i> -BuSnClL ² ₂
[R ₂ SnOO] ⁺	–	306(5)	–	–
[R ₃ Sn] ⁺	–	351(60)	–	–
[RSn] ⁺	177(3)	195(37)	177(11)	177(3)
[C ₆ H ₄] ⁺	76(48)	76(456)	76(63)	76(22)
[Sn] ⁺	120(22)	120(6)	120(32)	120(53)
[OCOL ²] ⁺	242(67)	242(6)	242(66)	242(33)
[C ₁₃ H ₁₁ N ₂ O ₂] ⁺	227(100)	–	–	–
[C ₆ H ₄ O ₂ N] ⁺	–	–	–	122(100)
[C ₁₃ H ₁₃ N ₂] ⁺	197(68)	197(100)	197(100)	197(54)

CONCLUSIONS

Organotin(IV) derivatives were synthesized in quantitative yield by refluxing the synthesized carboxylic acids and respective organotin(IV) compounds in dry toluene. Elemental analyses showed good agreement between the calculated

and observed % of C, H and N. It is proposed from the FT-IR spectral data that the organotin(IV) moieties react with the [O,O] atoms of the ligand, which behaves as bidentate. NMR data showed that the bidentate nature of carboxylate group is probably lost in solution and that the tri-organotin(IV) derivatives contained four-coordinated tin with a tetrahedral arrangement, while the mono- and di-organotin(IV) derivatives exhibit penta- or hexa-coordinated geometry due to fluxional behavior.

Acknowledgements. M. Hussain and M. Hanif are thankful to the Higher Education Commission, Pakistan for financial support. M. Hanif is also thankful to PAEC (Pakistan Atomic Energy Commission) for study leave.

ИЗВОД

СИНТЕЗА И СТРУКТУРНА КАРАКТЕРИЗАЦИЈА ОРГАНОКАЛАЈ(IV) КОМПЛЕКСА СА [O,O] ДОНОРИМА КАРБОКСИЛНИХ КИСЕЛИНА

MUKHTIAR HUSSAIN¹, MUHAMMAD ZAMAN¹, MUHAMMAD HANIF¹, SAQIB ALI¹ и MUHAMMAD DANISH²

¹Department of Chemistry, Quaid-i-Azam University, Islamabad-45320 и ²Department of Chemistry, University of Sargodha, Sargodha, Pakistan

У раду су добијени органокалај(IV)-карбоксилати опште формуле R_nSnL_{4-n} (где је R = Me, n-Bu и Ph група, а L = α -фенил-2,3-(метилендиокси)-цинаматни анјон и 2-(2,3-диметиланилино)-никотинатни анјон). Моно-, ди- и три- органокалај(IV) карбоксилати синтетисани су реакцијом органокалајних оксида или хидроксида са стехиометријском количином киселине на повишеној температури у сувом толуену. Састав изолованих органокалај(IV)-комплекса, понашање везујућих донорских група и структурно означавање испитивани су елементалном анализом, FT-IR, ¹H-, ¹³C-NMR и масеном спектрометријом. Спектрални подаци указују на то да је лиганд бидентантно везан, координирајући се преко кисеоникових атома. Ове спектроскопске технике потврдиле су дисторговану тетраедарску геометрију у раствору за триорганокалај, а координациони број између пет и шест за диорганокалај(IV)-дикарбоксилате. У чврстом стању, три-органокалајна једињења су претежно тригонално-бипирамидални полимери, а ди-органокалајна октаедарска. Међутим, за моноорганокалајне трикарбоксилате предложено је да су октаедарски, и у раствору и у чврстој фази.

(Примљено 14. маја, ревидирано 22. октобра 2007)

REFERENCES

1. M. Gielen and E. R. T. Tiekink, in *Metallotherapeutic Drug and Metal-based Diagnostic Agents: Tin Compounds and Their Therapeutic Potential*, M. Gielen and E. R. T. Tiekink Eds., Wiley, New York, 2005, p. 421
2. W. Seinen and M. I. Willems, *Toxicol. Appl. Pharmacol.* **35** (1976) 63
3. K. Miller, M. P. Scott, J. R. Foster, *Clin. Immunol. Immunopathol.* **30** (1983) 62
4. M. Gielen, P. Lelieveld, D. de Vos, R. Willem, in *Metal Complexes in Cancer Chemotherapy*, B. K. Keppler Ed., VCH, Weinheim, 1993, p. 369.
5. M. Gielen, M. Biesmans, R. Willem, E. R. T. Tiekink, *Eur. J. Inorg. Chem.* (2004) 445
6. V. I. Bregade, S. A. Glazun, P. V. Petrovski, Z. A. Starikova, V. Y. Rochev, H. Dalil, M. Biesmans, R. Willem M. Gielen, D. de Vos, *Appl. Organomet. Chem.* **17** (2003) 453
7. M. Gielen, *J. Braz. Chem. Soc.* **14** (2003) 870

8. S. W. Ng, V. G. K. Das, *J. Crystallogr. Spectrosc. Res.* **23** (1993) 925
9. A. K. Saxena, F. Huber, *Coord. Chem. Rev.* **95** (1989) 109
10. M. Gielen, *Coord. Chem. Rev.* **151** (1996) 41
11. M. Gielen, *Appl. Organomet. Chem.* **16** (2002) 481
12. P. Yang, M. Guo, *Coord. Chem. Rev.* **185** (1999) 41
13. T. P. Lockhart, *Organometallics* **7** (1988) 1438
14. J. Meunier-Piret, M. Boualam, R. Willem, M. Giellen, *Main Group Met. Chem.* **16** (1993) 329
15. G. Prabusankar, R. Murugavel, *Organometallics* **23** (2004) 5644
16. W. L. F. Armarego, C. L. L. Chai, *Purification of Laboratory Chemicals*, 5th Ed., Butterworth-Heinemann, New York, 2003
17. A. Altmore, M. Cascarano, C. Giacobozzo, A. Guagliardi, SIR92, *J. Appl. Cryst.* **26** (1993) 343
18. E. A. Nodiff, K. Tanabe, C. Seyfried, S. Matsuura, Y. Kondo, E. H. Chen, M. P. Tyagi, *J. Med. Chem.* **14** (1971) 921
19. M. A. Chaudhary, M. Mazhar, S. Ali, X. Song, G. Eng, *Met. Based Drugs* **8** (2002) 275
20. X. N. Fang, X. Q. Song, Q. L. Xie, *J. Organomet. Chem.* **619** (2001) 43
21. Q. L. Xie, Z. Q. Yang, Z. X. Zhang, *Appl. Organomet. Chem.* **6** (1992) 193
22. B. Y. K. Ho, J. J. Zuckerman, *Inorg. Chem.* **12** (1973) 1552
23. D. H. Williams, I. Fleming, *Spectroscopic Methods in Organic Chemistry*, 4th Ed., McGraw-Hill Book Company (UK) Ltd., 1987
24. R. Twari, G. Srivastava, R. C. Mehrotra, A. J. Crowe, *Inorg. Chim. Acta* **111** (1986) 161
25. A. Saxena, J. P. Tandon, *Polyhedron* **3** (1984) 681
26. P. G. Harrison, *Chemistry of Tin*, Blackie Academic and Professional, Glasgow, 1989
27. A. Badshah, M. Danish, S. Ali, M. Mazhar, S. Mahmood, M. I. Choudhry, *Synth. React. Inorg. Met.-Org. Chem.* **24** (1994) 1155
28. H. O. Kalinowski, S. Berger, S. Brown, *¹³C NMR Spektroskopie*, Thieme, Stuttgart, 1984
29. M. Gielen, A. Tzschach, M. Biesmans, F. Kayser, R. Willem, *J. Fluorine Chem.* **64** (1993) 279
30. M. Danish, S. Ali, M. Mazhar, A. Badshah, M. I. Choudhary, H.G. Alt, G. Kehr, *Polyhedron* **14** (1995) 3115
31. M. Gielen, M. Boualam, E. R. T. Tiekink, *Appl. Organomet. Chem.* **8** (1994) 19.



www.shd.org.yu

J. Serb. Chem. Soc. 73 (2) 189–195 (2008)

JSCS–3701

Journal of
the Serbian
Chemical Society



JSCS@tmf.bg.ac.yu • www.shd.org.yu/JSCS

UDC 519.17:547.233'237+546.922:547.97

Original scientific paper

Q-Conjugacy character and Markaracter tables of tetraammineplatinum(II)

ALI MOGHANI*

Department of Color Physics, Institute for Colorants, Paints and Coatings (ICPC), Tehran, Iran

(Received 7 May, revised 8 June 2007)

Abstract: The Q-conjugacy character and Markaracter tables of finite groups were introduced by Fujita, who applied his results in this area of research to enumerate isomers of molecules. In this paper, these tables are computed for tetraammineplatinum(II).

Keywords: Q-conjugacy character table; tetraammineplatinum(II); pigments.

INTRODUCTION

The enumeration of chemical compounds has been accomplished by various methods.^{1–3}

The Pólya–Redfield theorem is a standard method for combinatorial enumerations of graphs, polyhedra and chemical compounds. Only finite groups are treated throughout this paper. The notation is standard and mainly taken from Ref. 4 and the papers by Fujita.^{5–17}

For the sake of completeness, some necessary definitions are mentioned below.

Definition 1. Let G be a finite group and $h_1, h_2 \in G$. If there exists $t \in G$ such that $t^{-1} < h_1 > t = < h_2 >$, then h_1, h_2 are said to be Q-conjugate and are denoted by $h_1 \sim_Q h_2$.

It is easy to see that the Q-conjugacy is an equivalence relation and generates equivalence classes which are called dominant classes, *i.e.*, the group G is partitioned into dominant classes as follows: $G = K_1 + K_2 + \dots + K_s$.

Definition 2. A permutation representation P of a finite group G is obtained when the group G acts on a finite set $X = \{x_1, x_2, \dots, x_t\}$ from the right, which means that one is given a mapping $P: X \times G \rightarrow X$ via $(x, g) \rightarrow xg$ such that the following holds: $(xg)g' = x(gg')$ and $x_1 = x$ for each $g, g' \in G$ and $x \in X$.

Now let it be assumed that one is given an action P of G on X and a subgroup H of G . One considers the set of its right cosets H_{g_i} and the corresponding partition of G into these cosets: $G = H_{g_1} + H_{g_2} + \dots + H_{g_m}$. If the cosets from the right are multiplied by a group element g , these cosets are permuted, in fact one

* E-mail: moghani@icrc.ac.ir

doi: 10.2298/JSC0802189M

obtains an action of G on the set X of cosets and, correspondingly, a permutation representation which is denoted by G/H , following Fujita's notation. When H and H' are conjugate subgroups of G then the induced or coset-representations G/H and G/H' are equivalent.

Recalling from the theory of group actions that the sets $xG = \{xg \mid g \in G\}$, the orbits, form a set partition of X and that the action is called transitive if there is exactly one such orbit. Fujita⁶⁻¹¹ introduced the notations SSG_G and $SCSG_G$. A group contained in $SCSG_G$ is called a dominant subgroup. Any action of G on X induces the set partition of X into its orbits, *i.e.*, into transitive permutation representations. Moreover it can easily be seen that a complete set of pairwise inequivalent transitive permutation representations is formed by the set $\{G/G_1, \dots, G/G_r\}$. Thus each permutation is a unique linear combination $P = \sum \alpha_i G/G_i$ (*). The multiplicities α_i can be obtained by using the table of marks⁵ introduced by Burnside.¹²⁻¹⁷

Definition 3. The table of marks of G is the matrix $M(G) = (m_{ik}), \{1 \leq i, k \leq r\}$, where m_{ik} is the number of right cosets of G_k in G which remain fixed under right multiplication by the elements of G_i , $m_{ik} = |\{G_k \mid \text{for all } s \in G_i : G_k s = G_k\}|$.¹⁸ If $M(G)$ is restricted to rows and columns that belong to cyclic groups, the Markaracter table of G^9 is obtained and denote it by M^C .

Definition 4. Let H be a cyclic subgroup of G , the maturity of a finite group G is defined by examining how a dominant class (Q-conjugacy class) corresponding to H contains conjugacy classes. If the integer $m(H) = |N_G(H)|/|C_G(H)|$ (called the maturity discriminant) is less than $\varphi(|H|)$ where φ is the Euler function, the group G is concluded to be unmatured concerning H , where $N_G(H)$ and $C_G(H)$ denote the normalizer and centralizer of H within G , respectively.

Corollary 5. Let H be a cyclic group of G , the dominant class $K \cap H$ in the normalizer $N_G(H)$ is the union of $t = \varphi(|H|)/m(H)$ conjugacy classes of G , see Refs. 12-17.

Definition 6. Let $C_{u \times u}$ be the matrix of the character table of G . $C_{u \times u}$ is transformed to a more concise form called the Q-conjugacy character table, the $s \times s$ -matrix of which is denoted by $C^Q(s \leq u)$ as follows: if $u = s$ then $C = C^Q$, *i.e.*, G is a maturated group. Otherwise $s < u$, according to Corollary 5 and Definition 2, since the dimension of the Q-conjugacy character table is equal to that of the corresponding Markaracter table¹² for each $G_i \in SCSG_G$ and the corresponding dominant class K_i , where $i = 1, \dots, s$.

If $t = 1$ (K_i is exactly a conjugacy class), then there is no reduction in row and column of C but if $t > 1$ (K_i is a union of t conjugacy classes of G , *i.e.*, reduction in column), then the sum of the t -rows of irreducible characters, *via* the same degree in C (reduction in rows), give one a reducible character, which are called Q-conjugacy characters in both cases. See Section 2.2 of Ref. 12 and in the special case (Q-conjugacy characters of cyclic groups) Ref. 5 for more details.

COMPUTATIONAL METHOD AND DISCUSSION

Here, a free software package for group theory, named GAP (Groups, Algorithms and Programming), which greatly facilitates these calculations (see <http://www.gap-system.org>), should be brought to the attention of the spectroscopy community. For example, the table of marks of any finite group G is afforded by the following command: "TableOfMarks(G)".

The full, non-rigid group and symmetry properties of tetraammineplatinum(II) of order 5184 with C_{2v} and C_{4v} point groups were computed.^{19,20}

Let G be the symmetry group of tetraammineplatinum(II) (see Fig. 1), then by the following program in GAP:

```
gap>G:=Group((2,3,4,5)(6,9,12,15,7,10,13,16,8,11,14,17),(2,3,4,5)(6,9,12,15,7,10,
13,17,8,11,14,16),(2,5)(3,4)(6,15)(7,17)(8,16)(9,12)(10,14)(11,13));
gap> t:=TableOfMarks(G); Sort("t");
gap> c:=CharacterTable(G);
gap>Display(t); Display(c);
```

one obtains the mark and the character tables of tetraammineplatinum(II), hence its $SCSG_G$ can be calculated as follows:

$$SCSG_G = \{G_1 = \text{id}, G_2 = \langle (6,7,8)(9,11,10)(12,14,13)(15,16,17) \rangle,$$

$$G_3 = \langle (9,11,10)(15,16,17) \rangle, G_4 = \langle (12,14,13)(15,17,16) \rangle,$$

$$G_5 = \langle (6,7,8)(9,11,10)(12,13,14) \rangle, G_6 = \langle (15,16,17) \rangle, G_7 = \langle (6,7,8)$$

$$(9,11,10)(12,14,13)(15,17,16) \rangle,$$

$$G_8 = \langle (9,11,10)(15,16,17), (6,7,8)(9,11,10)(12,14,13)(15,16,17) \rangle,$$

$$G_9 = \langle (12,14,13)(15,17,16), (6,7,8)(9,11,10)(12,14,13)(15,16,17) \rangle,$$

$$G_{10} = \langle (12,14,13)(15,17,16), (9,11,10)(15,16,17) \rangle,$$

$$G_{11} = \langle (12,14,13)(15,17,16), (6,7,8)(9,10,11)(12,14,13)(15,17,16) \rangle,$$

$$G_{12} = \langle (6,7,8)(9,11,10)(12,13,14), (9,11,10)(15,16,17) \rangle,$$

$$G_{13} = \langle (15,16,17), (6,7,8)(9,11,10)(12,14,13)(15,16,17) \rangle,$$

$$G_{14} = \langle (15,16,17), (9,11,10)(15,16,17) \rangle, G_{15} = \langle (15,16,17), (6,8,7)(12,13,14) \rangle,$$

$$G_{16} = \langle (15,16,17), (12,14,13)(15,17,16) \rangle,$$

$$G_{17} = \langle (15,16,17), (9,11,10)(15,16,17), (6,7,8)(9,11,10)(12,14,13)(15,16,17) \rangle,$$

$$G_{18} = \langle (15,16,17), (12,14,13)(15,17,16), (6,7,8)(9,11,10)(12,14,13)(15,16,17) \rangle,$$

$$G_{19} = \langle (12,13,14), (9,11,10)(12,14,13), (6,7,8)(9,10,11)(12,14,13)(15,16,17), (12,$$

$$14,13)(15,17,16), (2,4)(3,5)(6,12,7,13,8,14)(9,15,10,16,11,17) \rangle,$$

$$G_{20} = \langle (12,14,13)(15,17,16), (6,7,8)(9,10,11)(12,14,13)(15,17,16),$$

$$(2,4)(3,5)(6,12,7,13,8,14)(9,15,10,16,11,17) \rangle,$$

$$G_{21} = \langle (15,16,17), (9,11,10)(15,16,17), (2,4)(3,5)(6,14)(7,12)(8,13)(9,17)(10,15)$$

$$(11,16) \rangle,$$

$$G_{22} = \langle (6,7,8)(9,11,10)(12,14,13)(15,17,16), (6,8,7)(12,13,14), (2,4)(3,5)(6,14)(7,$$

$$12)(8,13)(9,17)(10,15)(11,16) \rangle,$$

$$G_{23} = \langle (7,8)(10,11)(13,14)(16,17) \rangle,$$

$$G_{24} = \langle (6,7,8)(9,11,10)(12,14,13)(15,16,17), (7,8)(10,11)(13,14)(16,17) \rangle,$$

$$\begin{aligned}
G_{25} &= \langle (15,16,17), (7,8)(10,11)(13,14)(16,17) \rangle, \\
G_{26} &= \langle (12,14,13)(15,17,16), (6,7,8)(9,11,10)(12,14,13)(15,16,17), (7,8)(10,11)(13,14)(16,17) \rangle, \\
G_{27} &= \langle (12,14,13)(15,17,16), (9,11,10)(15,16,17), (7,8)(10,11)(13,14)(16,17) \rangle, \\
G_{28} &= \langle (15,16,17), (6,8,7)(12,13,14), (7,8)(10,11)(13,14)(16,17) \rangle, \\
G_{29} &= \langle (15,16,17), (6,8,7)(9,10,11)(15,16,17), (7,8)(10,11)(13,14)(16,17) \rangle, \\
G_{30} &= \langle (6,7,8)(9,11,10)(12,14,13)(15,17,16), (9,11,10)(15,16,17), (7,8)(10,11)(13,14)(16,17) \rangle, \\
G_{31} &= \langle (6,7,8)(9,11,10)(12,14,13)(15,17,16), (12,14,13)(15,17,16), (7,8)(10,11)(13,14)(16,17) \rangle, \\
G_{32} &= \langle (6,8,7)(9,10,11)(12,13,14), (9,10,11)(12,14,13)(15,16,17), (7,8)(10,11)(13,14)(16,17) \rangle, \\
G_{33} &= \langle (6,7,8)(15,16,17), (9,11,10)(15,16,17), (12,14,13)(15,17,16), (7,8)(10,11)(13,14)(16,17) \rangle, \\
G_{34} &= \langle (6,7,8)(12,14,13), (9,11,10), (15,16,17), (7,8)(10,11)(13,14)(16,17) \rangle, \\
G_{35} &= \langle (15,16,17), (12,14,13)(15,17,16), (6,7,8)(9,11,10)(12,14,13)(15,16,17), (7,8)(10,11)(13,14)(16,17) \rangle, \\
G_{36} &= \langle (15,16,17), (12,14,13)(15,17,16), (9,11,10)(15,16,17), (7,8)(10,11)(13,14)(16,17) \rangle, \\
G_{37} &= \langle (6,7,8)(9,11,10)(12,14,13)(15,17,16), (12,14,13)(15,17,16), (9,11,10)(15,16,17), (7,8)(10,11)(13,14)(16,17) \rangle, \\
G_{38} &= \langle (9,11)(15,16) \rangle, G_{39} = \langle (6,8,7)(12,13,14), (6,7,8)(9,10)(12,14,13)(15,17) \rangle, \\
G_{40} &= \langle (15,16,17), (9,11)(15,16) \rangle, G_{41} = \langle (12,14,13), (9,11)(12,14,13)(16,17) \rangle, \\
G_{42} &= \langle (6,8,7)(12,13,14), (15,16,17), (6,7,8)(9,10)(12,14,13)(15,17) \rangle, \\
G_{43} &= \langle (6,7,8)(12,14,13), (9,11,10)(15,16,17), (3,5)(6,7)(9,15)(10,17)(11,16)(13,14) \rangle, \\
G_{44} &= \langle (6,8,7), (12,14,13), (3,5)(6,7)(9,15)(10,17)(11,16)(13,14) \rangle, \\
G_{45} &= \langle (6,7,8)(12,14,13), (9,11,10), (15,16,17), (3,5)(6,7)(9,15)(10,17)(11,16)(13,14) \rangle.
\end{aligned}$$

Now by Definitions 4 and 6, the 45×45 matrices M^C and C^Q of G can be found, which are given in Tables I and II, respectively. Therefore the symmetry of tetraammineplatinum(II) is an unmatred group of order 5184. The reader is encouraged to consult Refs. 20–23 for other monster molecules and pigments.

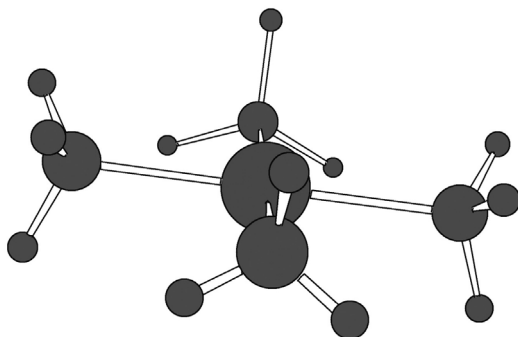


Fig 1. The structure of tetraammineplatinum(II).

ИЗВОД
ТАБЛИЦЕ КАРАКТЕРА Q-КОНЈУГАЦИЈЕ И МАРК-КАРАКТЕРА ЗА
ТЕТРААМИН-ПЛАТИНУ(II)

ALI MOGHANI

Department of Color Physics, Institute for Colorants, Paints and Coatings (ICPC), Tehran, Iran

Fujita је увео таблицу карактера Q-конјугације и таблицу марк-карактера, применивши их за пребројавање изомера. У овом раду ове две таблице су израчунате за тетраамин-платину(II).

(Примљено 7. маја, ревидирано 8. јуна 2007)

REFERENCES

1. N. S. Barta, J. R. Stille, *J. Chem. Educ.* **71** (1994) 20
2. P. S. Beauchamp, *J. Chem. Educ.* **61** (1984) 666
3. A. Kerbe, K. Thurlings, *Combinatorial Theory*, Springer, Berlin, 1982, p. 191
4. J. H. Conway, R. T. Curtis, S. P. Norton, R. A. Parker, R. A. Wilson, *Atlas of Finite Groups*, Oxford University Press, Oxford, 1985
5. S. Fujita, *Bull. Chem. Soc. Jpn.* **71** (1998) 2071
6. S. Fujita, *J. Graph Theory* **18** (1994) 349
7. S. Fujita, *J. Org. Chem.* **67** (2002) 6055
8. S. Fujita, *J. Comput. Chem. Jpn.* (2004) 113
9. S. Fujita, *Theor. Chim. Acta* **91** (1995) 291
10. S. Fujita, *J. Math. Chem.* **5** (1989) 99
11. S. Fujita, *J. Math. Chem.* **12** (1999) 173
12. S. Fujita, *Bull. Chem. Soc. Jpn.* **71** (1998) 2309
13. S. Fujita, *MATCH Commun. Math. Comput. Chem.* **54** (2005) 251
14. S. Fujita, *MATCH Commun. Math. Comput. Chem.* **55** (2006) 5
15. S. Fujita, *MATCH Commun. Math. Comput. Chem.* **55** (2006) 237
16. S. Fujita, *MATCH Commun. Math. Comput. Chem.* **57** (2007) 5
17. S. Fujita, *Diagrammatical Approach to Molecular Symmetry and Enumeration of Stereoisomers*, MCM, Kragujevac, 2007
18. A. Kerber, *MATCH Commun. Math. Comput. Chem.* **46** (2002) 151
19. A. R. Ashrafi, M. Hamadani, *Croat. Chem. Acta* **76** (2003) 299
20. A. Moghani, A. R. Ashrafi, M. Hamadani, *J. Zhejiang Univ. Sci.* **6B** (2005) 222
21. M. R. Darafsheh, Y. Farjami, A. R. Ashrafi, *Bull. Chem. Soc. Jpn.* **78** (2005) 996
22. A. Moghani, A. R. Ashrafi, *Croat. Chem. Acta* **79** (2006) 465
23. A. Moghani, S. Naghdi, A. R. Ashrafi, A. Ahmadi, *London Math. Soc.* **340** (2007) 630.



www.shd.org.yu

J. Serb. Chem. Soc. 73 (2) 197–209 (2008)

JSCS–3702

JSCS@tmf.bg.ac.yu • www.shd.org.yu/JSCS

UDC 546–328+54–145.2:543.422.25

Original scientific paper

A study of 12-tungstosilicic and 12-molybdophosphoric acids in solution

DANICA BAJUK-BOGDANOVIĆ¹, IVANKA HOLCLAJTNER-ANTUNOVIĆ^{1*#},
MARIJA TODOROVIĆ², UBAVKA B. MIOČ^{1#} and JOANNA ZAKRZEWSKA³

¹Faculty of Physical Chemistry, P.O. Box 47, 11158 Belgrade 118, ²Faculty of Chemistry,
P.O. Box 157, 11001 Belgrade and ³Institute of General and
Physical Chemistry, P.O. Box 551, 11001 Belgrade, Serbia

(Received 21 February, revised 19 September 2007)

Abstract: The behaviour of two heteropolyacids (HPAs) with quite different stability in aqueous solutions was systematically investigated by UV, IR and NMR spectroscopy and potentiometric titration. It was shown that the Keggin structure of 12-tungstosilicic acid ($H_4SiW_{12}O_{40}$, WSiA) anion was sustained over a wide range of pH from 1.0 to 7.0, while the same anion type of 12-molybdophosphoric acid ($H_3PMo_{12}O_{40}$, MoPA) was present only at pH 1.0. This means that under physiological conditions WSiA is dominantly present in the form of a Keggin-anion, whereas the structure of MoPA is completely decomposed to molybdate and phosphate. The obtained results are of special importance for bio-medical and catalytic applications of these compounds and for a better understanding of the mechanism of their action.

Keywords: heteropolyacids of Keggin structure; 12-tungstosilicic acid; 12-molybdophosphoric acid; hydro-stability; UV; IR and NMR spectroscopy.

INTRODUCTION

Polyoxometalates (POMs) of various classes are very interesting compounds with unusual behaviour: they are good catalysts, superionic proton conductors, compounds with photoconductive and magnetic characteristics and biochemical active species.^{1–6}

The properties of POMs in the solid state are extensively studied and rather well established but their behaviour in the liquid state is not well understood and explained in spite of numerous publications. However, the behaviour of these interesting compounds in solution is important from the aspect of their bio-medical and catalytic applications and from the aspect of their formation and degradation.

For more than 20 years, the antiviral, antitumour and anticoagulant activities of POMs have been studied.^{1–3,6} A fundamental limitations in the interpretation

* Corresponding author. E-mail: ivanka@ffh.bg.ac.yu

Serbian Chemical Society member.

doi: 10.2298/JSC0802197B

and application of the results on the behaviour of these compounds in physiological media, as well as their application as biochemical active compounds derives from their nature and equilibrium between different molecular forms in aqueous solutions. Namely, the problem of all biological/medicinal investigations of POMs is whether these compounds reside in their original form during biomedical treatment, and for how long and under which conditions. Generally, it is considered that the parent form of the POMs anion is active.^{1-3,6} In order to consider and elucidate the proper mechanism of the bio-medical activity of POMs, it is indispensable to identify the real active species under physiological conditions, both *in vitro* and *in vivo*.

Due to their properties, POMs are also used as catalysts in oxidation reactions, in acid catalyzed reactions and as bifunctional catalysts both in homogeneous and heterogeneous catalysis.^{1-3,7,8} With the purpose of improving the catalytic characteristics of these compounds and explaining the mechanism of their action, it is also (as in the case of bio-medical applications) important to specify the nature of the active species present. Many studies considered the hydro stability of heteropolyacids (HPA), mostly of Keggin type, and their reaction pathways in solution.^{1,3,9-15}

It was shown that many POMs degrade into a mixture of inorganic products in aqueous solution.¹ Kepert and Kyle^{16,17} studied the decomposition of Keggin anions containing silicon, phosphorus or boron as the central, heteroatom and tungsten as the addenda metal atom. These authors found that the equilibrium reaction in solution proceeds in three distinct stages, with $[\text{SiW}_{11}\text{O}_{39}]^{8-}$ and $[\text{SiW}_9\text{O}_{34}]^{10-}$ as intermediates. A few years later, stopped-flow kinetics studies of 12-molybdophosphate formation and decomposition were performed by Kircher and Crouch.¹⁸ Molybdophosphate complexes in aqueous solutions were identified by ^{31}P -NMR and Raman spectroscopy, as well as by differential pulse polarography.¹⁹ Additionally, ^{31}P -NMR spectroscopy was applied in a stability study of HPAs through the rate of exchange of structural units between WPA and MoPA.¹⁵ Moreover, McGarvey and Moffat followed the major species present in tungstophosphate and molybdophosphate solutions as a function of pH by NMR and IR spectroscopy.¹³ They found that both acids decompose to a lacunary form of the Keggin anion, which further decomposes to phosphate species in alkaline solutions. The same system was investigated over a wide pH range (1–12) using preparative high performance liquid chromatography combined with IR, UV–Vis and ICP spectroscopy.^{20,21} Smith and Patrick applied ^{31}P - and ^{183}W -NMR spectroscopy in a detailed study of tungstophosphoric and tungstosilicic acids in aqueous solutions.²²⁻²⁴ The species present in these systems were identified and quantified as a function of pH.

The conclusions reached in all these studies were not consistent, although the conditions of the investigations were similar. Generally, it can be concluded

that the hydrolytic stability of HPAs depends on the anion structure, the nature of the heteroatom and the peripheral metal atom which comprise the anion, as well as on the conditions of the solution.

The aim of this study was to investigate thoroughly the behaviour of two HPAs of the Keggin type with quite different hydro-stability, *i.e.*, 12-phosphorsilicic (WSiA) and 12-molybdophosphoric (MoPA) acids, in order to contribute to a better explanation of their base hydrolysis. For this purpose, UV, IR and ^{31}P -NMR spectroscopic methods and potentiometric titration were applied and the results were summarized and compared in order to determine the dominant species present in aqueous solutions at various pH values, with special attention to physiological conditions.

EXPERIMENTAL

Materials

MoPA was prepared by literature method²⁵ and confirmed by infrared spectroscopy, while WSiA was commercially available (Fluka). Both acids were recrystallized prior to use.

Methods

The pH values of the solutions were adjusted by the addition of NaOH or HCl solutions and measured using a pH meter with a glass electrode. The pH values of the solutions were monitored until no apparent changes were observed. The samples were prepared one day prior to the measurements.

The UV spectra of aqueous 2.0×10^{-5} mol dm⁻³ solutions of the HPAs were obtained using a Cintra 10e (GBS) spectrophotometer.

Solid samples for IR measurements were obtained by evaporation of the water from 5.0×10^{-2} mol dm⁻³ solutions of the HPAs of different pH values. The IR spectra were recorded on a Perkin-Elmer 983G spectrophotometer using the KBr pellets technique, in the wave number range 1500–300 cm⁻¹, where the bands characteristic for Keggin anions are to be found.

Sample solutions for NMR measurement were prepared by adding the estimated quantities of NaOH just after dissolving. The NMR experiments were performed with a Bruker MSL 400 spectrometer at 161.978 MHz. The concentration of the HPAs was 5.0×10^{-2} mol dm⁻³, with 2048 scans, 9.0 μs pulse and 500 ms repetition time at 25 °C. The sample volume was about 2.5 ml in a 10 mm tube. Methylenediphosphonate (MDP) at 17.05 ppm was used as the external reference relative to 85 % H₃PO₄.

The UV, IR and ^{31}P -NMR spectra were recorded at pH values of 1.0, 2.0, 3.5, 5.0, 7.0, 8.5, 10 and 11.5.

Potentiometric titrations were performed by adding 0.192 mol l⁻¹ NaOH standard aqueous solution into each of the solutions of the HPAs (20 ml, 0.064 mol l⁻¹ MoPA and 0.087 mol l⁻¹ WSiA) at a rate of 2 drops per second at room temperature.

RESULTS AND DISCUSSION

UV Spectra

In the UV range, the electronic spectra of HPAs having a Keggin structure exhibit two intense absorption bands at about 200 and 260 nm, attributed to the transitions O_d-M and O_b/O_c-M, respectively.²⁶

The UV spectra of the WSiA solutions at various pH values, presented in Fig. 1, show that this HPA was stable in the pH range from 1.0 to 8.5, with an absorption maximum at 262.6 nm. This band disappeared in solutions of higher pH values.

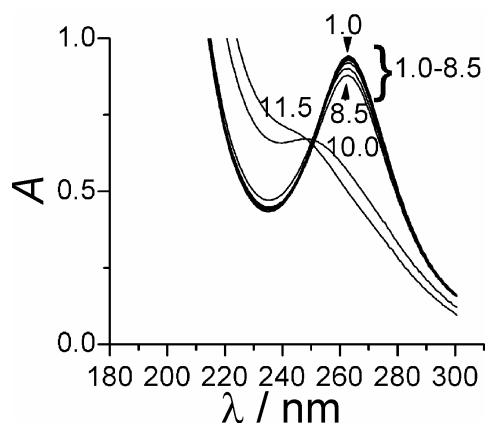


Fig. 1. UV spectra of WSiA solutions of various pH values.

In contrast, the UV spectra of the MoPA solutions changed drastically in the pH range from 1.0 to 7.0 (Fig. 2a) but remained unchanged with further increase in the pH value of the solution (Fig. 2b). This finding could be explained by the fact that the Keggin anions were completely decomposed into PO_4^{3-} and MoO_4^{2-} at pH 7.0. At pH 1.0 and 2.0, the absorption maximum was at about 220 nm, while at pH 3.5 and 5.0, there was a maximum at 210 nm with shoulder at about 230 nm (Fig. 2a).

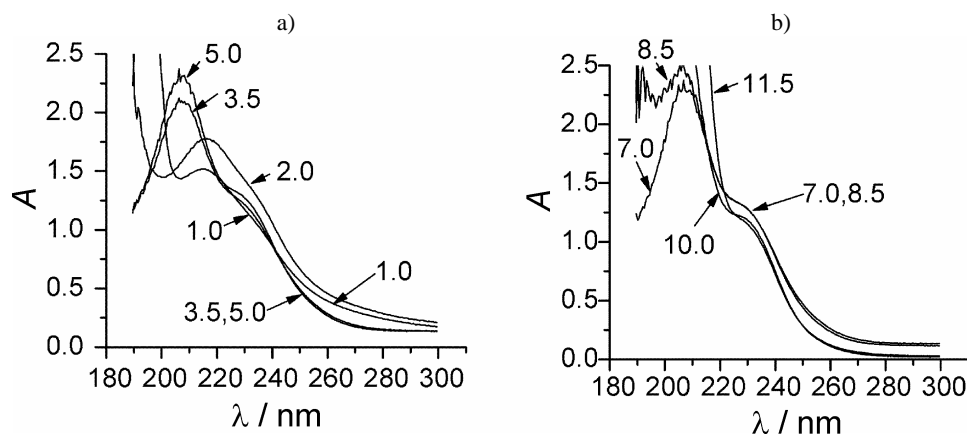


Fig. 2. UV Spectra of MoPA solutions of various pH values:
a) from pH 1.0 to 5.0 and b) from pH 7.0 to 11.5.

All the changes in the UV spectra of HPA solutions of different pH can be attributed to changes in the structure of the individual forms of the HPAs. However, it is difficult to conclude about the nature of the observed changes and to identify with certainty the formed products.

IR Spectra

IR Spectra of evaporated and dried sample solutions were recorded over the same pH range 1.0 to 11.5 as in the case of the UV spectra and are presented in Figs. 3 and 4. It is necessary to point out that although the pH values of solutions changed during evaporation of the water, there was no reversible change of the given forms of HPAs to the parent Keggin anion.

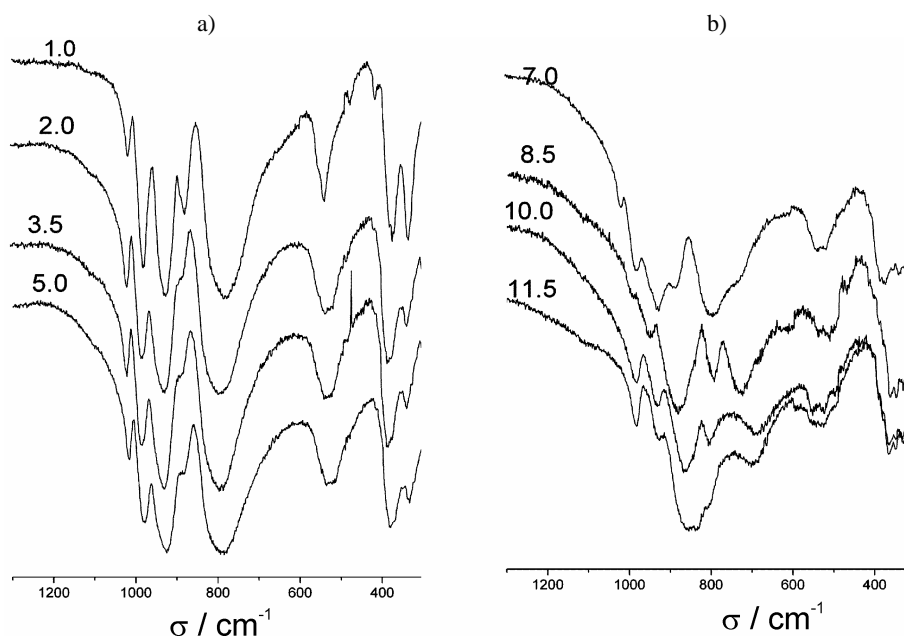


Fig. 3. IR Spectra of evaporated aqueous WSiA solutions of various pH values:
a) from pH 1.0 to 5.0 and b) from pH 7.0 to 11.5.

As in the case of the UV spectra, the changes in the IR spectra of the dry residues of aqueous solutions of WSiA (Fig. 3) appeared at higher pH values than in the case of MoPA. The spectrum at pH 1 corresponds to the spectrum of solid acid. It is characterized by four bands characteristic for the Keggin anion $[\text{SiW}_{12}\text{O}_{40}]^{4-}$: 981, 928, 880 and 785 cm^{-1} ,²⁷ corresponding to vibrations $\nu_{\text{as}}(\text{W}-\text{O}_{\text{d}})$, $\nu_{\text{as}}(\text{Si}-\text{O}_{\text{a}})$, $\nu_{\text{as}}(\text{W}-\text{O}_{\text{b}}-\text{W})$ and $\nu_{\text{as}}(\text{W}-\text{O}_{\text{c}}-\text{W})$, respectively.

It can be noticed from the data given in Fig. 3 and Table I, that there was almost no change in the positions of the characteristic bands for samples up to pH 7.0, confirming that the Keggin anion was preserved in the solutions up to this pH value. However, the first changes in spectrum were registered at pH 7.0, which indicate the appearance of some new species in solution. This species present at pH 8.5 can be identified as the lacunary anion, $[\text{SiW}_{11}\text{O}_{39}]^{8-}$, characterized by bands at 952, 885, 870, 797 and 725 cm^{-1} .²⁸ Some of these bands disappeared at pH 10 and pH 11.5. It is evident that at pH 11.5, the WSiA had

completely decomposed to SiO_4^{4-} (bands at about 1000 cm^{-1}) and WO_4^{2-} ions (bands at about $860, 700$ and 525 cm^{-1}).

TABLE I. Vibration bands for the solid residues of aqueous WSiA solutions of various pH values

pH							
1.0	2.0	3.5	5.0	7.0	8.5	10.0	11.5
1017w	1017m	1016m	1016m	1018w			
					1000sh		
980s	979s	979s	978s	980w		982w	983w
					952w		
925vs	924vs	926vs	925vs	923m			927sh
879sh	880sh	880sh	880sh	880w	885s,b		
					865sh	868s,b	860s,b
800vs,b	800vs,b	800vs,b	800vs,b	800vs,b	795m	807w	
					726s,b		
						690w,b	700w,b
538m	535m,b	535m,b	535m,b	535m,b	530m,b	530m,b	525w,b
373m	383m	380m	380m	375m			
					360w	360w	365w
334m	335w	335w	335w	335w			
					325w	324w	321w

The present results are in accordance with the generally accepted knowledge that tungstosilicates are more stable than other tungsten heteropolyanions. A general scheme for the decomposition of WSiA in aqueous solution with increasing pH was proposed in the literature.^{16,17} In the first stage, $[\text{SiW}_{12}\text{O}_{40}]^{4-}$ is hydrolyzed to the lacunary $[\text{SiW}_{11}\text{O}_{39}]^{8-}$ anion, a further increase in the pH results in the formation of the $[\text{SiW}_9\text{O}_{34}]^{10-}$ anion, which finally decomposes to SiO_4^{2-} and WO_4^{2-} . A quantitative determination of speciation of WSiA over the pH range 3–13.5, performed by Smith and Patrick by NMR spectroscopy,²² showed that the Keggin $[\text{SiW}_{12}\text{O}_{40}]^{4-}$ anion is stable up to pH 3.7; the main component in the pH range from 3.8–9.2 is the lacunary $[\text{SiW}_{11}\text{O}_{39}]^{8-}$ monovacant anion, which is decomposed with further increase in the pH value. The present results confirm that the decomposition pathways of WSiA in solution proceed through the formation of the lacunary monovacant anion, which is completely decomposed at $\text{pH} > 8.5$. However, contrary to the findings of Smith and Patrick,²² the presented UV and IR spectra show that the Keggin anion is stable up to pH 7.0. Based on IR spectra, it can also be concluded that the degradation to tungstate and silicate occurs in alkaline solution of $\text{pH} > 10.0$.

The IR spectra recorded for the samples of MoPA are shown in Fig. 4, while the major vibration bands are listed in Table II. It can be seen that only spectrum at pH 1.0 of dry residue of aqueous solution of acid have the four characteristic bands of the Keggin anion $[\text{PMo}_{12}\text{O}_{40}]^{3-}$ at $1067, 975, 870$ and 810 cm^{-1} .²⁷ The

changes in the spectrum started even at pH 2.0. The splitting of the band corresponding to the vibration P–O into two bands at about 1063 and 1035 cm^{-1} can be ascribed to the presence of the lacunary $[\text{PMo}_{11}\text{O}_{39}]^{6-}$ anion.¹³ The spectra for pH 2.0 and 3.5 are complex, indicating the presence of different structures, which cannot be exactly identified from the IR spectra. At pH 5.0, the decomposition of the MoPA anion to molybdate and phosphate commenced. In alkaline solutions (pH > 7.0), complete decomposition is evident. In contrast to these results, Song and Barteau²⁹ found no change in the IR spectra of $\text{H}_3\text{PMo}_{12}\text{O}_{40}$ evaporated from aqueous solutions of pH 2.6–3.1. The authors explained their results as being the consequence of the short time interval between acid dissolution and IR measurements (20 min). However, in the present study it was found that equilibrium with respect to the decomposition process was attained within the time required to prepare the solutions for WSiA and MoPA, which is in accordance with the conclusions of Jurgensen and Moffat.³⁰

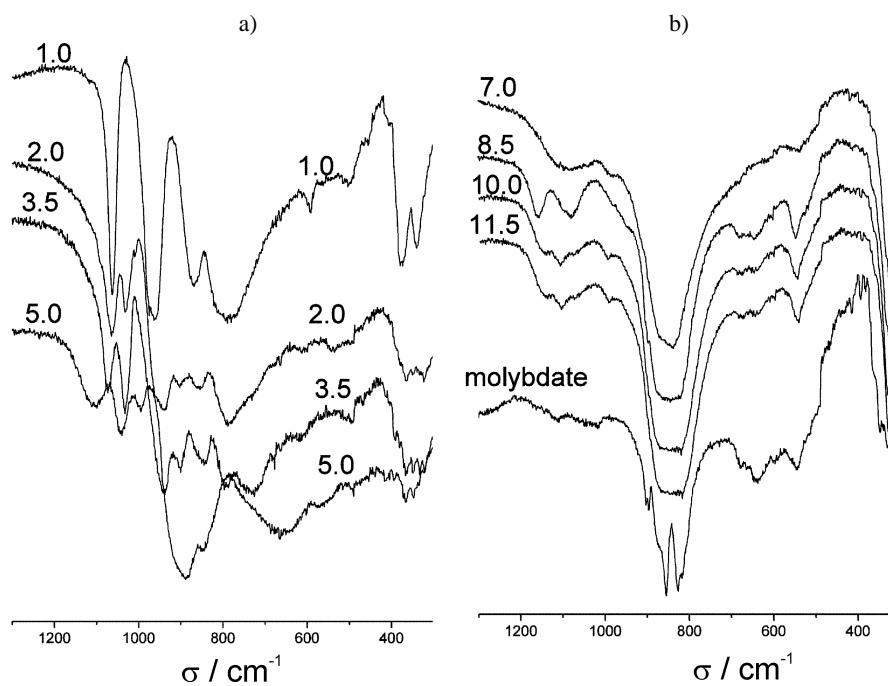


Fig. 4. IR Spectra of evaporated aqueous MoPA solutions of various pH values: a) from pH 1.0 to 5.0 and b) from pH 7.0 to 11.5.

The solutions of MoPA, in contrast to other solutions of HPAs, are coloured and with increasing pH values, the change in their colour can be followed visually, *i.e.*, from the intense yellow of the pure acid, through green to light blue at pH > 5.0, which indicates the reduction of molybdenum.

It is obvious that pH influences the stability of both the investigated HPAs but in different ways. The present results indicate that the Keggin anion of WSiA is sustained in aqueous solutions up to pH 7.0, while this structure of MoPA is present only at pH 1.0, with other Keggin anion structures appearing with further increase in the pH value.

TABLE II. Vibration bands for the solid residues of aqueous MoPA solutions of various pH values

pH								Molybdate
1.0	2.0	3.5	5.0	7.0	8.5	10.0	11.5	
					1155 <i>m</i>	1157 <i>sh</i>	1155 <i>sh</i>	
			1099 <i>m</i>			1107 <i>w</i>	1107 <i>w</i>	
		1074 <i>s</i>		1077 <i>w,b</i>	1079 <i>m</i>			
1063 <i>s</i>	1065 <i>s</i>							
	1032 <i>m</i>	1033 <i>s</i>	1040 <i>s</i>					
			995 <i>m</i>	983 <i>sh</i>		995 <i>vw</i>	995 <i>vw</i>	
964 <i>vs</i>								
	940 <i>w,b</i>	938 <i>m</i>			937 <i>sh</i>			
	903 <i>vw</i>	901 <i>w</i>						902 <i>w</i>
			889 <i>vs,b</i>					880 <i>sh</i>
869 <i>s</i>	855 <i>vw,b</i>	846 <i>w</i>	848 <i>sh</i>	836 <i>w</i>	844 <i>vs,b</i>	845 <i>vs,b</i>	843 <i>vs,b</i>	855 <i>vs</i>
								827 <i>vs</i>
790 <i>vs,b</i>	789 <i>m,b</i>	797 <i>w</i>						
		726 <i>w</i>						
			660 <i>m,b</i>					
					675 <i>w</i>	674 <i>w</i>	674 <i>w</i>	680 <i>w</i>
					645 <i>w</i>	643 <i>w</i>	650 <i>w</i>	640 <i>w</i>
592 <i>w</i>								
				536 <i>w</i>	546 <i>m</i>	545 <i>m</i>	544 <i>m</i>	547 <i>w</i>
504 <i>w</i>								
459 <i>sh</i>								
374 <i>m</i>	365 <i>w</i>	365 <i>w</i>	365 <i>w</i>					
341 <i>m</i>								
	324 <i>w</i>	325 <i>w</i>	325 <i>w</i>	320 <i>s</i>	320 <i>s</i>	318 <i>s</i>	318 <i>s</i>	320 <i>s</i>

All the changes in the UV spectra of the HPAs solutions of different pH can be attributed to changes in the structure of the individual HPA, but identification of the formed products is limited. The IR spectra present a further improvement in the identification of the dominant chemical species present in the HPAs solutions of differing pH, in relation to the UV spectra, but it is difficult to identify all the structures present. The IR spectra at higher pH values indicate the total degradation of the parent anion to tungstate and silicate or molybdate and phosphate anions.

NMR Spectra

In order to overcome the drawbacks of UV and IR spectroscopy in the identification of molybdophosphate species in solutions of differing pH values, the complementary method of ^{31}P -NMR spectroscopy was applied.

The ^{31}P -NMR spectra and chemical shifts of the peaks for solutions of MoPA of different pH values are shown in Fig. 5 and Table III, respectively. At pH 1.0, the most intensive peak corresponding to $[\text{PMo}_{12}\text{O}_{40}]^{3-}$ is at -2.87 ppm, while the peaks at -2.16 ppm and -0.65 can be assigned to $[\text{P}_2\text{Mo}_{18}\text{O}_{62}]^{6-}$ and $[\text{Mo}_9\text{PO}_{31}\text{OH}(\text{OH}_2)_2]^{4-}$, respectively.^{19,31} The presence of these structures manifests the very complex reaction pathway of MoPA in acidic solution. The most intensive peaks in solutions of pH 2.0 (-0.95 ppm) and 3.5 (-0.77 ppm) correspond to the lacunary $[\text{PMo}_{11}\text{O}_{39}]^{6-}$ ion, which is the dominant component under these conditions. In solution with pH 5.0, the strong peak with a chemical shift of 2.15 ppm is ascribed to $[\text{P}_2\text{Mo}_5\text{O}_{23}]^{6-}$, a structure with two P atoms, the peak at 0.65 ppm is assigned to $[\text{PMo}_6\text{O}_{25}]^{9-}$ and the peak at -0.49 ppm is assigned to $[\text{PMo}_{11}\text{O}_{39}]^{6-}$.³¹ The difference between chemical shifts of the $[\text{PMo}_{11}\text{O}_{39}]^{6-}$ ion observed at low and at high pH (at -0.95 to -0.49 ppm, respectively) can be explained by extensive protonation.¹⁹ In solutions of pH 7.0 and higher, peaks corresponding to phosphate ions, H_2PO_4^- , HPO_4^{2-} and PO_4^{3-} appear, which means that the complex structure of MoPA is completely destroyed under physiological conditions.

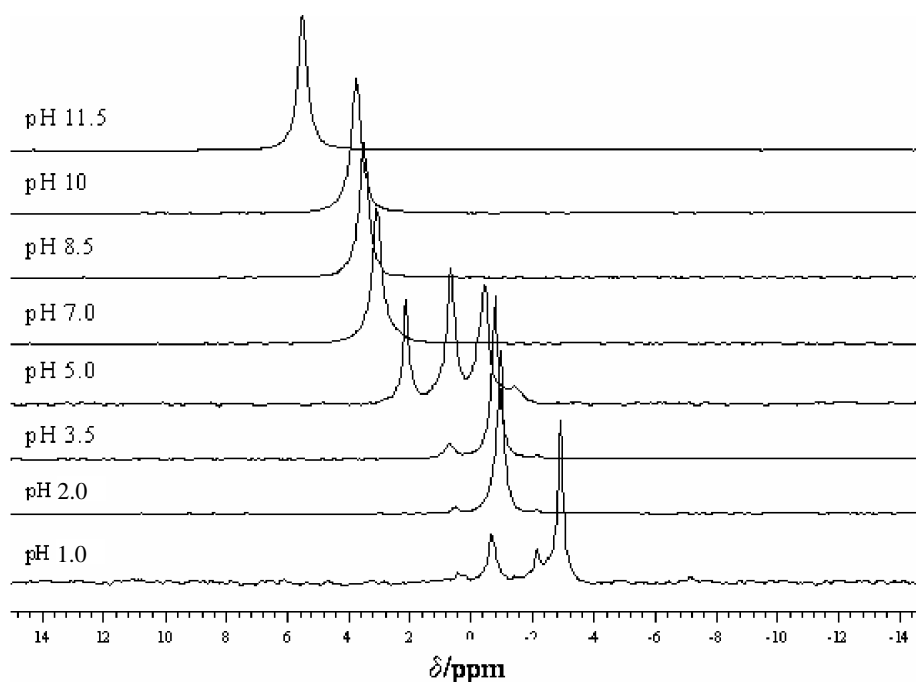


Fig. 5. ^{31}P -NMR Spectra of MoPA solutions of different pH values.

Table III. Chemical shifts of the signals in the ^{31}P -NMR spectra of MoPA solutions of various pH values

pH	1.0	2.0	3.5	5.0	7.0	8.5	10.0	11.5
Chemical shift, ppm	0.44	0.53	0.71	2.15	3.10	3.51	3.78	5.50
	-0.65	-0.95	-0.77	0.65	-	-	-	-
	-2.16	-2.16	-2.16	-0.49	-	-	-	-
	-2.87	-	-	-1.39	-	-	-	-

Potentiometric titration

The potentiometric titrations showed how the pH of the solutions of the HPAs changed on addition of 0.192 mol l^{-1} NaOH. Initially, the pH increased slowly from pH 1.7 to 3.0 as the NaOH was added. Continued addition of NaOH to the solution of WSiA led to a rapid increase in the pH, with the endpoint at a hydroxide to acid ratio of 4.0 (Fig. 6a). This is in accordance with conclusions obtained from the spectroscopic results. In this pH region, WSiA is stable and behaves as a tetrabasic acid in water. On the contrary, the potentiometric titration of MoPA, $\text{H}_3[\text{PMo}_{12}\text{O}_{40}]$ showed a broad endpoint at about 4 mole equivalences of base at $\text{pH} \approx 3.8$ (Fig. 6b). The spectroscopic results showed that at this pH value, the Keggin anion is decomposed and that aqueous solutions of MoPA contain mixture of various species, resulting in a higher basicity than expected based on its parent structure.

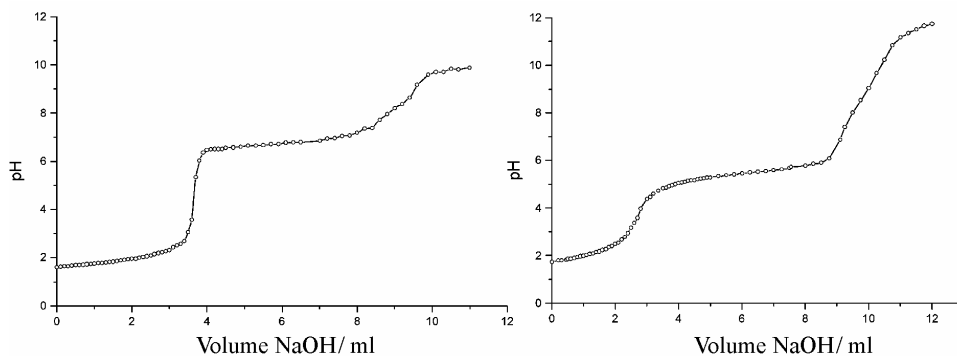


Fig. 6. Potentiometric curves for the base decomposition of:
a) $\text{H}_4[\text{SiW}_{12}\text{O}_{40}]$ and b) $\text{H}_3[\text{PMo}_{12}\text{O}_{40}]$.

Further addition of base to the acid solution caused no change in the pH, indicating the ability of the POMs to maintain the pH of the solution, *i.e.*, both acids have a high buffering capacity.

The second broad endpoint in the potentiometric curve signifies the total decomposition of the HPAs.

It is evident that the electrochemical results are in agreement with the spectroscopic ones.

CONCLUSIONS

In this study, special attention was placed on the importance of the molecular species of the POMs present in solution and their role in catalytic and biochemical and biomedical processes on a molecular level. When POMs are employed as catalysts for homogeneous or heterogeneous catalysis, their activity depends on the general characteristics of the solution, *i.e.*, the nature of the solvent—organic or aqueous, their concentration, the pH of the solution and the reduction potential of the hetero- and addenda atoms, as well as on the strength of the acid centres. Such studies are important if one wishes to follow the mechanism of catalytic processes, the formation of activation complexes, as well as in formation of complex catalysts on different supports by the sol–gel process or impregnation. All the bonds formed in the activation complexes and between the substrate and the parent catalysts depend on the molecular forms of the POMs.

It would seem that hitherto in spite of the large number of references, insufficient attention has been paid to this problem. In order to contribute to the solution of the molecular forms of the PMOs existing in solution, spectroscopic methods, *i.e.*, UV, IR and ^{31}P -NMR spectroscopy, and a potentiometric method were employed to gain more information.

It can be concluded that all the spectroscopic methods employed in this work indicate the existence of different forms of HPAs in aqueous solutions with a considerable dependence on pH with regard to the parent acid. Considering this, literature data are not always consistent due to the complexity of the system; many factors influence the equilibrium, primarily the pH and concentration of the HPA, while the performances of different analytical techniques used for identification should also be taken into account.

Based on the results presented in this paper, the following can be concluded: UV spectroscopy only indicates that some changes occur in the system but they cannot be specified with certainty. IR Spectroscopy gives more information, which enables the identification of the dominant species as a function of the pH of the solution. However, in some cases, because of the similar spectra, it is not possible to perform an exact identification of the major components. NMR Spectroscopy provides unique data which can be employed for more accurate interpretations of the changes in the solutions in dependence on pH.

The presented results indicate that the reaction pathway of MoPA in acidic solution is very complex. Only at pH 1.0 is the parent Keggin anion the dominant molecular form, with additionally two other minor components, $[\text{P}_2\text{Mo}_{18}\text{O}_{62}]^{6-}$ and $[\text{Mo}_9\text{PO}_3\text{OH}(\text{OH}_2)_2]^{4-}$. The main component in solutions of pH 2.0 and 3.5 was the lacunary $[\text{PMo}_{11}\text{O}_{39}]^{6-}$ anion. In the solution of pH 5.0, in addition to the lacunary anion, $[\text{P}_2\text{Mo}_5\text{O}_{23}]^{6-}$ and $[\text{PMo}_6\text{O}_{25}]^{9-}$ ions were present. In the solution of pH 7.0, and in more alkaline solutions, complete decomposition to phosphate and molybdate occurred.

The results concerning aqueous solutions of WSiA confirmed that the tungstosilicate is more stable than the molybdophosphate and that the decomposition pathways of WSiA in solution proceed *via* the formation of the lacunary monovacant anion, which decomposes into SiO_4^{2-} and WO_4^{2-} at $\text{pH} > 8.5$. However, in contrast to literature data, it was shown that the Keggin anion structure is preserved over a wide range of pH values, from pH 1.0 to 7.0.

Considering the activity of POMs, it is not sufficient to define only the concentration of the POM, but also the molecular forms of the species present in solution under the experimental conditions. It is important to point out that under physiological conditions WSiA is dominantly present as the Keggin anion, while the parent structure of MoPA is completely destroyed.

These conclusions are of special importance for both biomedical and catalytic applications of heteropolyacids and other compounds of this type and for a better understanding of the mechanism of their activities.

Acknowledgement. This study was financially supported by the Serbian Ministry of Science (Grant 142047/2006).

ИЗВОД

ИСПИТИВАЊЕ 12-СИЛИЦИЈУМВОЛФРАМОВЕ И 12-ФОСФОРМОЛИБДЕНОВЕ КИСЕЛИНЕ У РАСТВОРУ

ДАНИЦА БАЈУК-БОГДАНОВИЋ¹, ИВАНКА ХОЛЦЛАЈТНЕР-АНТУНОВИЋ¹, МАРИЈА ТОДОРОВИЋ²,
УБАВКА Б. МИОЧ¹ И JOANNA ZAKRZEWSKA³

¹Факултет за физичку хемију, бр. 47, 11158 Београд 118, ²Хемијски факултет, бр. 157, 11001 Београд и
³Институт за општу и физичку хемију, бр. 551, 11001 Београд

У раду је систематски испитано понашање две хетерополи-киселине (НРА) различите стабилности у воденом раствору, применом метода UV, IR и NMR спектроскопије и потенциометријске титрације. Показано је да је структура родитељског анјона 12-силицијумволфрамове киселине (WSiA) сачувана у широкој области pH вредности, од 1,0 до 7,0, док је иста структура анјона 12-фосформолибденеве киселине (MoPA) присутна само при pH 1,0. Ово значи да је при физиолошким условима WSiA присутна у облику Кегиновог анјона, док је структура анјона МоРА потпуно разграђена до фосфата и молибдата. Добијени резултати су од посебног значаја за биомедицинске и каталитичке примене ових једињења као и за боље разумевање механизма њиховог деловања.

(Примљено 21. фебруара, ревидирано 19. септембра 2007)

REFERENCES

1. M. T. Pope, *Heteropoly and Isopoly Oxometalates*, Springer-Verlag, Berlin, 1983
2. M. T. Pope, A. Muller, *Polyoxometalates: From Platonic Solids to Anti-Retroviral Activity*, Kluwer Academic Publishers, Dordrecht, 1994
3. M. T. Pope, A. Muller, *Polyoxometalates Chemistry, From Topology via Self-Assembly to Applications*, Kluwer Academic Publishers, Dordrecht, 2001
4. U. Mioč, Ph. Colomban, A. Novak, *J. Mol. Struct.* **218** (1990) 123

5. U. B. Mioč, M. R. Todorović, M. Davidović, Ph. Colomban, I. Holclajtner–Antunović, *Solid State Ionics* **176** (2005) 2837
6. J. T. Rhule, C. L. Hill, D. A. Judd, R. F. Schinazi, *Chem. Rev.* **98** (1998) 327
7. I. V. Kozhevnikov, *Chem. Rev.* **98** (1998) 171
8. N. Mizuno, M. Misono, *Chem. Rev.* **98** (1998) 199
9. A. Teze, G. Herve, *Inorg. Synth.* **27** (1990) 85
10. G. F. Tourne, C.M. Tourne, *Top. Mol. Org. Eng.* **10** (1994) 59
11. L. C. W. Baker, M. T. Pope, *J. Am. Chem. Soc.* **82** (1960) 4176
12. C. Hill, M. Weeks, R. Schinazi, *J. Med. Chem.* **33** (1990) 2767
13. G. B. McGarvey, J. B. Moffat, *J. Mol. Catal.* **69** (1991) 137
14. M. Witvrouw, H. Weigold, C. Pannecouque, D. Schols, E. De Clerq, G. Holan, *J. Med. Chem.* **43** (2000) 778
15. M. A. Schwegler, J. A. Peters, H. van Bekkum, *J. Mol. Catal.* **63** (1990) 343
16. D. L. Kepert, J. H. Kyle, *J. Chem. Soc. Dalton Trans.* (1978) 137
17. D. L. Kepert, J. H. Kyle, *J. Chem. Soc. Dalton Trans.* (1978) 1781
18. C. C. Kircher, S. R. Crouch, *Anal. Chem.* **55** (1983) 242
19. J. A. R. van Veen, O. Sudmeijer, C. A. Emeis, H. de Wit, *J. Chem. Dalton Trans.* (1986) 1825
20. Z. Zhu, R. Tain, C. Rhodes, *Can. J. Chem.* **81** (2003) 1044
21. J. Toufaily, M. Soulard, J.–L. Guth, T. Hamieh, M.–B. Fadlallah, *J. Phys. IV France* **113** (2004) 155
22. B. Smith, V. Patrick, *Aus. J. Chem.* **55** (2002) 281
23. B. Smith, V. Patrick, *Aus. J. Chem.* **56** (2003) 283
24. B. Smith, V. Patrick, *Aus. J. Chem.* **57** (2004) 261
25. N. V. Apolonov, E. M. Feklichev, N. V. Timofeeva, A. Kalashnikov, V. E. Svinticki, *Dokl. ANSSSR* **191** (1970) 1048
26. J. Liu, W. J. Mei, *Antivir. Res.* **62** (2004) 65
27. C. Rocchiccioli–Deltcheff, M. Fournier, R. Franck, R. Thouvenot, *Inorg. Chem.* **22** (1983) 207
28. D. Li, Y. Guo, C. Hu, L. Mao, E. Wang, *Appl. Catal. A: General* **235** (2002); G. N. Alekar, *Ph.D. Thesis*, (2000) University of Pune, India
29. I. Song, M. Barteau, *J. Mol. Catal. A* **212** (2004) 229
30. A. Jurgensen, J. Moffat, *Catal. Lett.* **34** (1995) 237
31. L. Petterson, I. Andersson, L. O. Ohman, *Inorg. Chem.* **25** (1986) 4726.



www.shd.org.yu

J. Serb. Chem. Soc. 73 (2) 211–219 (2008)

JSCS–3703

JSCS@tmf.bg.ac.yu • www.shd.org.yu/JSCS

UDC 546.74'22+66.094.3:531.3+541.124

Original scientific paper

Mechanism and kinetics of the oxidation of synthetic α -NiS

NADA ŠTRBAC^{1#}, DRAGANA ŽIVKOVIĆ^{1*#}, IVAN MIHAJLOVIĆ^{1#},
BOYAN BOYANOV² and ŽIVAN ŽIVKOVIĆ¹

¹University of Belgrade, Technical Faculty, Vojske Jugoslavije 12, Bor, Serbia and

²University "Paisiy Hilendarsky", Tsar Assen 24, 4000 Plovdiv, Bulgaria

(Received 29 March, revised 4 September 2007)

Abstract: The results of an investigation of the mechanism and kinetics of the oxidation process of synthetic α -NiS are presented in this paper. The mechanism of α -NiS oxidation was investigated based on the comparative analysis of DTA–TG–DTG and XRD results, as well as the constructed phase stability diagrams (PSD) for the Ni–S–O system. The kinetic investigations of the oxidation process were performed under isothermal conditions (temperature range 823–1073 K). The obtained degrees of desulfurization were used in the calculation process according to the Sharp model and the kinetic parameters, including the activation energies and the rate constants of the characteristic reactions, for the oxidation of α -NiS were determined. These results enabled the formulation of a kinetic equation for the desulfurization process: $-\ln(1 - \alpha) = k_1\tau = 27.89 \exp(-9860/T)\tau$, with an activation energy of 82 ± 4 kJ mol⁻¹, for the first stage of the process and $-\ln(1 - \alpha) = k_2\tau = 1.177 \exp(-4810/T)\tau$, with an activation energy of 40 ± 2 kJ mol⁻¹, for the second stage.

Keywords: α -NiS; oxidation; mechanism; kinetics; DTA.

INTRODUCTION

Knowledge of the mechanism and kinetics for oxidation processes of metallic sulfides is of great significance in practical applications.^{1–3} The problematic nickel sulfides (millerite – NiS, heazlewoodite – Ni₃S₂, pentlandite – (Fe,Ni)₉S₈, etc.) oxidation processes have been the subject of investigation,^{4–13} due to their importance in nickel metallurgy. However, the documentation concerning on this subject is still incomplete and some discrepancy may be noticed when comparing different references.

Regarding to the mechanism of NiS oxidation, Dunn and Kelly⁴ explored the oxidation of synthetic millerite (Ni_{0.994}S) using DTA, TG and MS analyses up to 1273 K and defined the following: a) complete oxidation of millerite followed by

Serbian Chemical Society member.

* Corresponding author. E-mail: dzivkovic@tf.bor.ac.yu

doi: 10.2298/JSC0802211S

the formation of NiSO₄, Ni₃S₂ and NiO in the temperature range 823–973 K; b) continuation of NiSO₄ formation and oxidation of Ni₃S₂ between 973 and 1073 K and c) the existence of only NiO above 1073 K. The newest research dealing with the oxidation of α -NiS is presented in the work of Wang *et al.*,⁶ in which a three-step mechanism, including 1) the oxidation of α -NiS to NiO, occurring in the temperature range 943–953 K; 2) oxidation of α -NiS to Ni₃S₂ at 973 K and 3) oxidation of Ni₃S₂ to NiO above 973 K. Ni₃S₂ is a transient/intermediate species during the oxidation of α -NiS and is not an end product of α -NiS oxidation once the reaction reaches equilibrium.

The kinetics of the processes occurring during the oxidation of NiS was also investigated by Wang *et al.*^{6,12} and Bishop *et al.*,¹¹ in which the values of the characteristic kinetic parameters were given.

As a contribution to a better understanding of the process of α -NiS oxidation, the results of an investigation of the mechanism and kinetics of the oxidation of synthetic α -NiS are presented in this paper.

EXPERIMENTAL

The main characteristics of different nickel(II) sulfide types¹ are presented in Table I, one of which, *i.e.*, α -NiS, was synthesized and investigated in this study.

TABLE I. The main characteristics of different types of nickel(II) sulfide types¹

Nickel sulfide	Color	Crystal structure	Melting temperature, K	Solubility
α -NiS	Black	Amorphous	–	HCl
β -NiS	Black	NiAs type	810	HCl
γ -NiS	Black	Hexagonal	–	Sparingly in dilute HCl

Synthesis of α -NiS samples

Samples of α -NiS synthesized at the University “Paisiy Hilendarsky”, Plovdiv, Bulgaria, were used in this investigation.

The α -NiS sample was synthesized according to the following procedure: an aqueous solution of Na₂S was added slowly in proportions to an aqueous solution of NiSO₄ under continuous stirring with a magnetic bar, whereby nickel sulfide precipitated. The black precipitate of α -NiS was washed a few times with water and filtered. The filtered precipitate was placed in a crucible and then dried in a furnace at 373 (1 h), 473 (1 h) and 673 K (5 h). In order to prevent the oxidation of the obtained α -NiS, all operations are performed in a nitrogen environment, for which special equipment was created.^{15,16}

Applied experimental techniques

The analyses of the thermal behavior and mass changes of the starting sample during oxidation under non-isothermal conditions were performed using the results of simultaneous DTA–TG–DTG analysis. The thermal analysis was performed using a Derivatograph-Q (MOM, Hungary) with the conditions: sensitivity DTA – 1 mV and DTG – 1 mV, TG – 100 mg, heating rate of 10 °C min⁻¹, sample mass 100 mg and T_{\max} = 1273 K. A ceramic crucible was used. All experiments were performed in an air atmosphere.

X-Ray diffraction analysis was performed in order to characterize the investigated samples after oxidative roasting at different temperatures. The phase composition was determined

on a Siemens X-ray equipment with a Cu anticathode and Ni filter at a voltage of 40 kV and a current of 18 mA.

The investigations under isothermal conditions were performed using standard equipment. The experiments were performed using an electric resistance furnace with thermostatic control. A measured volume of air was introduced into the reaction volume, while the gaseous reaction products (mainly SO_2) were passed from the furnace tube to absorption tubes filled with an aqueous solution of hydrogen peroxide, whereby sulfuric acid was produced. The formed sulfuric acid produced was titrated against a standard solution of sodium hydroxide in the presence of indicator to determine of the sulfur content. Thus, the degree of desulfurization during oxidation roasting was calculated with an error expected to be $\pm 0.1\%$.

RESULTS AND DISCUSSION

Mechanism of synthetic α -NiS oxidation process

The Ni–S–O system is of interest for the investigation of the oxidation of NiS in air. Therefore, characteristic phase stability diagrams were constructed based on the starting thermodynamic data for the reactions occurring in the system of interest at temperatures of 923 and 1073 K, as shown in Fig. 1.

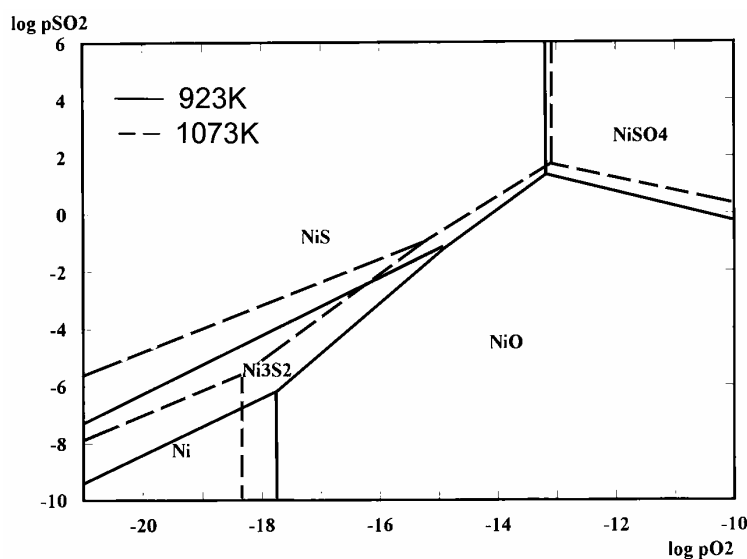


Fig. 1. Constructed phase stability diagrams (PSD) for the Ni–S–O system at 923 and 1073 K.

The obtained results show equilibrium between the phases: Ni–NiS–Ni₃S₂–NiSO₄–NiO, with NiO as the final product of the oxidation process for defined concentrations of SO₂ and O₂.

The results of the thermal analysis of the synthesized sample of α -NiS, obtained using the simultaneous DTA–TG–DTG method, are presented in Fig. 2, while the results of the X-ray diffraction measurements, including diffractograms of samples heated at 923 and 1073 K and then recorded at room temperature, are presented in Fig. 3.

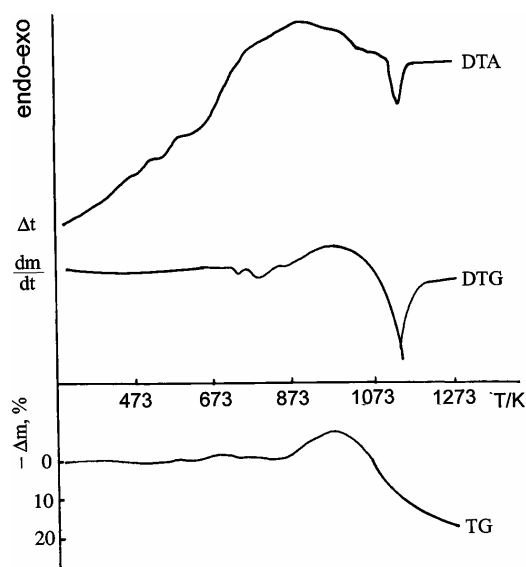


Fig. 2. DTA–TG–DTG Curves of NiS oxidation (atmosphere: air, heating rate: $10\text{ }^{\circ}\text{C min}^{-1}$).

Comparative analysis of the presented results was performed in order to obtain the mechanism of the process of NiS oxidation.

The first small endothermic peak in the DTA curve, shown in Fig. 2, occurred at a temperature near 550 K. It was not accompanied with a mass change on the TG curve and could correspond to the $\alpha \rightarrow \beta$ phase transition of NiS, as given in the literature.¹²

The oxidation of NiS commences in the temperature range 873–973 K, accompanied by a large exothermic effect with a maximum at 903 K and a significant mass, evidenced on the TG curve, which corresponds to the oxidation of nickel sulfide according to the reaction:



The process of NiSO₄ dissociation commences at 973 K, showing intensive a minimum on the DTA curve at the temperature of 1123 K and a significant decrease of the sample mass on the TG curve, due to the occurrence of the following reaction:



The reactions proposed using the results of thermal analysis are in accordance with the obtained XRD data. Namely, the results of X-ray diffractometry showed the existence of NiSO₄ and NiO, as well as the presence of NiS still non-oxidized at 923 K, and the existence of NiO at the higher temperature of 1073 K, which is also in accordance with the constructed PSD diagram.

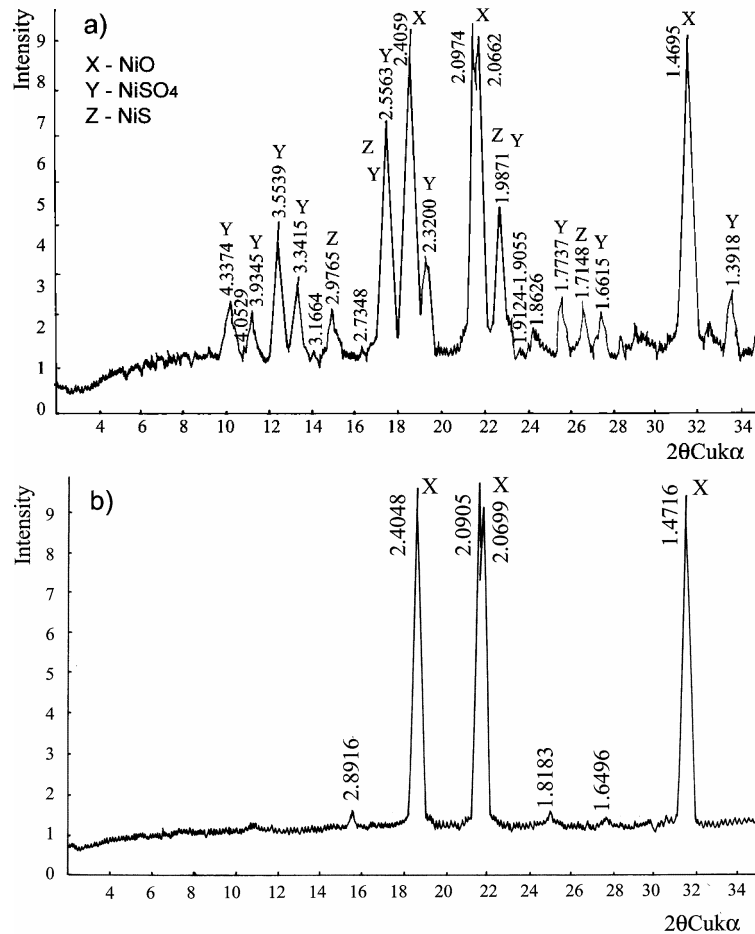


Fig. 3. X-Ray diffractograms of the investigated sample at 923 (a) and 1073 K (b).

Kinetics of the process of synthetic NiS oxidation

The degree of desulfurization was used to determine the kinetic parameters of the process, using the Sharp isothermal model.¹⁷ The degree of desulfurization presents the ratio of the sulfur reacted during the oxidation process compared to the starting concentration of sulfur in the sample.

In the course of the experiments, samples of NiS were oxidized and the amounts of emitted SO₂ were successively registered. These results are presented in Fig. 4.

The most important information concerning the desulfurization process of nickel sulfide, which may be concluded from the SO₂ emission curves, is that the process proceeds intensely only during several minutes at the beginning (*i.e.*, the first five to six minutes), thereafter, the SO₂ emission almost completely ceases.

The process is very rapid, particularly at higher temperatures, which means that several first minutes are essential for the degree of sulfide transformation.

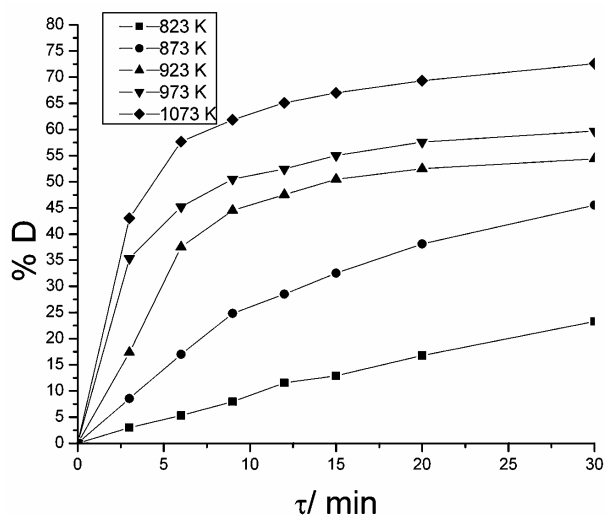


Fig. 4. Amount of sulfur which reacted with oxygen during the oxidative roasting of the NiS sample (D – degree of desulfurization, τ – time).

Linearization of the experimental results presented in Fig. 4 was tested using nine different kinetic equations proposed by Sharp.¹⁷ The criteria for accepting an equation as the best for linearization of the experimental data was the least standard deviation of the linear data in comparison with linear fitting of the experimental data obtained by the iteration program provided by MLAB software (MLAB, Civilized Software).¹⁸ This method for selection of the kinetic equation for the optimal fit of the experimental data points was described earlier.^{19,20}

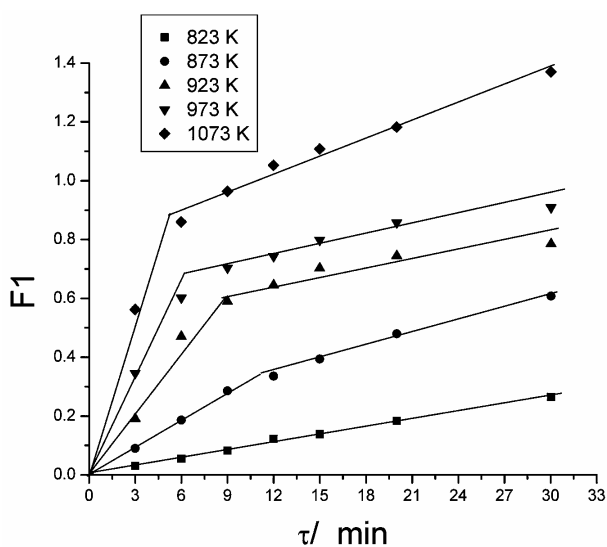


Fig. 5. Linearization of the experimental data points using the kinetic equation $F_1: -\ln(1 - \alpha) = k\tau$ for the process.

The best linearization of the experimental data (*i.e.*, the minimum standard deviation for all the isotherms) was obtained using equation F_1 : $-\ln(1 - \alpha) = k\tau$ for desulfurization, where: α – degree of reaction, τ – time and k is the rate constant (Fig. 5). According to the Sharp theory, Equation F_1 describes a random nucleation of the new phase, with singular nuclei for each particle.¹⁷ This stage could be considered as being dominant in controlling the reaction rate during the first period of time. An infraction of the linear isotherms (Fig. 5) was noticed for temperatures above 873 K, after the first 5–6 min. From the slopes of these linear isotherms, the rate constants were determined at the investigated temperatures (k_1 before the infraction and k_2 after the infraction) and a characteristic Arrhenius diagram was constructed, Fig. 6.

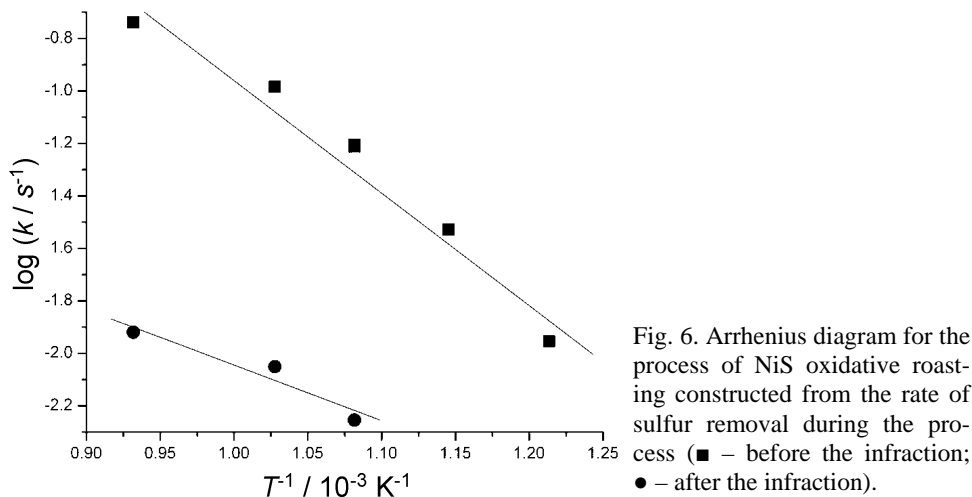


Fig. 6. Arrhenius diagram for the process of NiS oxidative roasting constructed from the rate of sulfur removal during the process (■ – before the infraction; ● – after the infraction).

According to the Arrhenius diagrams, the activation energy of the process under isothermal conditions was calculated. The kinetic equation for the oxidation stage of the desulfurization process was found to be: $-\ln(1 - \alpha) = k_1\tau = 27.89 \exp(-9860/T)\tau$, with an activation energy of $82 \pm 4 \text{ kJ mol}^{-1}$, and $-\ln(1 - \alpha) = k_2\tau = 1.177 \exp(-4810/T)\tau$, with an activation energy $40 \pm 2 \text{ kJ mol}^{-1}$ for the dissociation stage of the desulfurization process, as given above. The expected errors were calculated using the error in the slope of the relevant regression line for each Arrhenius plot.

CONCLUSIONS

The results of this investigation of the process of synthetic α -NiS are presented in this paper. Based on the experimental results of thermal and X-ray diffraction analysis, as well as thermodynamic analysis of the stability of the phases in the Ni–S–O system in the investigated temperature range, the mechanism of NiS oxidation was deduced. It was shown that α -NiS firstly transforms to β -NiS

at temperatures around 550 K, after which the oxidation process commenced between 873 and 973 K, when NiS was oxidized to NiSO₄ and NiO, while with further increasing of the temperature, at 973 K, dissociation of the formed NiSO₄ started. Hence, the final product of oxidation was NiO. The kinetics of the process was investigated using the Sharp method and it was determined that the oxidation process commences quite fast at the beginning of the process (during the first 5–6 min, depending on the temperature), with an activation energy which places the process in the kinetic region. After this first period of the reaction, the activation energy fell to the value on the limit of the kinetic-to-transition region, meaning that diffusion of the reactants and the reaction products began to have an influence on the overall rate of reaction.

ИЗВОД

МЕХАНИЗАМ И КИНЕТИКА ПРОЦЕСА ОКСИДАЦИЈЕ СИНТЕТИЧКОГ α -NiS

НАДА ШТРБАЦ¹, ДРАГАНА ЖИВКОВИЋ¹, ИВАН МИХАЈЛОВИЋ¹, ВОЈАН ВОЈАНОВ² и ЖИВАН ЖИВКОВИЋ¹

¹Универзитет у Београду, Технички факултет у Бору, Војске Југославије 12, Бор, Србија и ²University "Paisiy Hilendarsky", Plovdiv, Tsar Assen 24, 4000 Plovdiv, Bulgaria

У овом раду су представљени резултати истраживања механизма и кинетике оксидационог процеса пржења синтетичког α -NiS. Механизам оксидације α -NiS је испитиван при меном компаративне анализе DTA–TG–DTG и XRD резултата, као и конструисања дијаграма стабилности фаза (PSD) за Ni–S–O систем. Кинетичка испитивања оксидационог процеса су урађена под изотермским условима у опсегу 823–1073 К. Резултати степена десулфуризације су употребљени у процесу прорачуна кинетичких параметара процеса оксидације α -NiS према Шарповој методи. Прорачунате су вредности енергије активације и константе брзине карактеристичних реакција. Ови резултати омогућили су формулацију кинетичке једначине процеса десулфуризације: $-\ln(1 - \alpha) = k_1 \tau = 27,89 \exp(-9860/T) \tau$, са енергијом активације од $82 \pm 4 \text{ kJ mol}^{-1}$, за први стадијум процеса и $-\ln(1 - \alpha) = k_2 \tau = 1,177 \exp(-4810/T) \tau$, са енергијом активације од $40 \pm 2 \text{ kJ mol}^{-1}$, за други стадијум.

(Примљено 29. марта, ревидирано 4. септембра 2007)

REFERENCES

1. G. V. Samsonov, S. V. Drozdova, *Sulfides*, Metallurgy, Moscow, 1972, p. 186 (in Russian)
2. D. J. Vaughan, J. R. Craig, *Mineral chemistry of metal sulfides*, Cambridge University Press, Cambridge, 1978, p. 67
3. N. Štrbac, D. Živković, Ž. Živković, I. Mihajlović, *Sulfides – thermal, thermodynamic and kinetic analysis*, Punta, Niš, 2005, p.229 (in Serbian)
4. J. G. Dunn, C. E. Kelly, *J. Therm. Anal. Calor.* **12** (1977) 43
5. J. G. Dunn, C. E. Kelly, *J. Therm. Anal. Calor.* **18** (1980) 147
6. H. Wang, A. Pring, Y. Ngothai, B. O'Neill, *Am. Mineral.* **91** (2006) 537
7. J. J. Talja, H. Y. Sohn, in *Proceedings of EPD Congress*, San Francisco, USA, 1994, p. 739
8. K. P. Lillerud, P. Kofstad, *Oxidation of Metals* **21** (1984) 233
9. D. Dollimore, J. Pearce, *J. Therm. Anal. Calor.* **6** (1972) 321

10. I. Ya. Mittova, I. M. Soshnikov, V. A. Terekhov, A.V. Shchukarev, *Inorg. Mater.* **33** (1997) 543
11. D. W. Bishop, P. S. Thomas, A. S. Ray, *J. Therm. Anal. Calor.* **56** (1999) 429
12. H. Wang, A. Pring, Y. Ngothai, B. O'Neill, *Am. Mineral.* **91** (2006) 171
13. D. L. Legrand, H. W. Nesbitt, G. M. Bancroft, *Am. Mineral.* **83** (1998) 1256
14. M. Singleton, P. Nash, K. J. Lee, in *Phase Diagrams of Binary Nickel Alloys*, P. Nash, Ed., ASM International, Materials Park, USA, 1991, p. 254
15. M. Baudler, G. Brauer, F. Feher, F. Huber, R. Klement, W. Kwasnik, P. W. Schenk, M. Schmeisser, R. Steudel, *Handbook on Inorganic Synthesis, Vol. 5*, Mir, Moscow, 1985, p. 345 (in Russian)
16. B. S. Boyanov, V. V. Konareva, N. K. Kolev, *Hydrometallurgy* **73** (2004) 163
17. H. J. Sharp, W. G. Brinduy, N. B. Harahari, *J. Am. Ceram. Soc.* **49** (1966) 379
18. MLAB, Civilized Software Inc., www.civilized.com (December 12, 2006)
19. I. Mihajlović, N. Štrbac, Ž. Živković, I. Ilić, *J. Serb. Chem. Soc.* **70** (2005) 869
20. D. Minić, N. Štrbac, I. Mihajlović, Ž. Živković, *J. Therm. Anal. Calor.* **82** (2005) 383.



www.shd.org.yu

J. Serb. Chem. Soc. 73 (2) 221–226 (2008)

JSCS–3704

Journal of
the Serbian
Chemical Society

ersion
lectronic

JSCS@tmf.bg.ac.yu • www.shd.org.yu/JSCS

UDC 546.47+546.175–323+544.35:66.082.2:620.193

Original scientific paper

Periodic current oscillations of zinc in nitric acid solutions

FLORIN CRISAN^{1*} and ERVIN SALLÓ²

¹County Lab for Pesticides Quality Control, Bodrogului Str. 3, 310059, Arad and ²Chemistry Institute of Romanian Academy, Mihai Viteazul Blvd. 24, 300223, Timisoara, Romania

(Received 23 May, revised 16 August 2007)

Abstract: This paper presents current oscillations of a Zn anode in solutions of nitric acid and potassium dichromate. The effects of the nitric acid concentration were investigated. The system was analyzed using cyclic voltammetry, current–time plots and attractors. It was found that the concentration of nitric acid has a major effect on the behavior of the system and it is proposed that zinc hydroxide precipitation–dissolution processes are responsible for the current oscillations.

Keywords: zinc; corrosion; dynamic behavior; current oscillations; attractor.

INTRODUCTION

The dynamic behavior of some metals in the transition region from the active to the passive state, from the steady state to simple, double or chaotic oscillations, presents a large area of research interest in the corrosion and protection of metals and, also, for an understanding of oscillatory phenomena which occur during solid/liquid interface processes.^{1–16}

Self-organization of electrochemical systems is not limited to temporal phenomena but can also involve spatial pattern formation.^{2,9,11,13} The most studied electrochemical system, from the point of view of dynamic behavior, is the anodization of iron in sulfuric acid media.^{2,4,6,9} In addition to iron, there are many other metals which exhibit current or potential oscillations (Ni, Cu, Co, Pb, Ag, Zn, alloys) in certain media (acid, alkaline or solutions of salts). The behavior of zinc electrodes were studied in alkaline solutions as cathodes but their behavior is almost unknown in acidic media.^{14,15}

Current oscillations are explained by a precipitation–dissolution mechanism or chemical reactions having an autocatalytic step.^{3,15} The precipitation–dissolution mechanism is the most extensive mechanism and it seems to be the closest to the real phenomena of current oscillations. This mechanism presumes that chemical species (salt, hydroxide or oxide) are precipitated at the electrode surface.

* Corresponding author. E-mail: florincrisan2000@yahoo.com; dfjarad@rdslink.ro
doi: 10.2298/JSC0802221C

It is well known that zinc, as well as certain other metals and alloys, exhibit the phenomenon of metallic passivity, *i.e.*, the metal becomes inert under certain environmental conditions since its surface is covered by a thin oxide film. In the passive state, defects in the protective film may induce propagating reaction zones, which lead to the dissolution of the pacifying layer and transform the electrode into its active state.

For iron in acidic media, an increase of the dissolution rate with increasing electrode potential is observed. At the passivation potential, the dissolution rate decreases dramatically and the electrode surface becomes passive again. Under these conditions, the system forms an excitable medium where passivation–activation phenomena occur successively, leading to current oscillations.

This paper presents the dynamic behavior of a zinc anode in nitric acid-oxidizing media and the influence of the acidity and the electrode potential on this behavior. In addition, the attractors generated by current–time series are presented. The dynamic behavior of zinc was studied in solutions of nitric acid (0.2–1.6 M) containing 0.15 M of potassium dichromate.

EXPERIMENTAL

The experiments were performed using a three-electrode system in a non-stirred electrolyte. The potential of the zinc electrode was controlled by a Voltalab 40 PGZ 301 potentiostat and the response current was monitored by Voltmaster 7.08 software. The working electrode was a zinc rod (8 mm diameter) of 99.9 % purity (Merck) embedded in an isolating muff, so that only the end of the rod was exposed to the solution. The counter electrode was a Pt wire and a saturated calomel electrode (SCE) was used as the reference electrode. The electrolytes were prepared with purified Millipore water ($> 18 \text{ M}\Omega \text{ cm}$ resistivity) and analytical grade potassium dichromate (Riedel-de-Haën, 99.8 % purity) and nitric acid (Fluka, 65 %). The total volume of the solution in each experiment was 100 ml. The working electrode was polished with 600 and 1000 grade emery paper, washed with water and wiped prior to each experiment. All experiments were performed at room temperature.

RESULTS AND DISCUSSION

Cyclic voltammetry

The four cyclic voltammograms for the four nitric acid concentrations (0.2, 0.3, 0.6 and 1.6 M), at the same potassium dichromate concentration (0.15 M), recorded at a potential scan rate, are presented in Fig. 1. For all of the voltammograms, in the positive sweep, a slow increase of the current, followed by a plateau at around zero current, then an abrupt increase of the current at $\approx 0.2 \text{ V}$, accompanied by gas evolution at the counter electrode, can be observed. The width of the plateau zone decreased as the nitric acid concentration increased, so that at a nitric acid concentration of 1.6 M, the plateau was very small. Nevertheless, a maximum of the current appeared and then the electrode passivates.

For the negative sweep, the current decreased continuously but presents higher values than in the positive sweep. At around -0.2 V , the current oscillated,

which is marked in Fig. 1 by A. The potential domain in which oscillations occurred increased up to a nitric acid concentration of 0.6 M and then decreased. Current oscillations seem to appear only after the passive layer had attained a critical thickness and the potential attained a certain value. At this moment, the system became unstable and transitions between the passive and active state occurred. If both conditions (film thickness and potential value) exist, oscillations may appear.

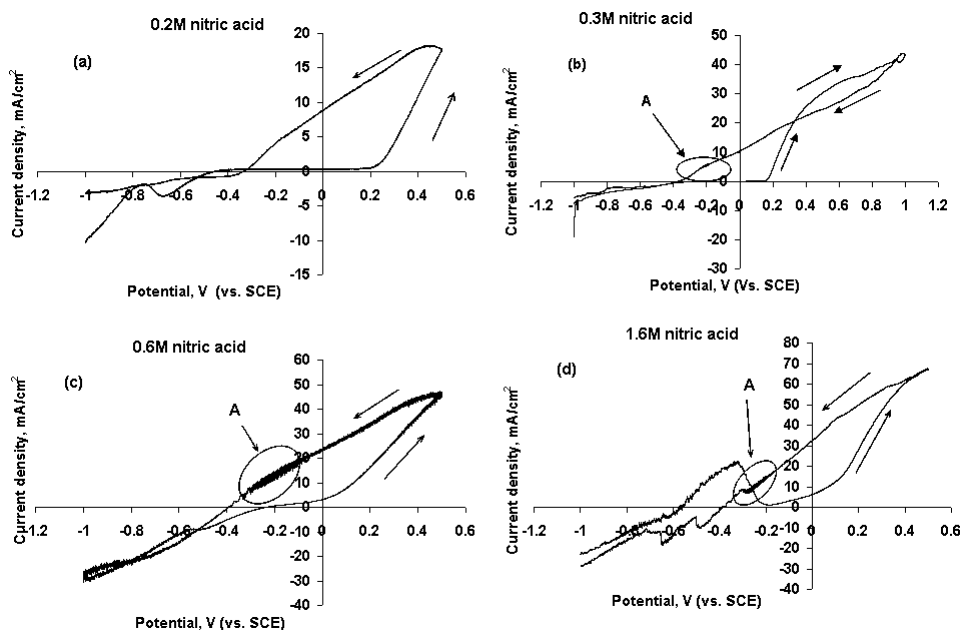


Fig. 1. Cyclic voltammograms recorded in a) 0.2 M HNO_3 , b) 0.3 M HNO_3 , c) 0.6 M HNO_3 and d) 1.6 M HNO_3 . The zones indicated with A denote oscillatory regions. The arrows indicate the direction of potential sweeping.

In the passive state, defects in the protective film may induce propagating reaction zones and electrode surface becomes active.¹³ Zinc dissolution leads to an accumulation of zinc ions and a migration of H^+ ions away from the vicinity of the electrode. Consequently, the pH increases and a temporary precipitation of zinc hydroxide may occur, whereby zinc dissolution ceases. The electrode surface becomes passive and the current decreases. Due to the precipitation of zinc ions, H^+ ions migrate back from the bulk to the surface of the electrode, leading to dissolution of the hydroxide layer, whereby the electrode reverts to its active state, the current increases and cycle repeats itself.

In order to obtain current oscillations, the electrode potential was swept from -1.0 V to 0.50 V then back to the potential value where oscillations occur (around -0.2 V). No oscillations were observed for a concentration of nitric acid of 0.2 M or lower.

Current–time series

The current vs. time plots for nitric acid concentrations of 0.3, 0.6 and 1.6 M at -0.20 , -0.10 and -0.05 V are presented in Fig. 2. The dynamic behavior of system changed, depending on the nitric acid concentration.

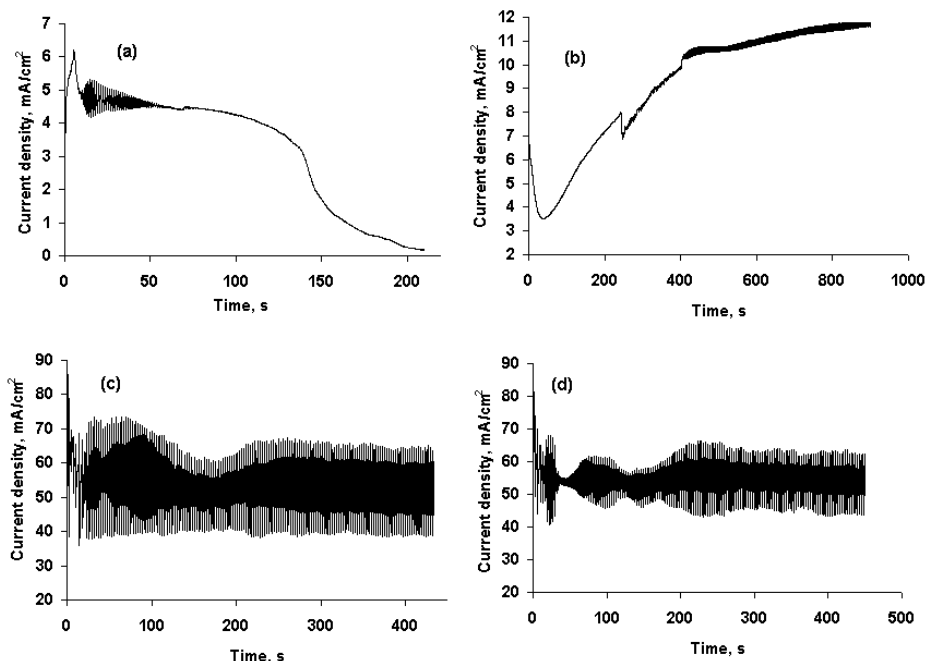


Fig. 2. Current–time series registered in a) 0.3 M HNO_3 at $E = -0.2$ V, b) 0.6 M HNO_3 at $E = -0.2$ V, c) 1.6 M HNO_3 at $E = -0.1$ V and d) 1.6 M HNO_3 at $E = -0.05$ V.

For 0.3 M nitric acid (Fig. 2a), the current passed through a maximum and oscillations appear after about 10 s but they rapidly ceased, then the current decreased to zero. For 0.6 M nitric acid (Fig. 2b), the current exhibited a minimum but oscillations did not appear even after 4 min. A short stir of the solution resulted in oscillations which occurred for 10 min. In this case, one period of oscillations could be observed but the amplitude was not very constant. For 1.6 M nitric acid (Figs. 2c and 2d), oscillations appeared immediately which become regular, with a double-period, after 4 min.

As observed, for 1.6M nitric acid solution, the oscillations were similar for different potential values (Figs. 2c and 2d,) but the amplitude was smaller at the lower potential (-0.05 V), than at the higher potential (-0.10 V) and the frequency increased.

Attractors

The attractors for the time series in Fig. 2 and the shape of the oscillations are presented in Fig. 3. Attractors 3a and 3b correspond to one period oscillation

(Figs. 2a and 2b, respectively) and 3c to double-period oscillation (2c), from which it can be concluded that as the concentration of nitric acid increased, the complexity of the oscillations increased and their shape changed. The oscillations for 0.3 and 0.6 M nitric acid are perfectly sinusoidal, while for 1.6 M nitric acid, the oscillations seem to be of the relaxation type.

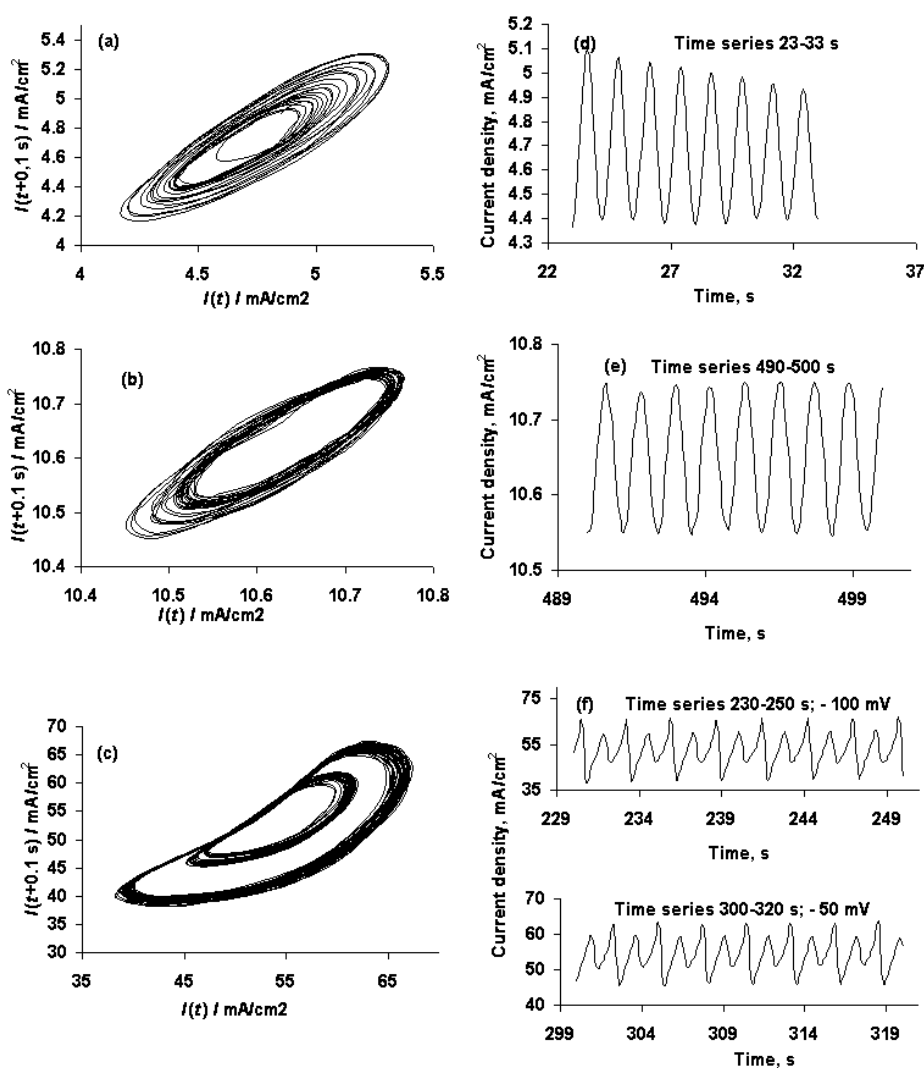


Fig. 3. Attractors and part of the time-series. a) 0.3 M HNO_3 (for 2a); b) 0.6 M HNO_3 (for 2b); c) 1.6 M HNO_3 (for 2c). The diagrams d–f present the shape of the oscillations for 2a–2d, respectively.

It is possible to find chaotic behavior for higher concentrations of nitric acid and the route to chaos is likely to be a period-doubling one. Further investigation is necessary to elucidate this mechanism and the role of potassium dichromate in it.

CONCLUSIONS

According to the experimental results, current oscillations in the Zn–nitric acid–potassium dichromate system occur within a certain potential range. In addition, the oscillations are strongly influenced by the nitric acid concentration but not enough information is available to explain the role of the potassium dichromate. The oscillations may be explained by the precipitation–dissolution mechanism and it is possible that a chemical reactions mechanism with participation of the potassium dichromate exists, which can lead to self-organization of the system.

Acknowledgements. The authors would like to acknowledge the West University “Aurel Vlaicu”, Arad, Romania, for partial support of this research. Especially, our thanks go to Ms. Florentina Munteanu for her help.

ИЗВОД

ПЕРИОДИЧНЕ СТРУЈНЕ ОСЦИЛАЦИЈЕ ЦИНКА У РАСТВОРИМА АЗОТНЕ КИСЕЛИНЕ

FLORIN CRISAN¹ и ERVIN SALLÓ²

¹County Lab for Pesticides Quality Control, Bodrogului Str. 3, 310059, Arad u ²Chemistry Institute of Romanian Academy, Mihai Viteazul Blvd. 24, 300223, Timisoara, Romania

Овај рад приказује струјне осцилације аноде од цинка у растворима азотне киселине уз додаток калијум-бихромата. Испитиван је утицај концентрације азотне киселине на ову појаву. Систем је анализиран коришћењем цикличних волтамограма, графика зависности струје од времена и атрактора. Нађено је да концентрација азотне киселине има одлучујући утицај на понашање система и претпостављено да је процес таложења и растварања цинк-хидроксида одговоран за струјне осцилације.

(Примљено 23. маја, ревидирано 16. августа 2007)

REFERENCES

1. J. L. Hudson, M. R. Basset, *Rev. Chem. Eng.* **7** (1991) 111
2. O. Teschke, D. M. Soares, F. Galembeck, *J. Electrochem. Soc.* **132** (1985) 741
3. C. Naitao, Z. Shiyong, W. Chao, C. Shenhao, *J. Serb. Chem. Soc.* **66** (2001) 563
4. L. Organ, I. Z. Kiss, J. L. Hudson, *J. Phys. Chem. B* **107** (2003) 6648
5. T. T. Lunt, J. R. Scully, V. Brusamarello, A. S. Mikhailov, J. L. Hudson, *J. Electrochem. Soc.* **149** (2002) B163
6. P. Parmananda, B. J. Green, J. L. Hudson, *Phys. Rev. E* **65** (2002) 035202-1
7. W. Wang, I. Z. Kiss, J. L. Hudson, *Ind. Eng. Chem. Res.* **41** (2002) 330
8. I. Z. Kiss, J. L. Hudson, *Phys. Chem. Chem. Phys.* **4** (2002) 2638
9. B. J. Green, J. L. Hudson, *Phys. Rev. E* **63** (2001) 026214-1
10. W. Wang, B. J. Green, J. L. Hudson, *J. Phys. Chem. B* **105** (2001) 7366
11. B. J. Green, W. Wang, J. L. Hudson, *Forma* **15** (2000) 257
12. I. Z. Kiss, V. Gaspar, L. Nykos, *J. Phys. Chem. A* **102** (1998) 909
13. K. Agladze, S. Thouvenel–Romans, O. Steinbock, *Phys. Chem. Chem. Phys.* **3** (2001) 1326
14. J. St.-Pierre, D. L. Piron, *J. Electrochem. Soc.* **137** (1990) 2491
15. J. L. Hudson, T. T. Tsotsis, *Chem. Eng. Sci.* **49** (1994) 1493
16. N. Potkonjak, Lj. Kolar–Anić, T. Potkonjak, S. N. Blagojević, S. Anić, *Mater. Sci. Forum* **518** (2006) 301.



www.shd.org.yu

J. Serb. Chem. Soc. 73 (2) 227–231 (2008) UDC 535.513+512.77+517968.2:541.138–034:681.5.017

JSCS–3705

Note

NOTE

The validity of the general polarization curve equation approximation for the process of metal deposition

PREDRAG M. ŽIVKOVIĆ*, BRANIMIR N. GRGUR and KONSTANTIN I. POPOV#

*Faculty of Technology and Metallurgy, University of Belgrade,
Karnegijeva 4, 11120 Belgrade, Serbia*

(Received 15 June, revised 28 September 2007)

Abstract: Digital simulation was employed for the solution of the general polarization curve equation of metal deposition processes. By approximating the dependence of the exchange current density on concentration with a linear function for one- and two-electron transfer processes, an error lower than 20 % was obtained.

Keywords: polarization curve equation; metal deposition; exchange current density; simulation.

INTRODUCTION

The general equation of the polarization curve for metal deposition process according to Newman,¹ can be given as:

$$j = j_{0,s} (f_a - f_c) \quad (1)$$

where j is the overall current density, f_a and f_c are defined as:

$$f_a = 10^{\frac{\eta}{b_a}} \quad (2a)$$

$$f_c = 10^{-\frac{\eta}{b_c}} \quad (2b)$$

where b_a and b_c are the anodic and cathodic Tafel slopes, respectively, η is the overpotential and $j_{0,s}$ is the concentration dependent exchange current density for a surface concentration c_s . The mathematical expression for the $j_{0,s}$ could be given as:¹

$$j_{0,s} = \left(\frac{c_s}{c_0} \right)^\gamma j_0 \quad (3)$$

* Corresponding author. E-mail: peca@tmf.bg.ac.yu

Serbian Chemical Society member.

doi: 10.2298/JSC0802227Z

where c_s and c_0 are the surface and bulk concentration of the reacting metal ion, respectively, j_0 is the exchange current density for a surface concentration equal to the bulk concentration of the solution and the coefficient γ is defined as:

$$\gamma = \frac{d \log j_0}{dc_0} \quad (4)$$

For a one-electron process of metal deposition:²



γ is defined as:

$$\gamma = 1 - \beta \quad (6)$$

where β is a symmetry factor of the energetic barriers.

For a two-electron process,¹ assuming the first electron transfer is rate determining in the overall mechanism:



γ is defined as:

$$\gamma = \frac{2 - \beta}{2} \quad (8)$$

If γ is not equal to 1, simple analytical solutions of the general equation of the polarization curve in terms of formal kinetics are not available and different numerical methods must be applied.

The aim of this work was to deduce whether the approximation of the value of γ equal to 1 could be applied for the solution of the general equation of the polarization curve in a qualitative or quantitative manner.

RESULTS AND DISCUSSION

For one-electron transfer processes given by Eq. (5), it can be calculated that the anodic and cathodic Tafel slopes have values of 120 mV/dec, while for two-electron transfer processes given by Eqs. (7) and (7a), the anodic and cathodic Tafel slopes have values of 40 and -120 mV/dec, respectively.

On the other hand, surface and bulk concentration of the reacting metal ion can be connected with current density using the following equation:

$$\frac{c_s}{c_0} = 1 - \frac{j}{j_L} \quad (9)$$

where j_L is the limiting diffusion current density (note: Eq. (9) is strictly valid only in the case of forced convection, *i.e.*, a stirred electrolyte, but many authors use this equation for non-stirred conditions). By substituting c_s/c_0 from Eq. (9) into Eq. (3) and $j_{0,s}$ from Eq. (3) into Eq. (1), the following is obtained:

$$j = j_0 \left(1 - \frac{j}{j_L} \right)^\gamma (f_a - f_c) \quad (10)$$

or:

$$\frac{j}{j_L} = \frac{j_0}{j_L} \left(1 - \frac{j}{j_L} \right)^\gamma (f_a - f_c) \quad (11)$$

as the general polarization curve equation.

In the first approximation, assuming the value for $\gamma \approx 1$, and with further rearrangement, a simplified version of Eq. (10) is obtained:

$$j = \frac{j_0(f_a - f_c)}{1 + \frac{j_0(f_a - f_c)}{j_L}} \quad (12)$$

or:

$$\frac{j}{j_L} = \frac{\frac{j_0}{j_L}(f_a - f_c)}{1 + \frac{j_0(f_a - f_c)}{j_L}} \quad (13)$$

Simplified mathematical treatments of Eqs. (12) and (13) are widely used in qualitative, and in many cases in quantitative, discussions of metal deposition and other electrochemical processes. It is again necessary to note that both equations are approximations because the value of γ is not unity in many cases. Different numerical methods should be applied in these cases, as suggested previously.³

Hence, in this work, digital simulation was performed for one- and two-electron transfer processes and $\beta = 0.5$. Obviously, for a one-electron transfer process, the values are as following: $\gamma = 0.5$, $f_a = 10^{\eta/120}$ and $f_c = 10^{-\eta/120}$, while for a two-electron transfer process $\gamma = 0.75$, $f_a = 10^{\eta/40}$ and $f_c = 10^{-\eta/120}$.

The polarization curves calculated using Eqs. (11) and (13) for the ratio between $|j_0/j_L| = 10, 1$ and 0.1 are shown in Figs. 1 and 2.

As can be seen from Figs. 1 and 2, the approximation of Eq. (11) by Eq. (13) is acceptable for qualitative purposes at practically all overpotentials and ratios of $|j_0/j_L|$. On the other hand, quantitative approximation is valid only in the overpotential region where the Tafel approximation could be applied.

The relative error, given as the percentage difference of the current density between Eqs. (11) and (13), is plotted as a function of the overpotential in Figs. 3 and 4.

From Figs. 3 and 4, it can be seen that the maximum difference between the values of current density calculated using Eqs. (11) and (13) is about 20 % if γ is 0.5 and about 9 % if γ is 0.75.

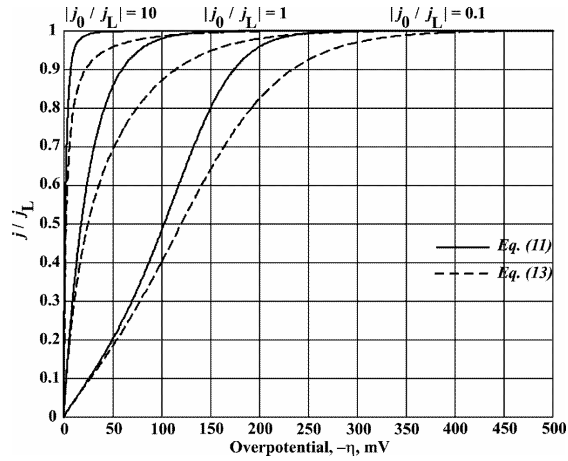


Fig. 1. Dependences of j/j_L vs. $-\eta$ calculated from Eq. (11) and Eq. (13), using $|j_0/j_L| = 10, 1$ and 0.1 , and $\gamma=1$ and $0.5, f_a = 10^{120}$ and $f_c = 10^{-\eta/120}$.

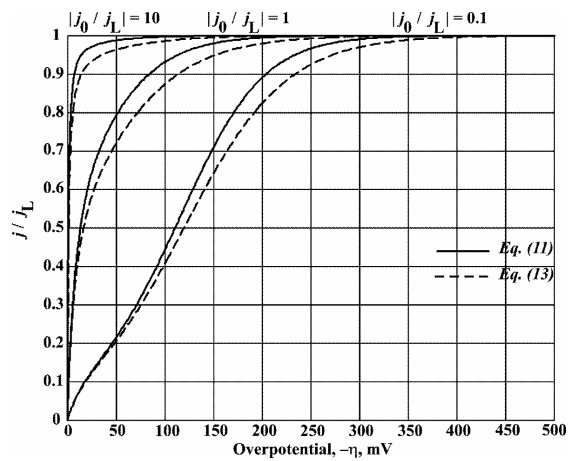


Fig. 2. Dependences of j/j_L vs. $-\eta$ calculated from Eq. (11) and Eq. (13), using $|j_0/j_L| = 10, 1$ and 0.1 , and $\gamma=1$ and $0.75, f_a = 10^{40}$ and $f_c = 10^{-\eta/120}$.

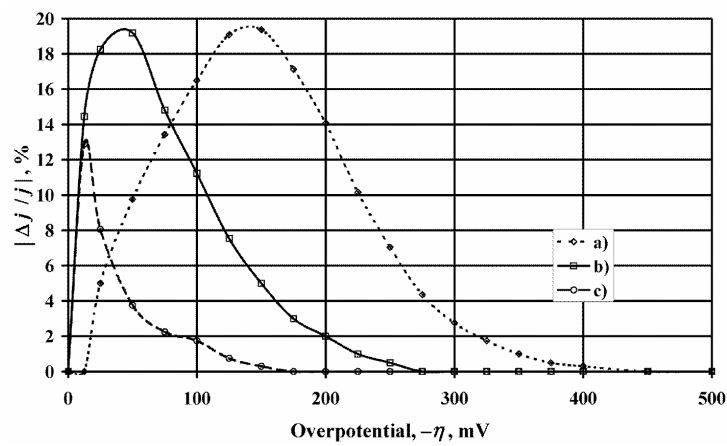


Fig. 3. Dependence $|\Delta j/j|$ vs. $(-\eta)$ from Fig. 1, for different $|j_0/j_L|$ ratios: a) 0.1 , b) 1 and c) 10 .

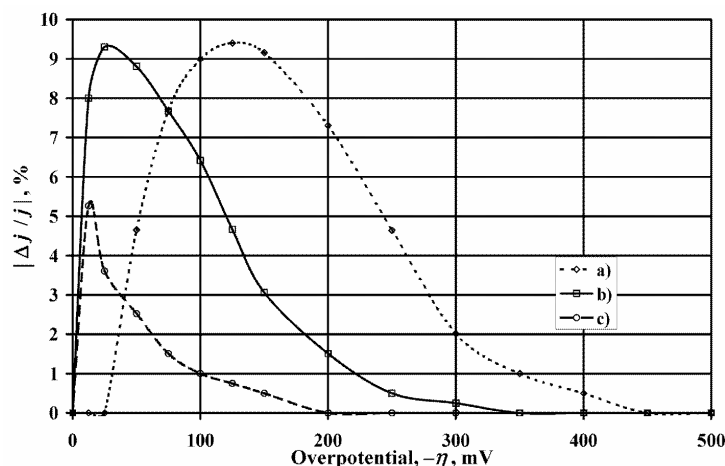


Fig. 4. Dependence $|\Delta j/j|$ vs. $(-\eta)$ from Fig. 2, for different $|j_0/j_L|$ ratios: a) 0.1, b) 1 and c) 10.

Hence, it can be concluded that approximation of the general polarization curve for the case of $\gamma = 1$ can be used in all qualitative and some quantitative estimations with a maximum error lower than 20 % for the cases under consideration.

Acknowledgements. This work was financially supported by the Ministry of Science of the Republic of Serbia, contract No. 142044.

ИЗВОД

ВАЛИДНОСТ ЈЕДНАЧИНЕ АПРОКСИМАЦИЈЕ ОПШТЕ ПОЛАРИЗАЦИОНЕ КРИВЕ ЗА ТАЛОЖЕЊЕ МЕТАЛА

ПРЕДРАГ. М. ЖИВКОВИЋ, БРАНИМИР. Н. ГРГУР И КОНСТАНТИН. И. ПОПОВ

Технолошко-металуршки факултет, Универзитет у Београду, Карнегијева 4, 11120 Београд

За решавање једначине опште поларизационе криве за процес таложeња метала примењена је дигитална симулација. Апроксимирајући зависност густине струје измене од концентрације линеарном функцијом, за процесе са једноелектронским и двоелектронским трансфером добијена је релативна грешка која не прелази 20 %.

(Примљено 15. јуна, ревидирано 28. септембра 2007)

REFERENCES

1. J. S. Newman, *Electrochemical Systems*, Prentice-Hall, Inc., Engelwood Cliffs, New Jersey, 1973, p. 177
2. J. O'M. Bockris, A. K. N. Reddy, M. Gamboa-Aldeco, *Modern Electrochemistry 2A*, 2nd Ed., Kluwer Academic /Plenum Publishers, New York, 2000, p. 1249
3. K. I. Попов, P. M. Živković, B. N. Grgur, *Electrochimica Acta* **52** (2007) 4696.



www.shd.org.yu

J. Serb. Chem. Soc. 73 (2) 233–247 (2008)

JSCS–3706

JSCS@tmf.bg.ac.yu • www.shd.org.yu/JSCS

UDC 547.869+615.32:543.4/.5

Original scientific paper

Individual and simultaneous determinations of phenothiazine drugs using PCR, PLS and (OSC)–PLS multivariate calibration methods

MOHAMMAD ALI KARIMI^{1,2,3*}, MOHAMMAD MAZLOUM ARDAKANI⁴,
REZA BEHJATMANESH-ARDAKANI², MOHAMMAD REZA HORMOZI NEZHAD⁵
and HAMZEH AMIRYAN²

¹Department of Chemistry, Payame Noor University of Sirjan, Sirjan, ²Department of Chemistry, Payame Noor University of Ardakan, Ardakan, ³Department of Chemistry, Shahid Bahonar University of Kerman, Kerman, ⁴Department of Chemistry, Yazd University, Yazd and ⁵Department of Chemistry, Persian Gulf University, Bushehr, Iran

(Received 14 September 2006, revised 24 July 2007)

Abstract: Individual and simultaneous determinations of some phenothiazine drugs are described. The individual determination method is based on the reaction of chlorpromazine hydrochloride (CPH), promethazine hydrochloride (PH), trifluoperazine hydrochloride (TFPH), trimipramine maleate (TPM) and thioridazine hydrochloride (TRDH) with complex of $[\text{Fe}(\text{Bpy})_3]^{3+}$. In the presence of phenothiazine derivatives, $[\text{Fe}(\text{Bpy})_3]^{3+}$ is reduced easily to the coloured complex $[\text{Fe}(\text{Bpy})_3]^{2+}$, which shows an absorption maximum at 525 nm. The individual method is highly sensitive and suitable for 0.3–190 $\mu\text{g ml}^{-1}$ concentrations, with detection limits in the range 0.18–2.46 $\mu\text{g ml}^{-1}$. Simultaneous kinetic–spectrophotometric determination of ternary mixture of CPH, PH and TPM using principal component regression (PCR), partial least squares (PLS) and orthogonal signal correction (OSC)–PLS multivariate calibration methods is also described. The simultaneous methods are based on the difference observed in the reduction rate of the $[\text{Fe}(\text{Bpy})_3]^{3+}$ complex with CPH, PH and TPM in acidic media. The results showed that the simultaneous determination of CPH, PH and TPM can be performed in the concentration ranges of 0.5–120.0, 0.3–80.0 and 5.0–100.0 $\mu\text{g ml}^{-1}$, respectively, for three methods (PCR, PLS and OSC–PLS). The root mean square errors of prediction (RMSEP) of CPH, PH and TPM were 0.346, 0.663 and 0.820 (for PCR) 0.317, 0.659 and 0.830 (for PLS) and 0.087, 0.124 and 0.085 (for OSC–PLS), respectively. The proposed methods were successfully applied to the individual and simultaneous determination of phenothiazine derivatives in pharmaceutical preparations, the results of which compared well with those obtained by the official method, and several synthetic (spiked) samples, whereby satisfactory results were obtained.

Keywords: individual and simultaneous determinations; phenothiazine drugs; PLS; PCR; OSC–PLS.

*Corresponding author. E-mail: m_karimi@pnu.ac.ir or ma_karimi43@yahoo.com

doi: 10.2298/JSC0802233K

INTRODUCTION

Phenothiazine derivatives, an important group of neuroleptics, are used as antihistamines, tranquilizers, anti-emetics and antiparkinson.¹ The therapeutic importance of these drugs has prompted many workers to develop methods for their individual and simultaneous determinations in body fluids, as well as in pharmaceutical.²⁻⁴ There are various analytical procedures for the individual assay of phenothiazines, the most important of which being titrimetry,⁵ conductometry,⁶ voltammetry,⁷ spectrofluorometry,⁸ chemiluminescence,⁹ HPLC¹⁰ and GLC¹¹ methods. Many spectrophotometric methods for their determination have already been proposed based on the oxidation of the drugs to a coloured radical cation and the subsequent measurement of absorbance.¹²⁻²⁰ Unfortunately, some of these methods have some disadvantages, such as the use of non-aqueous media,¹⁶ low sensitivity,¹⁷ a heating step,¹⁸ a very strong acid,¹⁹ a low linear range and critical working conditions,^{12,15} a narrow linear range of application²⁰ and a very narrow limit of detection.¹³ In addition to this, the simultaneous determination of phenothiazine derivatives in binary and ternary mixtures was also reported.²¹⁻²⁶ Gutierrez *et al.* proposed a stopped-flow method for the simultaneous determination of perphenazine (PP) and chlorpromazine hydrochloride (CPH).²¹ Chen *et al.* reported the simultaneous flow-injection determination of CPH and promethazine hydrochloride (PH) by a photochemical reaction.²² The simultaneous kinetic determination of phenothiazine drugs was also reported.²³ Fasanmade reported a multivariate calibration method based on principal component regression (PCR) for the simultaneous ultraviolet (UV) determination of an oxidation product of CPH sulphoxide.²⁴ Shamsipur *et al.* tested partial least-squares (PLS) regression, singular value decomposition-based PLS, and an artificial neural network (ANN) as calibration procedures for the simultaneous determination of PH, CPH, and PP by both conventional and derivative spectrophotometry.²⁵ Recently, Hemmateen-ejad *et al.* reported the simultaneous determination of a ternary mixture of PH, CPH and PP based on the net analyte signal (NAS)-ANN model using conventional and derivative absorbance spectra.²⁶ To the best of our knowledge, no chemometrics methods for the simultaneous determination of these drugs using kinetic-spectrophotometric methods have been reported.

The theories and applications of chemometric methods, such as PCR and PLS, to the analysis of multi-component mixtures have been discussed by several workers.²⁷⁻³² Multivariate calibration methods have been successfully applied to multi-component kinetic determination in order to overcome some of the drawbacks of classical methods. Soft algorithms, such as PCR, PLS and ANN, which avoid co-linearity problems, have been used for the simultaneous determination of analytes having the same chemical properties, which cannot be resolved with common methods.

The formation of the complex between Fe(III) and 2,2'-bipyridine (bpy) is the basis of existing spectrophotometric methods for the determination of trace amounts of reducing agents.³³ Reducing agents can be determined through reducing the $[\text{Fe}(\text{bpy})_3]^{3+}$ complex, followed by treating the coloured complex of $[\text{Fe}(\text{bpy})_3]^{2+}$. Recently, a kinetic-spectrophotometric determination of a ternary mixture of hydrazine and its derivatives by PCR and PLS methods based on the difference observe in the rate of reduction of $[\text{Fe}(\text{bpy})_3]^{3+}$ with hydrazine, thiosemicarbazide and phenylhydrazine in a micellar media of sodium dodecyl sulphate (SDS) and buffer of pH 3.0 was reported.³⁴ In this paper, a new, simple, rapid and sensitive indirect spectrophotometric method for the individual micro-determination of five phenothiazine drugs, containing CPH, PH, trifluoperazine hydrochloride (TFPH), trimipramine maleate (TPM) and thioridazine hydrochloride (TRDH). Also, in this study, principal component regression (PCR), partial least squares (PLS) and orthogonal signal correction (OSC)-PLS multivariate calibration methods for the analysis of ternary mixtures of CPH, PH and TPM, using the observed difference in the reduction rate of $[\text{Fe}(\text{bpy})_3]^{3+}$ with these drugs in acidic media, were used.

EXPERIMENTAL

Apparatus and software

A GBC UV-Visible Cintra 6 Spectrophotometer with 1-cm glass cells, attached to a Pentium IV computer was used for recording the absorbance spectra and the kinetic spectrophotometric data. A Metrohm 780 pH-meter furnished with a combined glass-saturated calomel electrode was calibrated with at least two buffer solutions at pH 1.00 and 7.00. Measurements of the pH were made with a Metrohm 691 pH-meter using a combined electrode. The data were treated in an AMD 2000 XP (256 Mb RAM) microcomputer using Matlab software. PLS and PCR analysis were performed using PLS and PCR toolboxes in the Matlab program version 7.0.

Reagents and standard solutions

All reagents were of analytical reagent grade. Triply distilled water was used throughout. Stock solutions ($1000 \mu\text{g ml}^{-1}$) of chlorpromazine hydrochloride, promethazine hydrochloride, trifluoperazine hydrochloride, trimipramine maleate and thioridazine hydrochloride (all from Biochemicals Inc., USA) were prepared by dissolving 100 mg each of the phenothiazine salts in distilled water and diluting to the mark in 100 ml volumetric flasks. These solutions were spectrophotometrically stable for at least 48 h. Standard solutions were prepared by appropriate dilution of the above solutions. A stock solution of 5.0×10^{-2} M 2,2'-bipyridine was prepared by dissolving 0.784 g of 2,2'-bipyridine (Merck) in water and diluting to the mark in a 100 ml volumetric flask. A stock solution of 5×10^{-2} M of Fe(III) was prepared by dissolving 2.43 g of $\text{Fe}(\text{NH}_4)(\text{SO}_4)_2 \cdot 12\text{H}_2\text{O}$ (Merck) in water and diluting to the mark in a 100 ml volumetric flask. A buffer solution of pH 4 was prepared using sodium acetate and hydrochloric acid at appropriate concentrations.

General procedure

The $[\text{Fe}(\text{bpy})_3]^{3+}$ complex as the oxidizing agent for both the individual and simultaneous method of determination was prepared daily in a 25 ml volumetric flask by the addition

of 2.5 ml of buffer solution (pH 4.0), 0.2 ml of Fe(III) solution (0.05 M) and 1.0 ml of bpy solution (0.05 M) and then diluting with water to the mark. For each measurement in the individual determination, 2.0 ml of the above solution was transferred to a spectrophotometer cell, then an appropriate volume of CPH, PH, TFPH, TPM or TRDH in the range of 0.5–120, 0.3–100, 7–190, 5–100 and 3–120 $\mu\text{g ml}^{-1}$, respectively, was injected into the cell using a micro-syringe and the absorbance was recorded at 525 nm after 200 s. In the simultaneous determination method, the temperature was thermostated at 25 °C for 10 min, 2.4 ml of solution was transferred into the glass cell of the spectrophotometer and the absorbance of this solution was zeroed before injecting the analyte(s). Then, an appropriate volume of CPH, PH, TPM or a mixture of them in their concentration ranges was injected into the cell using a micro-syringe and absorbance was recorded at 525 nm every 2.0 s.

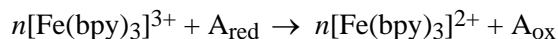
Sample preparation procedure for tablets and injections

Twenty tablets were weighed and finely powdered. An accurately weighed amount of the powder equivalent to 50 mg of phenothiazine salt was transferred into a 100 ml volumetric flask and diluted to the mark with water. The powder was completely dispersed using a mechanical stirrer and the solution was filtered. A suitable aliquot of this solution within the working range of the individual phenothiazine was treated as described in the recommended procedure.

An accurately measured volume from the injections was appropriately diluted to obtain 500 $\mu\text{g ml}^{-1}$ of phenothiazine salt solution. A suitable aliquot of this solution was taken and the recommended procedure followed for the analysis of the drug content.

RESULTS AND DISCUSSION

The Fe(III)–bpy system allows the spectrophotometric determination of a reducing agent, A_{red} , as follows:^{33,34}



The above reaction is completed with the formation of an equivalent amount of $[\text{Fe}(\text{bpy})_3]^{2+}$ with respect to the n -electron reductant, A_{red} . The reduction of $[\text{Fe}(\text{bpy})_3]^{3+}$ to the complex $[\text{Fe}(\text{bpy})_3]^{2+}$ (with $\lambda_{\text{max}} = 525 \text{ nm}$) is completed in the presence of a suitable reducing agent, such as phenothiazine derivatives, in a few minutes. A linear correlation was found between the absorbance at λ_{max} for each drug and the concentration in the range given in Table I. The intercepts, slopes and correlation coefficients for the calibration data of the phenothiazine drugs are also presented in Table I.

The reduction rate of $[\text{Fe}(\text{bpy})_3]^{3+}$ with CPH, PH and TPM is different. This difference provides the possibility for resolving their mixtures using PCR, PLS and OSC–PLS multivariate calibration methods. The characteristics of the calibration curves for the determination of CPH, PH and TPM for PCR, PLS and OSC–PLS are given in Table I.

A series of experiments was conducted to establish the optimum analytical parameters to achieve maximum sensitivity in the individual determination of CPH, PH, TFPH, TPM and TRDH and the simultaneous determination of CPH, PH and TPM. The experimental parameters, such as the concentrations of the reagents, temperature and pH of the solution were optimized. The optimization process gave similar results for both methods (individual and simultaneous determinations).

TABLE I. Analytical parameters for the determination of phenothiazine drugs

Parameter	CPH	PH	TFPH	TPM	TRDH
Colour	Pink	Pink	Pink	Pink	Pink
λ_{\max} / nm	525	525	525	525	525
Stability, h	48	48	48	48	48
The Beer law limits, $\mu\text{g ml}^{-1}$	0.5–120	0.3–80	7–190	5–100	3–120
Detection limit ^a , $\mu\text{g ml}^{-1}$	0.33	0.18	1.60	1.20	1.20
Molar absorptivity, $\text{cm}^2 \text{mol}^{-1}$	0.263	0.227	0.631	0.356	0.350
The Sandell sensitivity $\mu\text{g cm}^{-2}$ per A unit	13.5	14.1	7.6	11.5	11.6
	Regression equation ^b				
Regression coefficient (<i>r</i>)	0.9982	0.9984	0.9988	0.9989	0.9987
Slope (<i>b</i> / $\text{cm}^3 \text{mg}^{-1}$)	13.5	14.1	6.5	11.5	11.6
Intercept (<i>a</i>)	0.1688	0.0490	0.1238	0.0941	0.1149
RSD ^c / %	1.2	1.6	0.9	1.4	1.5

^aTheoretical detection limit ($3S_b$ or three times the standard deviation of the blank);²³ ^b $A = a + bC$, where *A* is the absorbance for concentration *c* in mg cm^{-3} ; ^crelative standard deviation (calculated from five determinations)

Absorption spectra

The reagent blank does not absorb in visible range of the spectrum but when CPH, PH, TFPH, TPM or TRDH has reacted with $[\text{Fe}(\text{bpy})_3]^{3+}$, a pink-coloured cationic product, $[\text{Fe}(\text{bpy})_3]^{2+}$, is formed, with a peak of absorbance at 525 nm. The absorption spectra of the products and reagent blank are shown in Fig. 1.

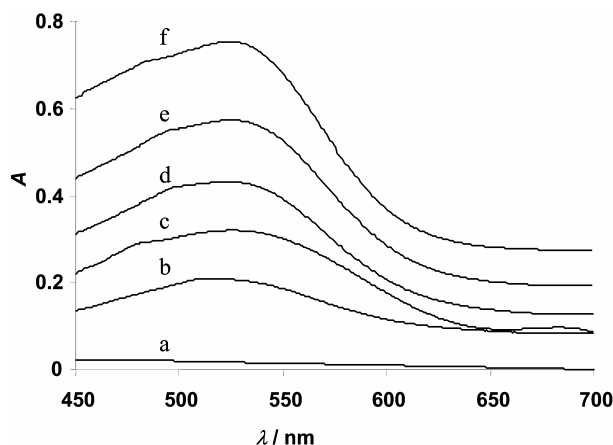


Fig. 1. Absorption spectra of the Fe(III)-bpy reagent blank (a), Fe(III)-bpy complex in the presence of $40 \mu\text{g ml}^{-1}$ of TFPH (b), TRDH (c), TPM (d), CPH (e) and PH (f).

Effect of Fe(III) and bpy concentrations

The effect of the Fe(III) and bpy concentrations, in the ranges 5.0×10^{-4} – 1.0×10^{-2} and 5.0×10^{-4} – 5.0×10^{-3} M, respectively, were studied. At a constant concentration of Fe(III) of 4.0×10^{-4} M, the bpy concentration was varied in the above-mentioned range. For each CPH, PH, TFPH, TPM and TRDH in their individual determination and in the ternary mixture of CPH, PH, and TPM in their simultaneous (for the three PCR, PLS and OSC-PLS methods) determi-

nation, increasing the bpy concentration up to 2.0×10^{-3} M resulted in an increase in the reaction rate and the absorbance. However, at higher concentrations of bpy, a decrease in the reaction rate and absorbance was observed. This might be due to the fact that high concentrations of bpy would result in a positive interference from Fe(III), which could have arisen from incomplete conversion of Fe(II) into the $[\text{Fe}(\text{bpy})_3]^{2+}$ complex *via* mixed ligand complex formation. Therefore, the bpy concentration of 2.0×10^{-3} M was selected as the optimum concentration.

The effect of the Fe(III) concentration on the reaction rate and absorbance of CPH, PH, TFPH, TPM and TRDH at constant concentration of bpy (2.0×10^{-3} M) was studied. Increasing the Fe(III) concentration up to 4.0×10^{-4} M resulted in an increase in the reaction rate and absorbance in the individual determinations of CPH, PH, TFPH, TPM and TRDH and the simultaneous determination of CPH, PH and TPM. However, at higher concentrations of Fe(III), a decrease in the reaction rate and absorbance was observed. Thus, for both the individual and simultaneous (for each three PCR, PLS and OSC-PLS methods) determinations of these drugs, a Fe(III) concentration of 4.0×10^{-4} M was chosen as the optimum concentration for further studies.

Effect of pH

The effects of pH on the absorbance and reduction of $[\text{Fe}(\text{bpy})_3]^{3+}$ by CPH, PH, TFPH, TPM and TRDH and the formation of the $[\text{Fe}(\text{bpy})_3]^{2+}$ complex, as well as on the reaction rates were studied over the pH range 1.0–6.0. The effect of pH on the absorbance of the solution mixture is shown in Fig. 2. The absorbance and reaction rate increased with increasing pH up to 4.0, but thereafter decreased. Therefore, for both the individual and simultaneous (for each three PCR, PLS and OSC-PLS methods) determinations of these drugs, a pH value of 4.0 (acetate buffer) was chosen as the optimal pH for further studies.

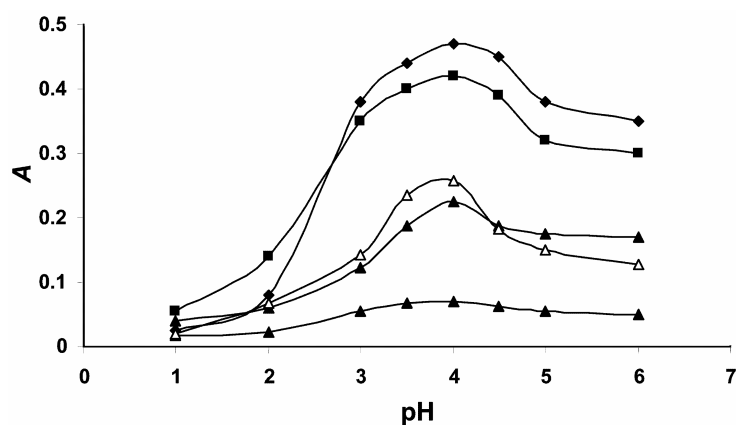


Fig. 2. Effect of pH on the absorbance of $20 \mu\text{g ml}^{-1}$ of TPM (●), TFPH (▲), TRDH (△), CPH (◆) and PH (■). Conditions: 4×10^{-4} M Fe(III); 2×10^{-3} M bpy; 25°C temperature.

Effect of temperature, reaction time and stability of the colour

The effect of temperature on the absorbance and reaction rates was studied in the range of 25–70 °C. From the results, it can be concluded that increasing the temperature led to an increase in the reaction rates for each five analytes but temperature had no effect on the absorbance. However, for the sake of simplicity and for a better control of temperature effects on the precision of determinations, 25 °C was chosen as the optimal temperature. In the individual determinations, at room temperature (25 °C), it was necessary to wait for at least 2 min after drug addition before the absorbance was measured to allow its reaction with the $[\text{Fe}(\text{bpy})_3]^{3+}$ complex to go to completion. Therefore, all absorbance values were measured after 200 s from the initiation of the reaction. The coloured products were stable for at least 48 h.

Absorbance–time behaviour

Under the optimized conditions, the reactions of CPH, PH and TPM with $[\text{Fe}(\text{bpy})_3]^{3+}$ complex showed different kinetic behaviours (Fig. 3). These differences in the reaction rates allowed multivariate calibration methods to be designed as techniques for the simultaneous determination of CPH, PH and TPM.

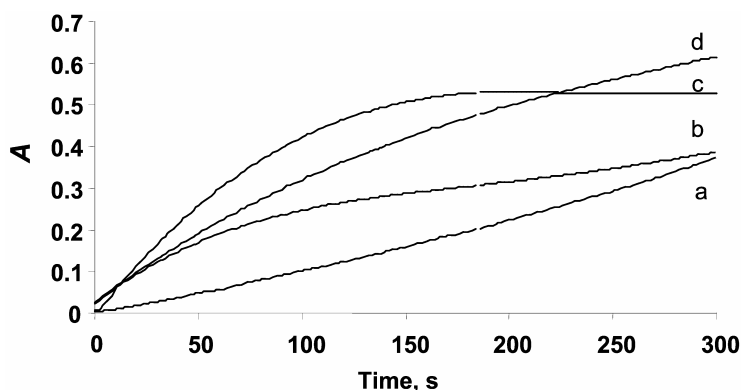


Fig. 3. Absorbance changes of the Fe(III)/bpy complex vs. time in the reaction with: 10 $\mu\text{g ml}^{-1}$ of TPM (a), CPH (b), 1 PH (c) and a mixture of them (d).

Accuracy and precision

In the individual determination method, the accuracy of the method was established by analyzing the pure drugs at three concentration levels and the precision by determining the relative standard deviation (*RSD*) for seven replicate analyses on the same solution containing three different concentration levels for each drug (Table II).

Multivariate calibration and statistical parameters

Multivariate calibration methods, such as PCR, PLS and OSC–PLS, require a suitable experimental design of a standard belonging to the calibration set in

order to provide for a good prediction. The first step in the simultaneous determination of the drugs by the PCR, PLS and OSC–PLS methodologies involved constructing a calibration mixture for the mixtures of CPH, PH and TPM. A synthetic set of 40 solutions of mixtures of CPH, PH and TPM were prepared according to the experimental design of three factors at three levels. The concentration ranges used were 0.5–120.0, 0.3–80.0 and 0.50–100.0 $\mu\text{g ml}^{-1}$ for CPH, PH and TPM, respectively. From these series, 27 solutions were chosen for the calibration set (Table III) and the other 13 were used as the prediction set (Table IV). Changes in the absorbance of the solutions were recorded during a period of 300 s.

TABLE II. Accuracy and precision data

Pheothiazine derivative	Amount, $\mu\text{g ml}^{-1}$		<i>RSD</i> / % (<i>n</i> = 7)
	Taken	Found	
CPH	2	2.0	1.9
	50	50.6	2.4
	110	111.7	2.9
TFPH	8	7.9	3.1
	60	61.1	2.0
	180	177.2	2.5
PH	0.5	0.5	2.8
	10	10.3	1.6
	60	59.2	2.5
TPM	5	4.8	2.7
	30	30.4	2.6
	70	68.9	2.1
TRDH	20	19.6	2.5
	75	76.4	1.9
	100	98.7	2.8

TABLE III. Calibration set for constructing the PCR and PLS models in the determination of CPH, PH and TPM

Sample	Concentration, $\mu\text{g ml}^{-1}$			Sample	Concentration, $\mu\text{g ml}^{-1}$		
	CPH	PH	TPM		CPH	PH	TPM
1	5.0	1.0	9.0	15	7.0	3.0	15.0
2	5.0	1.0	12.0	16	7.0	6.0	9.0
3	5.0	1.0	15.0	17	7.0	6.0	12.0
4	5.0	3.0	9.0	18	7.0	6.0	15.0
5	5.0	3.0	12.0	19	10.0	1.0	9.0
6	5.0	3.0	15.0	20	10.0	1.0	12.0
7	5.0	6.0	9.0	21	10.0	1.0	15.0
8	5.0	6.0	12.0	22	10.0	3.0	9.0
9	5.0	6.0	15.0	23	10.0	3.0	12.0
10	7.0	1.0	9.0	24	10.0	3.0	15.0
11	7.0	1.0	12.0	25	10.0	6.0	9.0
12	7.0	1.0	15.0	26	10.0	6.0	12.0
13	7.0	3.0	9.0	27	10.0	6.0	15.0
14	7.0	3.0	12.0				

TABLE IV. Prediction set for constructing the PCR, PLS and O-PLS models in the determination of CPH, PH and TPM

Sample	Amount added			Amount predicted, $\mu\text{g ml}^{-1}$								
	$\mu\text{g ml}^{-1}$			PCR			PLS			O-PLS		
	CPH	PH	TPM	CPH	PH	TPM	CPH	PH	TPM	CPH	PH	TPM
1	5.75	2.25	9.00	5.79	2.04	9.55	5.78	2.04	9.52	5.70	2.22	8.82
	6.00	2.00	9.00	5.85	2.08	8.21	5.84	2.08	8.21	5.95	1.90	8.92
2	6.00	3.10	9.75	5.94	3.17	9.67	5.94	3.16	9.61	5.95	3.14	9.75
3	4.50	3.50	8.25	4.87	2.92	10.20	4.86	2.91	10.19	4.60	3.43	8.21
4	9.00	1.75	12.75	8.95	1.74	13.01	8.94	1.75	13.04	8.92	1.81	12.69
5	9.50	1.25	13.00	9.41	1.36	12.55	9.41	1.36	12.55	9.5	1.22	13.05
6	7.75	3.25	12.25	7.91	3.08	13.25	7.90	3.10	13.33	7.78	3.35	12.25
7	8.50	3.25	13.25	8.62	3.21	13.06	8.61	3.23	13.13	8.65	3.18	13.25
8	9.25	5.00	15.00	9.36	4.47	16.63	9.33	4.50	16.73	9.12	4.91	15.02
9	8.50	6.00	15.25	9.00	5.43	18.74	9.03	5.45	18.80	8.57	6.35	15.26
10	8.75	4.50	14.25	9.42	3.21	19.97	9.39	3.23	20.00	8.67	4.69	14.28
11	7.50	5.50	13.00	8.24	3.75	20.06	8.21	3.75	20.02	7.33	5.53	13.11
12	15.50	3.20	21.50	15.23	3.08	21.90	15.2	3.12	22.06	15.20	3.16	21.68
13												

To select the number of factors in the PCR, PLS and OSC-PLS algorithm, a cross-validation leaving out one sample method was employed.³⁵ The prediction error was calculated for each compound for the prediction set. This error was expressed as the prediction residual error sum of squares (*PRESS*):

$$PRESS = \sum_{i=1}^m (c_i^E - c_i)^2 \quad (1)$$

where m is the total number of calibration samples, c_i^E represents the estimated concentration and c_i is the reference concentration for the i -th sample left out of the calibration during cross validation. A plot of *PRESS* against the number of factors for a mixture of the components is shown in Fig. 4. To find the smallest number of factors, F-statistics was employed to perform the significant determination.³⁵ The optimal number of factors yielding the smallest error (*PRESS*) for the three compounds was found to be 3 for PCR, PLS and OSC-PLS. The validation step of the methodologies was performed by running PCR, PLS and OSC-PLS on the prediction set.

For the evaluation of the predictive ability of a multivariate calibration model, the root mean square error of prediction (*RMSEP*) and the relative standard error of prediction (*RSE*) can be employed:²⁸

$$RMSEP = \sqrt{\frac{\sum_{i=1}^N (c_i^E - c_i)^2}{n}} \quad (2)$$

$$RSE = \sqrt{\frac{\sum_{i=1}^N (c_i^E - c_i)^2}{\sum_{i=1}^N c_i^2}} \times 100 \quad (3)$$

where c_i^E represents the estimated concentration, c_i and n are the actual analyte concentration and the number of samples, respectively.

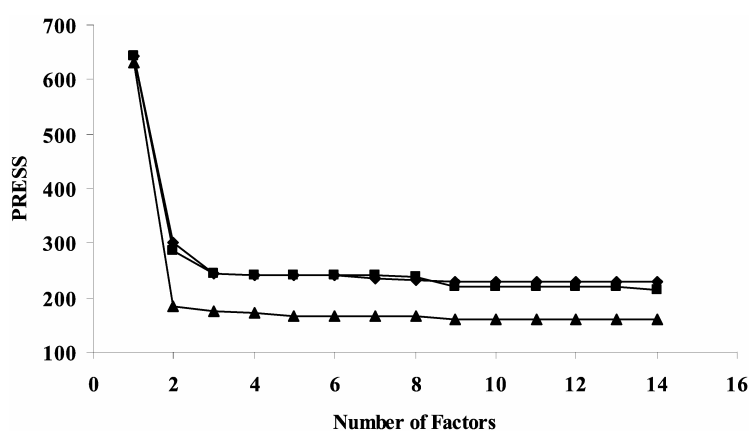


Fig. 4. Plot of *PRESS* against the number of factors for a mixture of CPH, PH, TPM for the PCR (◆), PLS (■) and O-PLS (▲) methods.

The square of the correlation coefficient (R^2), which is an indication of the quality fit of all the data to a straight line, is given by:

$$R^2 = \frac{\sum_{i=1}^N (c_i^E - c_m)^2}{\sum_{j=1}^N (c_j - c_m)^2} \quad (4)$$

where c_m represents the mean of the actual concentration in the prediction set.³⁶

The values of *RSE*, *RMSEP* and R^2 for each component using PLS, PCR and OSC-PLS are given in Table V, from which it can be seen that the obtained values for the statistical parameters were almost the same for the PLS and PCR methods, while the best results were obtained using the OSC-PLS method.

TABLE V. Statistical parameters calculated for the prediction set using the PCR, PLS and O-PLS models

Component	<i>RSE</i> / %			<i>RMSEP</i>			R^2		
	PCR	PLS	O-PLS	PCR	PLS	O-PLS	PCR	PLS	O-PLS
CPH	3.97	3.78	1.03	0.346	0.317	0.087	0.9869	0.9879	0.9988
PH	4.50	4.36	3.30	0.663	0.659	0.124	0.8836	0.8812	0.9949
TPM	5.08	4.80	0.65	0.820	0.830	0.085	0.7273	0.7335	0.9998

Interference studies

Interference by commonly associated excipients in pharmaceutical preparation, such as talc, glucose, starch, lactose, dextrose, sodium alginate and magnesium stearate, was investigated by preparing synthetic mixtures containing $20 \mu\text{g ml}^{-1}$ of each drug and 10-fold excess amounts of the excipients. The tolerance limit was defined as the concentration which gave an error of 3 % or less in the determination of $20 \mu\text{g ml}^{-1}$ of drug. The results are presented in Table VI, from which it is clear that the method is free from interferences of excipient species. Only ascorbic acid appeared to interfere with drugs in this method. The interference of ascorbic acid was eliminated when the synthetic sample solution was measured after times greater or equal to one hour.

TABLE VI. Recovery of $20 \mu\text{g ml}^{-1}$ of phenothiazine drugs from solutions with a 10-fold concentration of various additives used as excipients

Additive	Recovery of phenothiazine drug \pm RSD ^a , %				
	CPH	TPM	TRDH	PH	TFPH
Talc	100.6 \pm 1.1	101.0 \pm 0.8	100.8 \pm 0.9	101.8 \pm 1.4	101.0 \pm 0.6
Glucose	101.9 \pm 1.2	100.8 \pm 1.3	102.8 \pm 1.5	99.6 \pm 1.1	100.5 \pm 0.8
Starch	98.7 \pm 1.3	100.2 \pm 0.7	100.4 \pm 0.9	99.2 \pm 1.4	103.0 \pm 1.2
Lactose	102.5 \pm 1.0	100.6 \pm 1.7	101.9 \pm 1.3	100.8 \pm 0.8	98.0 \pm 1.5
Dextrose	98.5 \pm 1.3	101.3 \pm 0.8	101.6 \pm 1.3	102.6 \pm 1.4	101.4 \pm 1.1
Sodium alginate	101.6 \pm 1.0	100.9 \pm 1.5	01.6 \pm 1.0	100.2 \pm 0.7	101.4 \pm 1.4
Magnesium stearate	100.6 \pm 1.4	100.4 \pm 0.6	102.8 \pm 1.6	100.2 \pm 0.7	101.7 \pm 1.4

^aAverage of four determinations

Application

The proposed individual method was successfully applied to the determination of CPH, PH, TFPH, TPM and TRDH in pharmaceutical preparations. The same samples were also analyzed by the British Pharmaceutical (BP) official method,³⁷ and recovery percent, standard deviation (*SD*), T-test and F-test values were calculated (Table VII). The results reveal that similar degrees of accuracy and precision are afforded by both methods.

TABLE VII. Results of the determination of the studied drugs in pharmaceutical formulations

Drug and formulation ^a	Label claim mg/tablet or mg/ml	Found ^b (recovery \pm <i>SD</i> / %)			Student's T-value ^c	F-value ^d
		Proposed method	Official BP method			
CPH						
Tablet (1)	25	99.42 \pm 0.86	99.23 \pm 1.14	1.64	3.85	
Tablet (1)	100	98.89 \pm 0.96	100.76 \pm 0.92	1.44	1.90	
Injection (1)	25	99.85 \pm 0.54	101.24 \pm 0.82	1.96	2.65	
TFPH						
Tablet (2)	1	99.34 \pm 1.12	99.64 \pm 0.89	2.24	2.84	
Tablet (2)	5	100.8 \pm 0.70	99.36 \pm 0.58	1.85	2.75	

TABLE VII. Continued

Drug and formulation ^a	Label claim mg/tablet or mg/ml	Found ^b (recovery \pm SD / %)		Student's T-value ^c	F-value ^d
		Proposed method	Official BP method		
TFPH					
Tablet (2)	10	99.04 \pm 1.06	100.60 \pm 0.81	1.45	2.90
Injection (2)	1	98.96 \pm 0.70	100.34 \pm 0.58	1.76	3.85
PH					
Tablet (1)	25	99.10 \pm 0.82	99.56 \pm 0.76	2.34	2.65
Injection (1)	25	98.28 \pm 0.56	98.56 \pm 0.64	2.50	3.75
TPM					
Tablet (1)	25	101.60 \pm 0.48	99.42 \pm 0.72	1.90	1.82
Injection (1)	100	101.84 \pm 0.64	100.30 \pm 0.43	1.58	2.95
TRDH					
Tablet (3)	10	100.80 \pm 0.94	99.92 \pm 0.82	2.15	2.88
Tablet (3)	25	100.40 \pm 0.76	100.74 \pm 0.54	2.60	2.05
Tablet (3)	100	101.24 \pm 0.98	100.16 \pm 0.42	2.05	3.25

^aMarketed by: 1 – Tehran Chimi; 2 – Iran Daru Pakhsh; 3 – Pars Minoo; ^baverage of five determinations \pm standard deviation; ^ctabulated Student's T-value at the 95 % confidence level is 2.78; ^dtabulated F-value at the 95 % confidence level is 6.39

In order to assess the applicability of the proposed simultaneous determination methods (PCR, PLS and OSC-PLS) to the analysis of real samples, it was applied to the determination of the three phenothiazine derivatives in different synthetic mixtures. Thus, six different mixtures used in commercially available CPH, PH and TPM tablets were prepared and analyzed. Each measurement was repeated 3 times. The deviation results (Table VIII) show that the calculated values for all mixtures were in satisfactory agreement with the declared values.

TABLE VIII. Simultaneous determination of phenothiazines in tablet mixtures by application of PLS, PCR and OSC-PLS

Sample	Taken, mg			Recovery, %								
				PCR			PLS			O-PLS		
	CPH	PH	TPM	CPH	PH	TPM	CPH	PH	TPM	CPH	PH	TPM
1	6.00	3.00	11.00	95.66	103.53	95.63	102.42	101.24	101.25	100.64	101.20	97.36
				\pm 0.98	\pm 1.26	\pm 1.04	\pm 1.22	\pm 0.96	\pm 1.13	\pm 0.62	\pm 1.05	\pm 1.40
2	7.00	3.50	12.00	97.85	99.42	99.00	99.20	105.20	104.34	98.82	97.23	104.17
				\pm 1.06	\pm 0.86	\pm 0.92	\pm 0.82	\pm 1.15	\pm 0.74	\pm 1.30	\pm 0.65	\pm 0.81
3	10.00	5.00	17.00	98.50	104.00	95.52	98.50	102.10	96.47	103.23	105.32	96.25
				\pm 0.75	\pm 1.47	\pm 0.58	\pm 0.56	\pm 1.18	\pm 0.83	\pm 1.17	\pm 1.22	\pm 0.85
4	6.50	3.20	10.00	97.38	106.20	97.80	104.52	97.20	100.52	99.05	102.06	99.08
				\pm 0.68	\pm 1.80	\pm 0.66	\pm 0.67	\pm 1.24	\pm 0.89	\pm 0.57	\pm 1.25	\pm 0.98
5	9.50	5.00	16.50	96.31	103.20	96.54	100.66	102.76	101.35	94.78	98.32	103.45
				\pm 0.94	\pm 0.72	\pm 1.33	\pm 0.78	\pm 1.14	\pm 1.69	\pm 1.85	\pm 0.94	\pm 1.63
6	10.00	4.50	13.00	98.30	105.05	100.92	96.24	103.02	99.48	103.88	102.76	102.29
				\pm 0.63	\pm 1.08	\pm 0.90	\pm 0.66	\pm 0.88	\pm 0.96	\pm 0.86	\pm 1.56	\pm 1.39

CONCLUSIONS

This individual determination method is simple, rapid, quite selective and highly sensitive in comparison to other reported methods. The other advantages of the present method over the previous methods include rate of development and stability of the colour of the product, wide range of determination without the necessity for heating or extracting, low detection limit with high accuracy and precision. The high λ_{\max} (in the visible region) of the proposed method is a decisive advantage, since interference from associated excipients was not observed. Furthermore, in this method, toxic organic solvents are not required. In other words, it belongs to green chemistry. Thus, it is hoped that this method can be used as an alternative for the rapid and routine microdetermination of bulk samples and various pharmaceutical formulations. In short, the proposed method is a step towards this direction.

In this study, it was shown that the application of multivariate calibration methods, such as PCR, PLS and OSC-PLS, could be well applied for the simultaneous determination of CPH, PH and TPM. The three proposed methods are cheaper than chromatographic methods. Furthermore, in these methods, the use of toxic organic solvents is not required. In other words, they belong to green chemistry. The proposed methods as new, inexpensive and sensitive methods offers good selectivity, accuracy and precision and can be applied for a wide range of CPH, PH and TPM concentrations.

ИЗВОД

ПОЈЕДИНАЧАНА И УПОРЕДНА ОДРЕЂИВАЊА ФЕНОТИАЗИНСКИХ
ЛЕКОВА ПОМОЋУ CR, PLS И (OSC)-PLS КАЛИБРАЦИОНИХ
МЕТОДА СА ВИШЕ ПРОМЕНЉИВИХ

МОХАММАД АЛИ КАРИМИ^{1,2,3}, МОХАММАД МАЗЛУМ АРДАКАНИ⁴, РЕЗА БЕНЈАТМАНЕШ-АРДАКАНИ²,
МОХАММАД РЕЗА ХОРМОЗИ НЕЗХАД⁵ И ХАМЗЕН АМИРЈАН²

¹Department of Chemistry, Payame Noor University of Sirjan, Sirjan, ²Department of Chemistry, Payame Noor University of Ardakan, Ardakan, ³Department of Chemistry, Shahid Bahonar University of Kerman, Kerman, ⁴Department of Chemistry, Yazd University, Yazd and ⁵Department of Chemistry, Persian Gulf University, Bushehr, Iran

У раду је описано појединачно и упоредно одређивање неких фенотиазинских лекова. Метода појединачног одређивања заснована је на реакцији хлорпромазин-хидрохлорида (CPH), прометазин-хидрохлорида (PH), трифлуороперазин-хидрохлорида (TFPH), тримипрамин-малеата (TPM) и тиоридазин-хидрохлорида (TRDH) са комплексним јоном $[\text{Fe}(\text{bpy})_3]^{3+}$. У присуству фенитазинских деривата, $[\text{Fe}(\text{bpy})_3]^{3+}$ се лако редукује формирајући обојен комплексни јон $[\text{Fe}(\text{bpy})_3]^{3+}$, који показује апсорбциони максимум при таласној дужини од 525 nm. Метода је веома осетљива и погодна за одређивање у опсегу концентрација 0,3–190 $\mu\text{g ml}^{-1}$, са границом детекције од 0,18–2,46 $\mu\text{g ml}^{-1}$. У раду је такође описано спектрофотометријско одређивање тројних смеша CPH, PH и TPM применом мултиваријантних метода калибрације (PCR, PLS и OSC-PLS). Методе симултаног одређивања заснивају се на различитој брзини редукције комплексног јона $[\text{Fe}(\text{bpy})_3]^{3+}$ са CPH, PH и TPM у киселој средини. Резултати указују на то да CPH, PH и TPM могу бити упоредно одређени методама PCR, PLS и OSC-PLS у

областима концентрације 0,5–120,0; 0,3–80,0 и 5,0–100,0 $\mu\text{g ml}^{-1}$, респективно. Средња квадратна грешка предвиђања концентрације СРН, РН и ТРМ износи 0,346; 0,663 и 0,820 за методу PCR, 0,317; 0,659 и 0,830 за методу PLS и 0,087; 0,124 and 0,085 за методу OSC–PLS, респективно. Предложене методе су успешно примењене за појединачно и истовремено одређивање фенотиазинских деривата у фармацеутским препаратима, чији се резултати добро слажу са званичном методом, и на неколико синтетичких узорака, при чему су добијени задовољавајући резултати.

(Примљено 14. септембра 2006, ревидирано 24. јула 2007)

REFERENCES

1. C. O. Wilson, O. Gisvold, R. F. Doerge, *Text Book of Organic Medical and Pharmaceutical Chemistry*, 7th Ed., New York, 1977
2. H. P. Tarasiewicz, J. Karpinska, *Pharmazie* **47** (1992) 887
3. V. G. Belikov, G. F. Moiseeva, *Farmatsiya Moscow* **36** (1986) 87
4. J. Blazek, A. Dymes, Z. Stejskal, *Pharmazie* **31** (1976) 681
5. G. Dusinsky, O. Liskova, *Chem. Zvesti.* **12** (1958) 213
6. F. Dima, I. Bella, P. Gasper, *J. Chromatogr.* **156** (1978) 327
7. Z. Q. Zhaug, Z. G. Chen, H. Zhaug, *Microchem. J.* **53** (1996) 282
8. J. J. Menninger, C. E. Keeler, *Anal. Chem.* **36** (1996) 1840
9. J. L. Loez paz, A. Townshend, *Anal. Commun.* **33** (1996) 31
10. D. Deorsi, L. Gagliardi, D. Yonelli, *J. Pharm. Biomed. Anal.* **14** (1995) 1635
11. I. L. Zhuravleva, M. B. Terenina, R. V. Golovnya, M. A. Filiminova, *Khim–Farm. Zh.* **5** (1993) 58
12. K. Basavaiah, P. G. Ramma, *J. Inst. Chem. India* **56** (1984) 107
13. Jayarama, M. V. M. D'Souza, H. S. Yathirajan, Rangaswamy, *Talanta* **33** (1986) 352
14. S. M. Hassan, F. Bella, F. Ibrahim, F. A. Aly, *Anal. Lett.* **22** (1989) 1037
15. W. Misiuik, M. Tarasiewicz, *Pharmazie* **48** (1993) 66
16. M. M. El-Kerdway, M. A. Moustafa, S. M. El-Ashry, D. R. El-Wazzi, *Anal. Lett.* **26** (1993) 1669
17. W. Misiuik, M. Tarasiewicz, *Pharmazie* **51** (1996) 62
18. K. Basavaiah, G. Kreihnamurthy, *Anal. Lett.* **31** (1998) 1485
19. K. C. Srinivasamurthy, J. Seetharamappa, *Indian J. Pharm. Sci.* **62** (2000) 273
20. K. Basavaiah, J. M. Swamy, *Anal. Sci.* **17** (2001) 963
21. M. C. Gutierrez, A. Gomez–Hens, D. Perez–Bendito, *Anal. Lett.* **20** (1987) 1947
22. D. Chen, A. Rios, M. D. Luque de Castro, M. Valcarcel, *Talanta* **38** (1991) 1227
23. B. Gala, A. Gomez–Hens, D. Perez–Bendito, *Anal. Chim. Acta* **310** (1995) 453
24. A. A. Fasanmade, *Anal. Lett.* **27** (1994) 1955
25. M. Shamsipur, B. Hemmateenejad, M. Akhond, *J. AOAC Int.* **85** (2002) 555
26. B. Hemmateenejad, M. A. Safarpour, A. M. Mehranpour, *Anal. Chim. Acta* **535** (2005) 275
27. S. R. Crouch, T. F. Cullen, A. Scheeline, E. S. Kirkor, *Anal. Chem.* **72** (2000) 53
28. H. Goicoechea, C. A. C. Olivieri, *Anal. Chim. Acta* **453** (2002) 189
29. H. Abdollahi, J. Zolgharnein, G. H. Azimi, D. Jafarifar, *Talanta* **59** (2003) 1141
30. J. Ghasemi, H. R. Seraji, M. Noroozi, M. Hashemi, A. Jabbari, *Anal. Lett.* **37** (2004) 725
31. J. Ghasemi, A. Niazi, S. Ghobadi, *J. Chin. Chem. Soc.* **52** (2005) 1049
32. A. Niazi, A. Soufi, M. Mobarakabad, *Anal. Lett.* **39** (2006) 2359
33. A. A. Syed, A. Syeda, H. R. K. Mahesh, *Farmaco* **60** (2005) 47

34. M. A. Karimi, M. Mazloun Ardakani, R. Behjatmanesh Ardakani, O. Moradlou, F. Banifatemeh, *J. Chin. Chem. Soc.* **54** (2007) 15
35. D. M. Haaland, E. V. Thomas, *Anal. Chem.* **60** (1988) 1193
36. M. R. Majidi, K. Asadpour-Zeynali, *J. Chin. Chem. Soc.* **52** (2005) 21
37. *British Pharmacopoeia*, H. M. Stationary Office, London, 1993.



www.shd.org.yu

Determination of trace copper in water samples by flame atomic absorption spectrometry after preconcentration on a phosphoric acid functionalized cotton chelator

RENMIN GONG*, DEMIN ZHANG, KEDING ZHONG, MIN FENG and XINGYAN LIU

The Laboratory of Bio-Macromolecular Evolution, College of Life Science, Anhui Normal University, Wuhu, 241000, P. R. China

(Received 20 February, revised 8 August 2007)

Abstract: This paper reports the preparation of a phosphorylated cotton chelator (PCC) by solid phase esterification of phosphoric acid (PA) onto defatted cotton fibres using urea as the catalyst. The synthesized PCC was employed for the preconcentration of copper from water samples prior to its determination by flame atomic absorption spectrometry (FAAS). The preconcentration of copper was studied under both batch and column techniques. The pH range for the quantitative preconcentration of copper was 4.0–7.0. The sorption time required for each sample was less than 30 min by the batch method. The copper sorption capacity of the PCC was found to be 15.3 mg/g at the optimum pH value. Elution with 1.0 mol dm⁻³ hydrochloric acid was found to be quantitative. Feasible flow rates of the copper solution for quantitative sorption onto the column packed with PCC were 0.5–4.0 ml min⁻¹, whereas the optimum flow rate of the hydrochloric acid solution for desorption was less than 1.5 ml min⁻¹. An 80-fold preconcentration factor could be achieved under the optimum column conditions. The tolerance limits for common metal ions on the preconcentration of copper and the number of times of column reuse were investigated. The proposed method was successfully applied for the preconcentration and determination of trace copper in natural and drinking water samples by FAAS.

Keywords: phosphoric acid; PCC; trace copper; preconcentration; FAAS; determination.

INTRODUCTION

Determination of heavy metals at trace levels in environmental and food samples is of great importance nowadays due to the non-degradability, bioaccumulation and high toxicity of heavy metals in the environment and living organisms. Most heavy metals have a high affinity for thiol groups, carboxyl groups and/or amine groups; hence, they attack and inactivate enzymes and protein sites where these kinds of groups are present. It also has been demonstrated

* Corresponding author. E-mail: rmgong.nju@163.com

doi: 10.2298/JSC0802249G

that heavy metals bind to cell membranes, obstructing transport processes through the membranes. Therefore, heavy metals are of particular importance from the ecotoxicological point of view.¹

Copper, an important metal in many industries, is considered as an essential micronutrient for human health and plays an important role in carbohydrate and lipid metabolism and in the maintenance of heart and blood vessel activity. The requirement of an adult human is about 1–5 mg of copper per day, but excess amounts in the body can be toxic.² Acute symptoms from excessive ingested copper include salivation, epigastric pain, nausea, vomiting, diarrhoea, intravascular haemolytic anaemia, acute hepatic and renal failure, shock, and coma.

Flame atomic absorption spectrometry (FAAS) is a simple and well available technique for the determination of heavy metals in diverse samples. Due to the limited sensibility of FAAS and to the low concentration levels of heavy metal in natural samples, prior to FAAS analysis some preconcentration procedures based on liquid–liquid extraction,³ ion exchange⁴ and solid phase extraction⁵ have been developed. Solid phase extraction of heavy metals is considered superior to liquid–liquid extraction due to its simplicity, rapidity, low cost, and higher recovery. Macromolecular chelators have been found to be more selective for solid phase extraction in comparison to ion exchangers. Among different kinds of support materials used to design macromolecular chelator, cellulose appears attractive due to its good porosity, high hydrophilicity, low swelling, chemical resistance, wide availability and easy biodegradability.⁶

Cellulose sorbents containing diverse functional groups or reagents, such as pyrocatechol,⁶ iminodiacetate,⁷ diethylenetriaminetetraacetic acid,⁸ triethylenetetraminepentaacetic acid,⁹ 8-hydroxyquinoline,¹⁰ 2,3-dihydroxypyridine,¹¹ 8-hydroxyquinoline-5-sulphonic acid,¹² hexamethylenedithiocarbamates,¹³ methyliminodiacetic acid,¹⁴ have been reported for metal preconcentration. Lásztity *et al.*¹⁵ examined oxime, sulphoxine and 2,2'-diamino-diethylamine cellulose based macromolecular chelators for platinum. Aoki *et al.*¹⁶ investigated 6-deoxy-6-mercaptopcellulose and its S-substituted derivatives for their sorption characteristics. Dietz *et al.*¹⁷ functionalized acetoacetamide chelating groups onto microcrystalline cellulose and studied its affinity for Fe(III), Cu(II) and U(VI). In addition to cellulose, thiol cotton fibre (a functionalised cellulose sorbent)^{18–20} were also employed for methylmercury, selenium and multielement preconcentration.

This paper presents the preparation of a phosphorylated cotton chelator (PCC) by solid phase esterification of phosphoric acid (PA) onto defatted cotton fibre using urea as the catalyst. The synthesized PCC was employed for the preconcentration of copper in water samples prior to its determination by FAAS. The preconcentration of Cu on a column packed with PCC was investigated. The optimum conditions for the preconcentration and desorption procedures were also elucidated. By applying the proposed method, the Cu contents in natural and drinking water samples were determined.

EXPERIMENTAL

Reagents and Instrumentation

All chemicals were of analytical reagent grade unless otherwise stated. Doubly distilled deionised water was used throughout this study. A copper stock solution ($200 \mu\text{g ml}^{-1}$) was prepared by dissolving 0.3802 g of $\text{Cu}(\text{NO}_3)_2 \cdot 3\text{H}_2\text{O}$ (Merck) in 500 ml of water. Working solutions were prepared by diluting the stock solution to the required volumes. The esterification agent was prepared by dissolving 1.67 g of urea in 1 l of 0.5 mol dm^{-3} PA and then the pH value of the solution was adjusted to 3.5 with NaOH.

The glassware was washed with chromic acid, soaked in 10 % HNO_3 overnight and subsequently cleaned with doubly distilled water before use.

A Perkin–Elmer Model 5100PC flame atomic absorption spectrophotometer was used for the determination of copper under the manufacturer's recommended conditions. The calibration curve ($0.25\text{--}5.0 \mu\text{g ml}^{-1}$) for copper was established with solutions prepared from the $200 \mu\text{g ml}^{-1}$ stock solution.

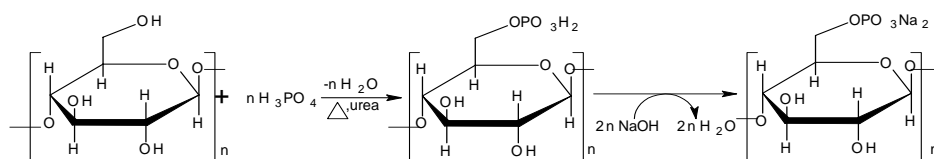
The reference measurements were made on Jobin-Yvon Panorama ICP–AES instrument using the axial viewing configuration. The operating condition was as follows: RF power 1.0 kW, nebuliser pressure 3.0 bar, plasma gas flow 16.0 l min^{-1} , auxiliary gas flow 1.7 l min^{-1} , sample uptake rate 0.8 ml min^{-1} , stabilization time 15 s, read time 1 s, emission line for Cu 324.754 nm.

Preparation of PCC

The PCC was prepared according to a method similar to one given in the literature but free of any solvent.²¹

Thus, defatted cotton fibre, purchased from a local drugstore, was mixed with the previously mentioned esterification agent in the ratio 1:12 (fibre:esterification agent, w/v) and stirred for 30 min. The esterification agent/fibre slurry was placed in a stainless steel tray and dried at 50°C in a forced air oven. After 24 h, the esterification reaction between PA and fibre was initiated by raising the oven temperature to 120°C for 90 min. After cooling, the PA-modified cotton fibre was extensively washed to neutral pH with doubly distilled deionised water. After filtration, the PA-modified cotton fibre was transformed into the Na form by suspension in a suitable amount of 0.10 mol dm^{-3} NaOH and stirring for 60 min. Subsequently, the residual alkali was removed by washing thoroughly with doubly distilled deionised water. The PCC was then dried at 50°C to constant weight and stored in a desiccator before use as the extractant for pre-concentration.

The preparation of PCC can be schematically expressed by the following Equation:

*Copper pre-concentration procedures*

Batch experiment. Batch experiments were conducted by adding 0.2 g of PCC to 250 ml shaking flasks containing 100.0 ml of copper solution having different concentrations or initial pH values. The initial pH values of the solution were previously adjusted with dilute HNO_3 or NaOH using a pH meter. After sealing to prevent volume change during the experiments, the flasks were maintained at ambient temperature ($20 \pm 2^\circ\text{C}$) and agitated at 150 rpm in a rotary shaker for predetermined time intervals. The PCC was separated by filtration through a

membrane filter (0.45 μm). The filtrate was analysed for the concentration of the remaining copper ions by FAAS. When the copper ion concentration in the filtrate was too low to be analysed by FAAS, the copper sorbed by the PCC was eluted into a suitable volume of 1.0 mol dm^{-3} hydrochloric acid for its determination.

Column procedure. A glass column (10 mm \times 200 mm) was packed with 0.1 g of PCC, then 100 ml doubly distilled deionised water was passed through the column for cleaning and preconditioning. A copper solution at the optimum pH value was loaded onto the column with a peristaltic pump at a flow rate of 2 ml min^{-1} , after which the column was washed with 5 ml of doubly distilled deionised water. The copper sorbed on the column was preconcentrated into a 5.0 ml volumetric flask by eluting with 5.0 ml of 1.0 mol dm^{-1} hydrochloric acid at a flow rate of 1 ml min^{-1} . The copper ion in the eluate was determined by FAAS.

RESULTS AND DISCUSSION

Batch experiment

Influence of initial pH. Preliminary studies indicated that the initial pH of the solution significantly affected Cu sorption. Hence, in all the experimental parameters affecting copper sorption by the PCC, the influence of the initial pH was studied first. The initial pH of copper solution was systematically examined over a range from 0.5 to 7.0, thus avoiding copper precipitation. As can be seen from Fig. 1, the percent copper sorbed was the lowest at the initial pH 0.5. The amount of Cu sorbed increased with increasing pH until a plateau was reached at about pH 4.0. These results show the strong pH dependence of Cu sorption on PCC. Thus, pH 4.5 was selected for the subsequent experiments.

At the optimal initial pH, the sorption equilibrium of Cu was attained after about 30 min.

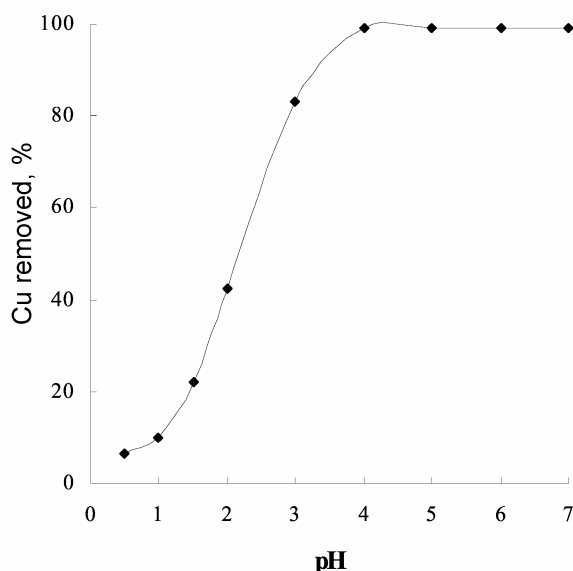


Fig. 1. Influence of the initial pH on the removal of Cu by PCC (Batch experiment: Cu concentration: 20 mg dm^{-3} ; PCC dose: 2 g dm^{-3} ; contact time: 1 h).

Effect of initial copper concentration. The influence of copper concentration on the sorption percent of Cu and sorption capacity of PCC for copper was investigated. As shown in Fig. 2, when the copper concentration was increased from 5 to 70 mg dm⁻³, the percent Cu sorbed on the PCC decreased from 99.4 to 44.4 %.

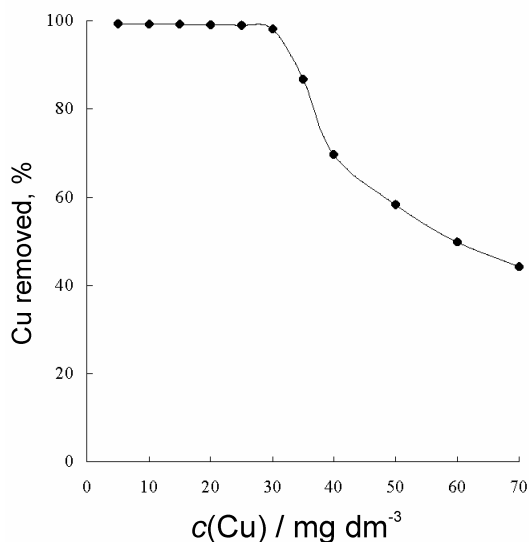


Fig. 2. Effect of the initial copper concentration on the removal of Cu by PCC (Batch experiment: PCC dose: 2 g dm⁻³; contact time: 1 h; pH 4.5).

Using the data in Fig. 2, the Langmuir equation was employed to study the sorption isotherm of Cu.

The Langmuir equation is based on the assumption that maximum sorption corresponds to a saturated monolayer of sorbate molecule on the sorbent surface, that the energy of sorption is constant and that there is no transmigration of sorbate in the plane of the surface.

The linear Langmuir equation is as follows:

$$c_e/q_e = 1/(aQ_m) + c_e/Q_m$$

where c_e (mg dm⁻³) is the concentration of the Cu solution at equilibrium, q_e (mg/g) is the amount of Cu sorbed at equilibrium, Q_m is the maximum sorption capacity and represents the practical limiting sorption capacity when the sorbent surface is fully covered with a monolayer of sorbate molecules and a is the Langmuir constant.

The Langmuir sorption isotherm of Cu sorbed on PCC is shown in Fig. 3. The experimental result indicate that the sorption isotherm of Cu trapped on PCC fitted the Langmuir model ($R^2 = 0.9988$). The maximum sorption capacity (Q_m) of PCC for Cu, obtained from the slope ($1/Q_m$) of the linear plot of c_e/q_e versus c_e , was 15.27 mg/g. The capacity of the PCC for other divalent metals is 12.62 mg/g for cobalt, 13.89 mg/g for zinc and 12.91 mg/g for nickel.

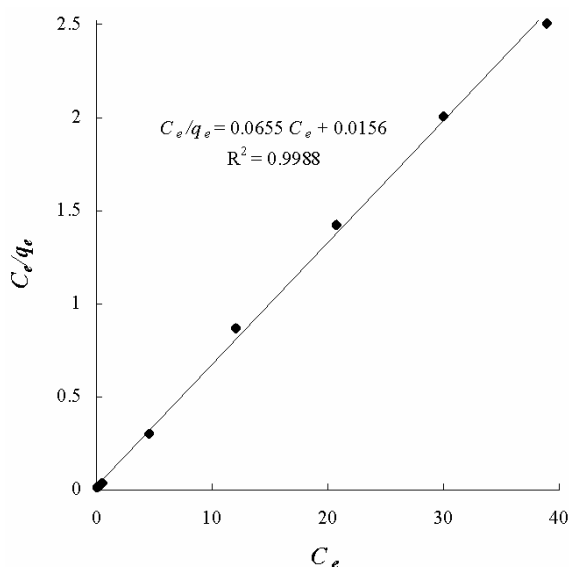


Fig. 3. Langmuir sorption isotherm of Cu by PCC.

Column procedure

Column operation conditions. The column operation conditions were examined with different volumes of a solution containing 20.0 μg copper at the optimum pH value. The volume of the copper solution was varied in the range of 50–500 ml under the optimum conditions, keeping the other variable constant. The experimental results indicated that the sorption was almost constant up to 400 ml. However, for convenience, all experiments were conducted with 100 ml of aqueous phase. The flow rate of the copper solution was varied from 0.5–5 ml min^{-1} . Figure 4 shows that the flow rate in the range 0.5–4 ml min^{-1} did not affect the copper sorption. A flow rate of 2 ml min^{-1} was used in all further experiments. Preliminary observations indicated that copper was eluted quantitatively with 5.0 ml of 1.0 mol dm^{-3} hydrochloric acid. It was found that a flow rate lower than 1.5 ml min^{-1} did not affect the elution of copper (Fig. 4). Therefore, 5.0 ml of 1.0 mol dm^{-3} hydrochloric acid and eluant flow rate of 1.0 ml min^{-1} were used in the present work. Thus, the quotient of the largest sample volume and the eluant volume was 80. After elution, the column was washed to neutral pH with doubly distilled deionised water and then 5 ml of 0.10 mol dm^{-3} sodium hydroxide was passed through before finally thoroughly washing with sufficient doubly distilled deionised water for reuse of the PCC.

Interference of foreign ions. The interference of common foreign metal ions on the preconcentration of copper were investigated by adding individual foreign metal ions to 100 ml of a 200 $\mu\text{g dm}^{-3}$ copper solution at the optimum pH value and determining the recoveries of copper applying the proposed procedure. The tolerance limits of the foreign metal ions, defined as the largest amount making

the recoveries of copper less than 95 %, were found to be 2.000 g dm⁻³ for Na⁺ and K⁺, 1.000 g dm⁻³ for Ca²⁺, 0.500 g dm⁻³ for Mg²⁺, 100 mg dm⁻³ for Co²⁺, Mn²⁺, Ni²⁺, Pb²⁺ and Zn²⁺. As the contents of these metal ions in common samples are within the tolerated concentration range, they will not interfere with the preconcentration of copper.

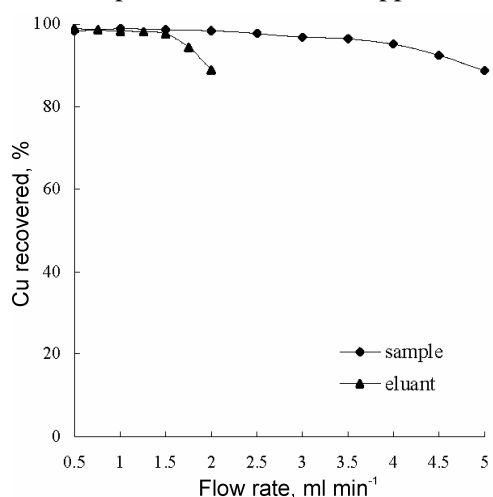


Fig. 4. Influence of the sample and eluant flow rate on the removal of Cu by PCC (Column experiment: Cu – 20 µg; sample volume – 100 ml; sample/eluant flow rate – 2/1 ml min⁻¹; pH 4.5).

Regeneration of column. The stability and potential regeneration of the column were investigated. Twenty sorption–elution cycles were performed by making four runs on the same day and the next four runs one day later. The column was stored in doubly distilled deionised water. As shown in Fig. 5, the column was relatively stable up to at least 20 preconcentration–elution cycles without an obvious decrease in the recovery of copper.

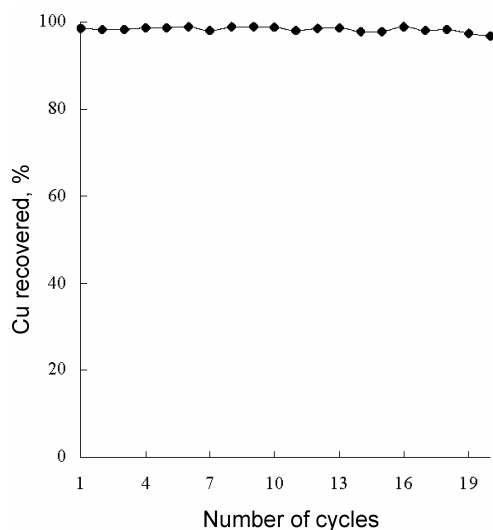


Fig. 5. Effect of recycle time on the removal of Cu by PCC (Column experiment: Cu – 20 µg; sample volume – 100 ml; sample/eluant flow rate – 2/1 ml min⁻¹; pH 4.5).

Copper determination in real water samples

In order to check the validity of the proposed method, the method was applied to determine trace amounts of copper in natural and drinking water samples. The natural water samples were collected from the Mirror Lake, the Yangtze River in or around Wuhu city, China. The drinking water sample was purchased from a local supermarket. The natural water samples were filtered through a membrane filter (0.45 μm), and then 100.0 ml of the filtrates or drinking water were subjected to the recommended column procedure for the preconcentration and determination of copper ions directly and after standard addition. The analysis was repeated five times and the results obtained were compared with the values determined by ICP–AES in Table I. It could be seen that the recovery obtained from the real water samples (97.9–102.1 %) was comparable to that gained by ICP–AES (97.8–100.5 %, data not shown), and the performance of the method was very good in natural and drinking water samples. Finally, the relative standard deviation of the copper determination in the examined real water samples ranged between 2.6 and 4.1 %.

TABLE I. The results of copper determination in natural and drinking water samples

Sample	Copper				
	Added $\mu\text{g dm}^{-3}$	Found $\mu\text{g dm}^{-3}$	Recovery %	RSD %	ICP–AES $\mu\text{g dm}^{-3}$
Lake water	0	23.5	–	3.6	24.4
	100	125.6	102.1	2.7	124.9
River water	0	28.6	–	3.8	28.2
	100	126.9	98.3	2.6	126.0
Nongfu spring [®] natural drinking water	0	8.4	–	4.1	8.2
	100	106.3	97.9	3.4	107.8

CONCLUSIONS

A simple, accurate and sensitive method for the preconcentration and determination of copper by FAAS in large volumes of water samples using PCC as the extractant has been developed. The preconcentration technique used in this work is very inexpensive since only 0.10 g of sorbent is required in column operation and which could be repeatedly used at least 20 times. An 80-fold preconcentration factor can be achieved under the optimum column conditions. The duration of the preconcentration step, which includes preconcentration of the sample and regeneration of the column, is about 70 min for 100 ml of sample solution. Moreover, as copper can be sorbed quantitatively over a wide pH range, no buffer was required to control precisely the pH values. The detection limit achieved was satisfactory for the examined samples. The proposed method was employed for preconcentration and determination of copper in natural and drinking water samples by FAAS with satisfactory results. In conclusion, the proposed method is excellent in regards to simplicity, sensitivity, selectivity, reliability, accuracy and column stability.

Acknowledgments. This work was sponsored by China Postdoctoral Science Funds, the Key Laboratory of Bioresource Protection and Utilization of Anhui Province, and the Key Laboratory of Biotic Environment and Ecological Safety in Anhui Province.

ИЗВОД

ОДРЕЂИВАЊЕ ТРАГОВА БАКРА У УЗОРЦИМА ВОДЕ ПЛАМЕНОМ АТОМСКОМ
АБСОРПЦИОНОМ СПЕКТРОСКОПИЈОМ ПОСЛЕ ПРЕКОНЦЕНТРИСАЊА НА
ПАМУЧНОМ ХЕЛАТОРУ ТРЕТИРАНОМ ФОСФОРНОМ КИСЕЛИНОМ

RENMIN GONG, DEMIN ZHANG, KEDING ZHONG, MIN FENG и XINGYAN LIU

*The Laboratory of Bio-Macromolecular Evolution, College of Life Science,
Anhui Normal University, Wuhu, 241000, P R China*

У раду је приказано добијање фосфорисаног памучног хелатора (РСС) естерификацијом фосфорне киселине (РА) у чврстој фази, на одмашћеним памучним влакнима помоћу урее као катализатора. Добијени РСС употребљен је за преконцентрисање бакра из узорака воде ради одређивања пламеном атомском абсорпционом спектроскопијом (FAAS). Преконцентрисање бакра испитивано је техникама груписања и колоне у области рН 4,0–7,0. Време сорпције за сваки узорак у методи груписања износи мање од 30 min. Добијено је да капацитет РСС за сорпцију бакра износи 15,3 mg/g при оптималној рН вредности. Квантитативно испирање постигнуто је раствором 1,0 mol dm⁻³ хлороводоничне киселине. Проток раствора бакра потребан за квантитативну сорпцију у колони са РСС пуњењем износи 0,5–4,0 ml min⁻¹, док је оптимални проток раствора хлороводоничне киселине потребног за десорпцију мањи од 1,5 ml min⁻¹. Фактор преконцентрисања од око 80 може се постићи под оптималним условима у колони. Иситивани су границе толеранције за преконцентрисање металних јона сличних бакру и број поновних коришћења колоне. Предложени метод успешно је примењен за преконцентрисање бакра у траговима и његово одређивање у узорцима природне и пијаће воде методом FAAS.

(Примљено 20. фебруара, ревидирано 8. августа 2007)

REFERENCES

1. H. T. Lu, S. F. Mou, Y. Yan, S. Y. Tong, J. M. Riviello, *J. Chromatogr. A* **800** (1998) 247
2. K. Ohta, H. Tanahasi, T. Suzuki, S. Kaneco, *Talanta* **53** (2001) 715
3. A. N. Anthemidis, G. A. Zachariadis, C. G. Farastelis, J. A. Stratis, *Talanta* **62** (2004) 437
4. S. B. Erdemoğlu, K. Pyrzyńska, Ş. Güçer, *Anal. Chim. Acta* **411** (2000) 81
5. G. A. Zachariadis, A. N. Anthemidis, P. G. Bettas, J. A. Stratis, *Talanta* **57** (2002) 919
6. V. Gurnani, A. K. Singh, B. Venkataramani, *Talanta* **61** (2003) 889
7. Y. Akama, K. Yamada, O. Itoh, *Anal. Chim. Acta* **485** (2003) 19
8. G. I. Tsysin, I. V. Mikhura, A. A. Formanovsky, Y. A. Zolotov, *Mikrochim. Acta* **105** (1991) 53
9. P. Burba, J. C. Rocha, A. Schulte, *Fresenius J. Anal. Chem.* **346** (1993) 414
10. V. Gurnani, A. K. Singh, B. Venkataramani, *Anal. Chim. Acta* **485** (2003) 221
11. V. Gurnani, A. K. Singh, B. Venkataramani, *Anal. Bioanal. Chem.* **377** (2003) 1079
12. K. Zih-Perényi, A. Lásztity, Zs. Horváth, Á. Lévai, *Talanta* **47** (1998) 673
13. P. Burba, P.-G. Willmer, M. Becker, R. Klockenkämper, *Spectrochim. Acta B* **44** (1989) 525
14. M. C. Gennaro, C. Sarzanini, E. Mentasti, C. Baiocchi, *Talanta* **32** (1985) 961
15. A. Lásztity, Á. Kelkó-Lévai, K. Zih-Perényi, I. Varga, *Talanta* **59** (2003) 393

16. N. Aoki, K. Fukushima, H. Kurakata, M. Sakamoto, K. Furuhashi, *React. Funct. Polym.* **42** (1999) 223
17. G. Dietz, T. Seshadri, H. J. Haupt, A. Kettrup, *Fresenius J. Anal. Chem.* **322** (1985) 491
18. V. Celo, R. V. Ananth, S. L. Scott, D. R. S. Lean, *Anal. Chim. Acta* **516** (2004) 171
19. L. Marin, J. Lhomme, J. Carignan, *Talanta* **61** (2003) 119
20. M. Q. Yu, W. Tian, D. W. Sun, W. B. Shen, G. P. Wang, N. Xu, *Anal. Chim. Acta* **428** (2001) 209
21. R. M. Gong, Y. B. Jin, J. Chen, Y. Hu, J. Sun, *Dyes Pigments* **73** (2007) 332.